[American Journal of Science, Vol. 306, September, 2006, P. 475–524, DOI 10.2475/10.2475/07.2006.01]

American Journal of Science

SEPTEMBER 2006

DEVELOPMENT OF SPATIAL VARIATIONS IN REACTION PROGRESS DURING REGIONAL METAMORPHISM OF MICACEOUS CARBONATE ROCKS, NORTHERN NEW ENGLAND

SARAH C. PENNISTON-DORLAND* and JOHN M. FERRY†

Department of Earth and Planetary Sciences, Johns Hopkins University, Baltimore, Maryland 21218 USA

ABSTRACT. Progress (ξ) of the infiltration-driven reaction, muscovite + ankerite + quartz + rutile + H_2O = biotite + calcite + plagioclase + CO_2, which occurred during Barrovian and Buchan regional metamorphism in east-central Vermont and south-central Maine, can vary by a factor of ten or more at all spatial scales down to that of adjacent lithologic layers <1 cm thick. Values of proxies for the activity of CO_2 and $\delta^{18}O_{fluid}$, $K_s(6) \equiv [(a_{phl})(a_{an})(a_{cal})^2]/[(a_{ms})(a_{dol})^3(a_{qtz})^2]$ and $\delta^{18}O_{Cal}$, are uniform within error of measurement over distances up to ≈1 m across layering. The conventional explanation of cm- to dm-scale variations in ξ in terms of layer-parallel channeled fluid flow cannot explain the uniformity in the proxies. Observed cm- to dm-scale variations in ξ are better explained by (a) mineral reactants and products that are solid solutions, (b) layer-by-layer variations in the amounts and compositions of minerals prior to reaction, and (c) uniformity of $K_s(6)$ on a spatial scale larger than the scale of variations in ξ during subsequent infiltration and reaction. The m-scale uniformity in $K_s(6)$ and $\delta^{18}O_{Cal}$ is interpreted as homogenization of a_{CO_2} and $\delta^{18}O_{fluid}$ caused by the combined effects of intergranular diffusion and hydrodynamic dispersion. Reaction progress therefore was driven by the interplay of layer-parallel advection of chemically-reactive H_2O-rich fluid at decameter and larger scales and cross-layer transport of CO_2 and H_2O by diffusion/dispersion at scales of ≈1 m and less. Regardless of whether mineral reactants and products are solid solutions, the geochemical tracer considered, or the mechanism of fluid-rock reaction, the geometry of fluid flow can never be determined at a scale smaller than the one over which the concentration of the tracer is homogenized in the fluid within error of measurement by diffusion and dispersion.

INTRODUCTION

It is now well documented that decarbonation reactions during metamorphism are commonly driven by infiltration of rock by chemically reactive fluid (Ferry and Gerdes, 1998). Ignoring the combined effects of diffusion and hydrodynamic dispersion (referred to in the rest of the paper for brevity as "diffusion/dispersion"), reaction progress (ξ) is related to molar time-integrated fluid flux (q) by

$$q = \nu_{CO_2}\xi(1 - X_{CO_2})/(\partial X_{CO_2}/\partial z), \quad (1)$$

where z is distance along the flow path, X_{CO_2} is mole fraction of CO_2 in fluid, and ν_{CO_2} is the stoichiometric coefficient of CO_2 in the reaction (Baumgartner and Ferry, 1991). Accordingly, the spatial distribution of the progress of infiltration-driven reactions in metamorphic rocks has been interpreted as a direct image of fossil fluid flow channels, some as small as several mm wide (for example, Ferry, 1987, 1994). Spatial variations in ξ directly image spatial variations in time-integrated fluid flux only if rocks considered

*Present address: Department of Geology, University of Maryland, College Park, Maryland 20742, USA
†Corresponding author: jferry@jhu.edu

were chemically isolated from each other during fluid flow and mineral reaction. Recent field (for example, Bickle and others, 1997; Evans and others, 2002; Ague, 2003), theoretical (for example, Ague and Rye, 1999; Ague, 2000, 2002), and experimental studies (for example, Wark and Watson, 2004), however, indicate that homogenization of fluid composition by diffusion/dispersion of H_2O, CO_2, and other volatile species should be very efficient at the scale of a m or greater at the conditions of regional metamorphism. Variations in ξ at the cm to dm scale therefore seem to require some explanation other than variations in time-integrated fluid flux. An alternative explanation is cm- to dm-scale variations in the amount and compositions of mineral solid solutions that participate in an infiltration-driven reaction prior to reaction coupled with uniformity in proxies for fluid composition during reaction at the same or larger scale, as could develop, for example, if fluid composition were homogenized by diffusion/dispersion (Ferry and others, 2005). In cases where the alternative interpretation is correct, cm- to dm-scale variations in ξ image variations in modes and mineral compositions prior to reaction rather than fluid flow channels.

We investigated occurrences of regionally metamorphosed micaceous carbonate rocks in east-central Vermont and south-central Maine to determine which of the two explanations better accounts for cm- to dm-scale variations in progress of infiltration-driven reaction, and correspondingly, how the variations in ξ are to be best understood in terms of metamorphic process. The two locations are appropriate for several reasons. First, the locations expose carbonate rocks in which ξ differs between cm-thick layers in some cases by more than an order of magnitude. The variations in ξ have previously been interpreted as a record of cm-scale differences in time-integrated fluid flux (Ferry, 1987, 1988a, 1988b, 1994). Second, the two areas permit comparison of metamorphic processes in a low-P Buchan terrain at the relatively shallow crustal depth of 10 to 15 km (Maine) with those in an intermediate-P Barrovian terrain at the mid-crustal depth of 25 to 30 km (Vermont). Third, for practical purposes, rocks experienced a single infiltration-driven decarbonation reaction during prograde regional metamorphism. Five of the minerals that participate in the reaction (ankerite, muscovite, biotite, calcite, plagioclase) are solid solutions. Fourth, rocks contain proxies that may be used to evaluate the spatial scale of the uniformity of the activity of CO_2 (a_{CO_2}), $\delta^{18}O_{fluid}$, and $\delta^{13}C_{fluid}$. Fifth, the study benefits from decades of geological and petrologic studies in both areas (as reviewed, for example, by Osberg and others, 1989 and Tucker and others, 2001).

GEOLOGIC SETTING

East-central Vermont

The location and geologic setting of outcrops investigated are illustrated in figure 1. Basic geologic relations in the area have been established by White and Jahns (1950), Lyons (1955), Doll and others (1961), Woodland (1977), Fisher and Karabinos (1980), Hatch (1988a), and Hueber and others (1990), among others. The study focused on the Siluro-Devonian Waits River Formation, a metamorphosed turbidite that is typically composed of interbedded pelitic schist and micaceous carbonate rock in variable proportions (Hatch, 1988b). The Waits River Formation was deformed and regionally metamorphosed during the Devonian Acadian orogeny (Thompson and others, 1968; Thompson and Norton, 1968; Osberg and others, 1989). Radiometric ages of monazite neoblasts in pelitic schists of the Gile Mountain Formation suggest mineral reactions that produced kyanite occurred at 353 ± 9 Ma (Wing and others, 2003). The study focused on large fresh roadcuts at locations 21-21, 21-32, and 21-35 (fig. 1). Locations 21-21 and 21-32 are entirely composed of micaceous carbonate rock, mostly bedded on a scale of ≈1 to 10 cm, and quartz veins; location 21-35 is composed of ≈21 percent carbonate rock, ≈75 percent pelitic schist, and ≈4 percent quartz veins

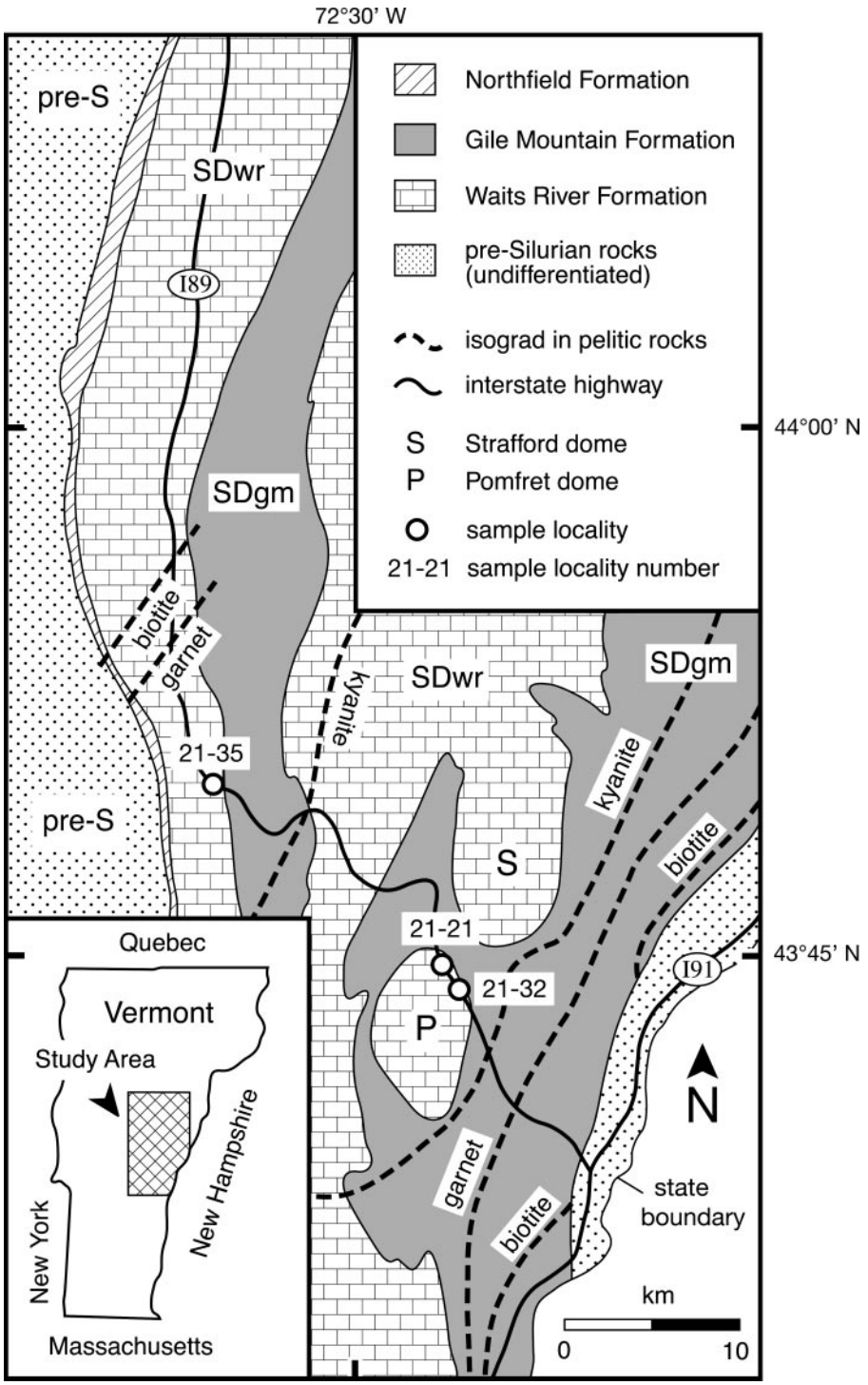

Fig. 1. Geologic sketch map of the study area in east-central Vermont (after Lyons, 1955; Doll and others, 1961; Ferry, 1994). Isograds are labeled on high-grade side. Sample location numbers are the same as in Ferry (1994). SDwr = Siluro-Devonian Waits River Formation; SDgm = Siluro-Devonian Gile Mountain Formation; pre-S = pre-Silurian units, undifferentiated.

(Ferry, 1994). Mineral equilibria in the area record P ≈ 7-8 kbar (Barnett and Chamberlain, 1991; Ferry, 1992, 1994; Menard and Spear, 1993, 1994); for purposes of calculations in this paper a value of P = 7.8 kbar was adopted. Locations 21-21 and 21-32 lie in the kyanite zone where mineral equilibria record T ≈ 550°C (Ferry, 1994). Mineral equilibria at location 21-35 in the garnet zone record T ≈ 500°C.

South-central Maine

The location and geologic setting of the outcrop investigated are illustrated in figure 2. Basic geologic relations in the area have been established by Osberg (1968, 1979, 1988) and Tucker and others (2001). The study focused on the limestone member of the Silurian Waterville Formation, a metamorphosed turbidite that is composed almost entirely of micaceous carbonate rock, usually bedded on a scale ≈1

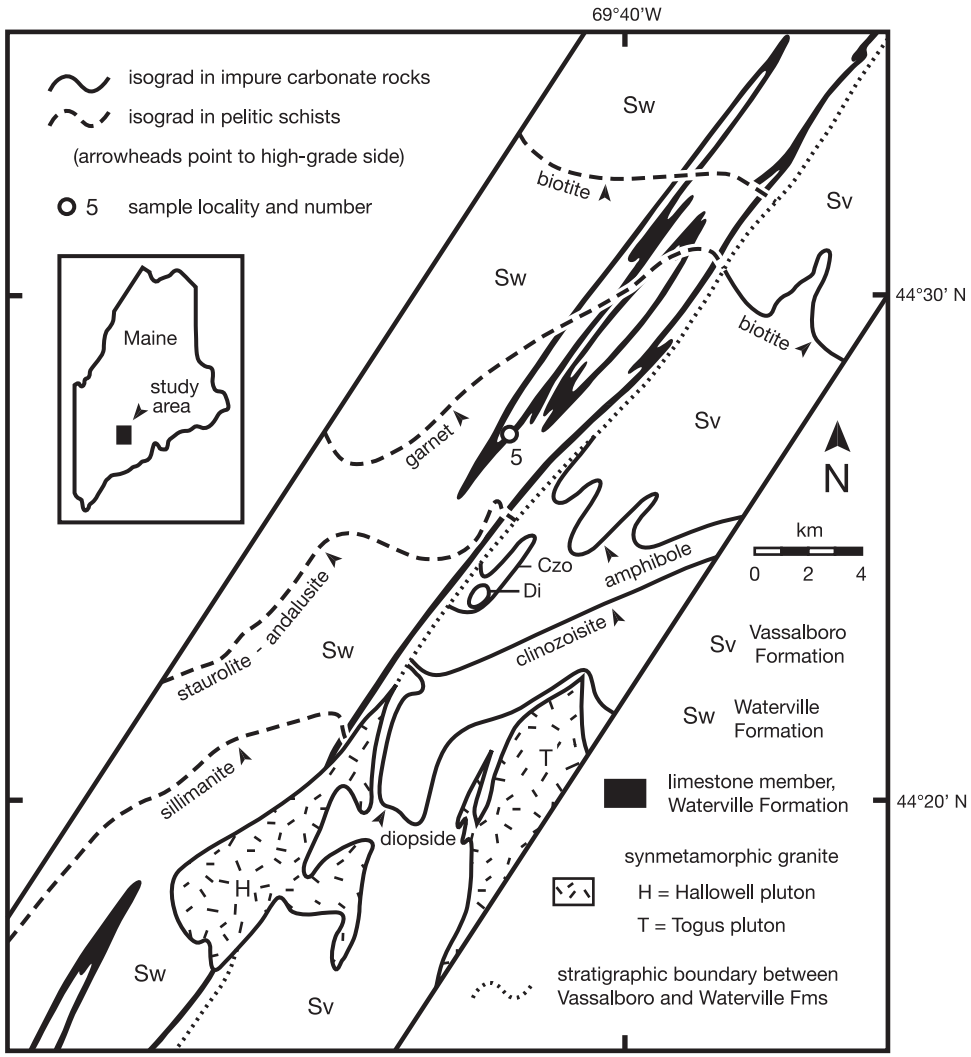

Fig. 2. Geologic sketch map of the study area in south-central Maine (after Osberg, 1968, 1979, 1988 and Ferry, 1976; 1980a,b; 1984; 1987; 1988b). Sample location 5 is the same as in Ferry (1994) and earlier publications.

to 50 cm. The Waterville Formation was deformed (Osberg, 1988), intruded by 378 ± 1 to 381 ± 1 Ma granites (Tucker and others, 2001), and regionally metamorphosed during the Devonian Acadian orogeny (Osberg, 1968, 1979, 1988). Radiometric ages of monazite neoblasts in pelitic schists of the normal Waterville Formation indicate mineral reactions that produced andalusite occurred at 364.3 ± 3.5 Ma (Wing and others, 2003). The study focused on a large working quarry at location 5 (fig. 2). Rare thin pelite layers constitute $<<1$ percent of the exposure. Mineral equilibria record $P \approx 3.5$ kbar in the area of figure 2 and $T \approx 450°C$ specifically at location 5. Rocks from location 5 have been the subject of numerous studies of fluid-rock interaction during regional metamorphism (Ferry, 1979, 1987, 1988b, 1994; Bickle and others, 1997; Evans and Bickle, 2005).

METHODS OF INVESTIGATION

Lithologic layering occurs at a variety of scales in micaceous carbonate rocks from both Vermont and Maine (for example, fig. 3), defined by differences in the amounts of calcite (Cal), quartz (Qtz), plagioclase (Pl), and micas. (These and all other abbreviations for minerals follow Kretz, 1983.) Samples were therefore collected along traverses across layering at a corresponding range of scales to investigate the distances over which variations in ξ and uniformity of proxies for fluid composition occurred during metamorphism. In Vermont, at the smallest scale, 9- and 16-cm traverses were examined from single large hand specimens obtained at locations 21-21 and 21-32, respectively (designated samples 9cm-a1 to 9cm-g and 16cm-a to 16cm-i in tables, figures, and text). In addition, 15 samples were collected along a 5-m-long traverse,

Fig. 3. Lithologic layering in metamorphosed micaceous carbonate rocks, location 21-32, Vermont (fig. 1). Layering occurs on a range of scales between several mm and several dm (notebook is ≈20 cm long). The 16-cm and 5-m sample traverses were obtained within and near the field of view.

and 24 samples were collected along a 35-m-long traverse at location 21-32 (designated samples 5m-1 to 5m-15 and 35m-1a to 35m-22). Finally, 12 samples were collected across each of two different carbonate beds at location 21-35 beginning and ending at their contacts with surrounding pelitic schist (designated samples 21-35-A to 21-35-L and 21-35-1 to 21-35-12). Sample positions along all but the longest traverse were measured with compass and steel measuring tape; positions along the longest traverse were measured to an accuracy of ±5 cm or better in three dimensions with a tripod-mounted laser rangefinder and digital fluxgate compass. All reported positions and spatial coordinates along each traverse were calculated by projecting actual sample positions to a line perpendicular to layering. Layering strikes 305° and dips 35°NE at location 21-21; 335° and 45°NE at location 21-32; 0° and 75°W along traverse A-L, location 21-35; and 5°, 40°W along traverse 1-12, location 21-35.

Samples from Maine are from collections made for earlier investigations (Ferry, 1979, 1987, 1994). At the largest scale, new data were obtained for 23 samples from a 100-m-long traverse oriented perpendicular to layering beginning at the contact between the normal and limestone members of the Waterville Formation (samples designated with a "T" or "TP" prefix in tables, figures, and text). Layering strikes ≈35° and is approximately vertical along the traverse except in rare hinges of isoclinal folds. At the smallest scale, pairs of adjacent cm-thick layers from the same thin section were examined from 7 samples along the 100-m traverse (designated samples TP-6, -8, -17, -29, -47, -72, -89) and from a large hand specimen from another part of the quarry (designated sample BB1). At an intermediate scale, 14 samples (designated F-A3 to F-A9 and F-B1 to F-B7) were examined from two different adjacent lithologic layers evenly-spaced over ≈1 m^2 in the hinge of an isoclinal fold (fig. 4). Finally, new data were obtained for 6 samples (designated FT-A to FT-F) along a 12-cm traverse across the contact between the two lithologic layers exposed in the hinge of the fold (fig. 4).

Mineral assemblages were determined in thin section with optical petrography and back-scattered electron (BSE) imaging using the JEOL JXA-8600 electron microprobe at Johns Hopkins University. Almost all mineral compositions were measured using wavelength-dispersive X-ray spectrometry with natural and synthetic mineral standards and a ZAF correction scheme (Armstrong, 1988) at Johns Hopkins University; mineral compositions in a few samples were measured with the Cameca SX50 electron microprobe at the Natural History Museum, London. For most thin sections, single spot analyses of ≈10 widely-spaced grains of Cal, biotite (Bt), muscovite (Ms), ankerite (Ank), and chlorite (Chl) were obtained, and the average composition is reported. Fewer analyses were collected in rare cases when a mineral occurred in very small abundance. For determination of average Pl composition in samples from Vermont, 12 to 42 spot analyses arranged on a square or rectangular grid were obtained from the Pl grain at or nearest each grid point. The composition of the most calcic Pl in each sample was obtained by additionally searching for the Pl grain with the brightest BSE image. For samples from Maine, the core and rim of the largest Pl grain in the field of view of the microprobe at ≈100x were analyzed in 10 areas evenly spaced along a traverse across a thin section or layer. Average Pl composition was estimated by averaging all 20 analyses, and the most calcic Pl in the sample was taken as the most calcic of the 20 analyses.

Mineral modes were measured for each sample by counting ≥2000 points in thin section using BSE imaging with the electron microprobe. Any question of mineral identification was resolved by obtaining an energy-dispersive X-ray spectrum. Uncertainties in modal analyses were estimated following Chayes (1956). Mineral modes were converted to moles per liter using mineral compositions and molar volumes of mineral components (Holland and Powell, 1998).

The O- and C-isotope compositions of bulk carbonate were measured in almost all samples from both Vermont and Maine. For samples along the 9- and 16-cm traverses

	layer A, lower ξ	layer B, higher ξ
ξ_2	0-0.10 mol/L	0.66-1.06 mol/L
$ln K_s(6)$	-1.292±0.088 (MSWD = 2.50, N = 6)	-0.921±0.053 (MSWD = 2.03, N = 7)
$\delta^{18}O_{Cal}$	19.39±0.10‰ (MSWD = 0.55, N=7)	19.92±0.10‰ (MSWD = 1.38, N = 7)
$\delta^{13}C_{Cal}$	-0.46±0.10‰ (MSWD = 0.18, N=7)	-0.35±0.10‰ (MSWD = 0.51, N=7)

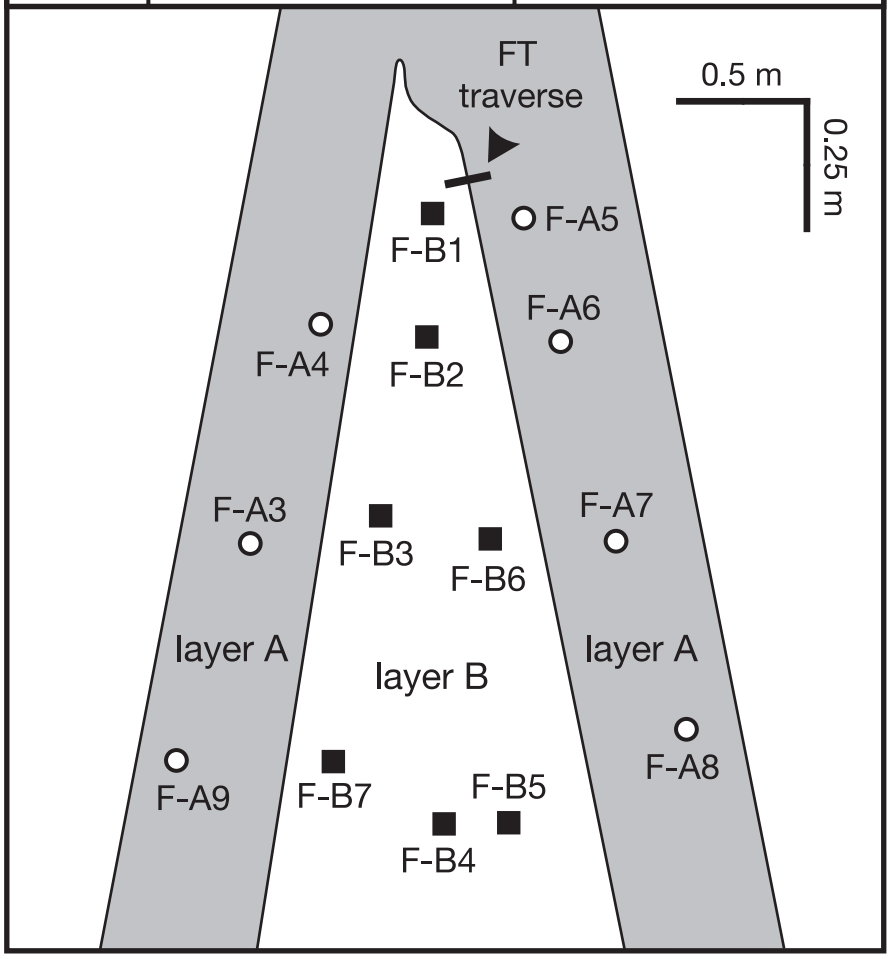

Fig. 4. Sketch of hinge area of isoclinal fold exposed on vertical quarry wall at location 5, Maine (fig. 2). Axis and axial plane of fold are perpendicular to plane of figure. Top of figure summarizes measurements of progress of reaction (2), $ln K_s(6)$, $\delta^{18}O_{Cal}$, and $\delta^{13}C_{Cal}$ for layers A and B based on data for the 14 samples whose locations are illustrated. Single values are weighted means; uncertainties are a 95% confidence interval based on the standard error. Bold line "FT traverse" denotes location of supplementary cm-scale sample traverse in figure 13. Figure and sample location numbers are the same as in figure 3 of Ferry (1994).

from Vermont and for the adjacent layer pairs from Maine, a powder was drilled from the center of each layer using a 2-mm-diameter diamond-tipped drill. For all other samples, a $\approx$4 cm^3 fragment was powdered for analysis with a tungsten carbide ball mill. Carbonate was dissolved from $\approx$2 to 10 mg of the powders in phosphoric acid for 1000 s at 90°C in the laboratory of A. J. Kaufman at the University of Maryland. Prior work in this laboratory demonstrated that a reaction time of 1000 s at 90°C is adequate for complete dissolution of calcite and ankerite. The released CO_2 was purified and analyzed for O- and C-isotope composition with a dual-inlet Micromass Isoprime mass spectrometer. Values of $\delta^{18}O$ and $\delta^{13}C$ are reported relative to VSMOW and VPDB respectively. The analytical precision could be evaluated for each analytical session because at least 10 measurements were made of one or two Cal working standards. In all cases for $\delta^{13}C$ and for most cases for $\delta^{18}O$, analytical precision was $\pm$0.1 permil (1σ). In a few sessions, however, the analytical precision for $\delta^{18}O$ was $\pm$0.1 to 0.2 permil (1σ). Duplicate analyses were made of all samples, and analyses were accepted only if they agreed within $\pm$2σ of the analytical precision. Samples containing less than $\approx$15 percent carbonate were not analyzed because they did not release sufficient CO_2. In most cases CO_2 was evolved from a mixture of Cal and Ank. The O-isotope acid fractionation factor, therefore, was computed from measured modes of Cal and Ank for each sample and equations for Cal-acid fractionation in Swart and others (1991) and Dol-acid fractionation in Rosenbaum and Sheppard (1986).

Thermodynamic calculations used the Berman (1988, updated June, 1992) database, the Kerrick and Jacobs (1981) equation of state for CO_2-H_2O fluids, metamorphic P-T conditions recorded by mineral equilibria, and activity-composition relations for minerals specified below.

MINERALOGY AND MINERAL CHEMISTRY

Modes and mineral compositions for representative samples of metamorphosed carbonate rock from Vermont and Maine are listed in tables 1 and 2. Modes and mineral compositions for all analyzed samples from Vermont are tabulated in Penniston-Dorland (ms, 2004). Most samples from both regions contain the same mineral assemblage: Cal, Ank, Ms, Bt, Chl, Pl, and Qtz with various combinations of accessory rutile (Rt), titanite, ilmenite, apatite, graphite, allanite, pyrrhotite, tourmaline, zircon, and garnet. Paragonite occurs additionally in one sample and sphalerite in another. Although all samples contain Cal, Pl, and Qtz, some samples may lack Ms, Ank, Bt, or Chl depending on whether prograde Bt- and Chl-forming reactions either did not occur (no Bt and/or Chl) or went to completion (no Ms and/or Ank). Modes in table 1 document that lithologic layering observed in the field (fig. 3) expresses layer-by-layer variations in carbonate, micas, Qtz, and Pl. Accessory garnet, titanite, ilmenite, paragonite, and sphalerite are restricted to samples from Vermont.

Biotite, Ms, Chl, Ank, and Cal are approximately Fe-Mg solid solutions with compositions (table 2) that deviate little from the average formulas in table 3. Furthermore, average formulas for each mineral for Vermont and Maine are almost the same. The range of measured Fe/(Fe+Mg) of Bt is between 0.14 and 0.45 in Vermont and between 0.23 and 0.43 in Maine; corresponding pairs of ranges are 0.11 to 0.39 and 0.20 to 0.41 for Ms, 0.12 to 0.39 and 0.21 to 0.37 for Chl, 0.04 to 0.26 and 0.11 to 0.25 for Ank, and 0.10 to 0.42 and 0.23 to 0.42 for Cal (table 3). The partitioning of Fe and Mg among Bt, Ms, Chl, Ank, and Cal is systematic (table 3). Average Fe-Mg exchange coefficients for mineral pairs from Vermont and Maine overlap at the $\pm$1σ level. Plagioclase in individual samples from both regions varies much more in composition than do Bt, Ms, Chl, Ank, and Cal. Variations in Pl composition result both from differences among individual grains in the same sample and from chemical zonation within grains. Chemical zonation is complicated and typically does not display a simple concentric pattern. In general, the rims of Pl are more calcic than cores, but the relationship in composition between rims and cores is

TABLE 1

Mineral assemblages and modes for selected samples of metacarbonate rock

A. East-central Vermont.

Sample*	16cm-a	16cm-c	16cm-g	16cm-i	5m-6	5m-8	5m-12	5m-14	35m-6	35m-7	35m-13a	35m-17
Muscovite	2.44	3.95	0.54	2.86	1.70	5.74	6.00	6.33	1.47	7.85	6.20	2.08
Biotite	3.62	14.44	4.98	8.10	8.18	0.35	5.78	2.30	tr	0	0.83	7.64
Chlorite	0.18	2.02	0.15	0.47	0.65	0.09	1.47	0.80	0.28	1.14	0.10	0.35
Ankerite	1.27	2.44	1.66	4.13	0.26	12.63	11.35	9.48	10.29	15.61	3.91	0.20
Calcite	66.05	50.44	50.61	50.89	1.52	35.45	33.79	41.23	39.09	32.84	36.98	0.60
Plagioclase	1.45	17.06	9.33	15.08	25.27	2.21	4.10	1.99	2.80	3.19	2.25	33.04
Quartz	24.86	8.46	32.44	17.60	60.90	43.05	36.56	37.07	45.87	38.70	49.34	53.92
Rutile	0	0.09	0.05	0.07	0.22	0.09	0.09	0.04	0.05	0.05	tr	0.25
Titanite	0	0	0	0	0.09	0	0.04	0	0	0	0	0.10
Apatite	0.14	0.51	0.15	0.67	0.39	0.13	0.39	0.22	tr	0.14	0.15	0.10
Allanite	0	0.37	0.05	0.13	0.30	0	tr	0.04	tr	0	0.05	0.25
Pyrrhotite	0	0.14	0.05	tr	0.48	0.22	0.17	0.35	0.14	0.33	0.10	1.39
Tourmaline	0	0.05	0	0	tr	0.04	0.26	0.09	0	0.14	0.10	0.10
Zircon	0	0.05	0	tr	0.04	0	tr	0	tr	0	tr	0

B. South-central Maine.

Sample*	TP-6a	TP-6b	TP-29b	TP-29c	T-52	T-57	T-66	T-78	TP-89b	TP-89c	F-A9	F-B7
Muscovite	2.49	1.55	3.07	3.78	2.38	4.32	1.42	4.71	4.03	2.69	4.48	6.93
Biotite	0	13.70	4.86	22.01	0	4.32	0.59	26.75	9.70	0.90	0.25	13.32
Chlorite	0.30	1.90	0.10	0.70	0	0.20	0.10	1.59	1.04	0.40	0.30	3.37
Ankerite	1.79	1.55	3.91	3.18	4.16	1.19	3.81	0.74	26.90	4.38	10.90	5.63
Calcite	81.99	61.20	68.63	46.15	77.83	77.90	71.23	43.87	32.07	72.79	57.71	52.96
Plagioclase	5.82	13.40	6.14	12.32	4.65	4.12	9.82	16.82	16.56	6.87	7.86	10.39
Quartz	7.41	5.90	13.08	11.67	10.69	7.45	12.41	3.77	9.00	11.59	17.96	6.40
Rutile	0.05	0.20	tr	0.05	0.05	tr	0.29	0.20	0.20	tr	0.10	0.19
Apatite	0.05	0.05	0.15	0.10	tr	0.05	0.05	0.05	0.25	0.15	0.10	0.10
Allanite	tr	tr	0	0	0	0.05	0	0.05	0	0	0	0
Pyrrhotite	0.10	0.45	0.05	0.05	0.25	0.40	0.24	1.39	0.10	0.25	0.20	0.72
Tourmaline	0	0.10	0	0	0	0	0	0.05	0.15	0	0.10	0
Zircon	0	0	0	0	0	0	0.05	0	tr	0	0.05	0

Values in volume percent; tr, <0.05%.

*Prefix for Vermont samples denotes sample traverse within location 21-32 (16-cm, 5-m, 35-m traverses). Suffix denotes sample along traverse. Prefix for Maine samples denotes adjacent layer pairs from 100-m traverse (TP), other samples from the 100-m traverse (T), or samples from the fold (F). Numerical suffixes for samples from 100-m traverse indicate distance in m along traverse to the SW from 0 at the contact between metacarbonate rock and pelitic schist; alphabetical suffixes, a and b or b and c, refer to the different members of adjacent pairs of layers from the same thin section. Suffix for samples from the fold indicate the layer and sample number (see fig. 4).

not universal. Accordingly, both average and maximum mole fraction of the $CaAl_2Si_2O_8$ component (X_{an}) are reported in table 2. The range in average and maximum X_{an} among all analyzed samples from Vermont is 0.10 to 0.82 and 0.19 to 0.92, respectively. The corresponding ranges for all analyzed Pl from Maine are nearly the same, 0.09 to 0.84 and 0.18 to 0.90.

STABLE ISOTOPE GEOCHEMISTRY

The O- and C-isotope compositions of bulk carbonate for all analyzed samples from Vermont and Maine are listed in table 4. Measured $\delta^{18}O_{carbonate}$ and $\delta^{13}C_{carbonate}$ fall within the fairly restricted ranges of 18.2 to 19.7 permil (VSMOW) and −1.4 to +0.5 permil (VPDB), respectively, for samples from locations 21-21 and 21-32 in Vermont. Values of $\delta^{18}O_{carbonate}$ are even more uniform for samples from location 21-35 (17.9 − 18.6‰); values of $\delta^{13}C_{carbonate}$ (−3.5 to −1.1‰), however, are generally lower and more variable. Measured $\delta^{18}O_{carbonate}$ and $\delta^{13}C_{carbonate}$ in table 4 fall within the range of values reported in other studies of the O- and C-isotope composition of carbonates from the Waits River Formation (Barnett and Chamberlain, 1991; Stern and others, 1992; Vyhnal and Chamberlain, 1996; Evans

TABLE 2

Compositions of minerals in selected samples of metacarbonate rock

A. Muscovite.

East-central Vermont

Sample*	16cm-a	16cm-c	16cm-g	16cm-i	5m-6	5m-8	5m-12	5m-14	35m-6	35m-7	35m-13a	35m-17
K	0.927	0.887	0.896	0.911	0.890	0.927	0.904	0.906	0.919	0.937	0.888	0.893
Na	0.060	0.064	0.064	0.067	0.068	0.052	0.057	0.060	0.066	0.053	0.081	0.076
Fe	0.078	0.079	0.070	0.086	0.082	0.040	0.036	0.042	0.038	0.038	0.058	0.067
Mg	0.147	0.143	0.134	0.157	0.138	0.182	0.187	0.200	0.190	0.193	0.143	0.117
Mn	0.000	0.001	0.001	0.000	0.000	0.001	0.000	0.001	0.001	0.000	0.001	0.000
Ti	0.048	0.064	0.057	0.049	0.053	0.050	0.030	0.034	0.042	0.069	0.038	0.058
Al^{VI}	1.746	1.730	1.751	1.737	1.742	1.758	1.774	1.752	1.748	1.706	1.792	1.769
Al^{IV}	0.880	0.845	0.859	0.887	0.840	0.901	0.855	0.847	0.858	0.851	0.901	0.878
Si	3.120	3.155	3.141	3.113	3.160	3.099	3.145	3.153	3.142	3.149	3.099	3.122
Oxide Sum	95.48	95.35	95.66	95.17	95.76	95.55	95.36	94.68	95.24	95.03	95.60	95.40

South-central Maine

Sample*	TP-6a	TP-6b	TP-29b	TP-29c	T-52	T-57	T-66	T-78	TP-89b	TP-89c	F-A9	F-B7
K	0.909	0.904	0.912	0.909	0.906	0.922	0.914	0.918	0.922	0.907	0.940	0.913
Na	0.061	0.054	0.061	0.062	0.057	0.047	0.060	0.051	0.052	0.053	0.042	0.051
Fe	0.052	0.047	0.060	0.063	0.049	0.052	0.081	0.049	0.056	0.056	0.051	0.050
Mg	0.159	0.147	0.112	0.112	0.158	0.157	0.149	0.158	0.150	0.154	0.166	0.146
Mn	0.000	0.000	0.000	0.000	0.000	0.000	0.000	0.000	0.000	0.000	0.000	0.000
Ti	0.022	0.025	0.029	0.027	0.023	0.037	0.025	0.038	0.031	0.028	0.030	0.032
Al^{VI}	1.798	1.807	1.815	1.821	1.793	1.776	1.773	1.767	1.781	1.784	1.777	1.793
Al^{IV}	0.873	0.866	0.878	0.893	0.848	0.862	0.853	0.835	0.852	0.849	0.874	0.877
Si	3.127	3.135	3.122	3.107	3.152	3.138	3.147	3.165	3.148	3.151	3.126	3.123
Oxide Sum	95.45	95.39	95.08	95.46	95.44	95.78	95.04	95.28	94.98	95.88	96.11	95.45

B. Biotite.

East-central Vermont

Sample*	16cm-a	16cm-c	16cm-g	16cm-i	5m-6	5m-8	5m-12	5m-14	35m-6	35m-13a	35m-17
K	0.892	0.893	0.871	0.883	0.932	0.874	0.878	0.883	0.896	0.831	0.906
Na	0.014	0.011	0.014	0.017	0.019	0.012	0.012	0.012	0.010	0.010	0.014
Fe	0.999	0.962	0.876	0.955	0.972	0.551	0.397	0.492	0.448	0.878	0.914
Mg	1.474	1.403	1.479	1.489	1.387	1.909	2.047	2.003	2.008	1.499	1.397
Mn	0.003	0.004	0.002	0.002	0.004	0.000	0.001	0.001	0.001	0.001	0.006
Ti	0.116	0.105	0.112	0.114	0.123	0.082	0.062	0.059	0.060	0.105	0.132
Al^{VI}	0.303	0.387	0.386	0.321	0.352	0.348	0.373	0.350	0.361	0.397	0.387
Al^{IV}	1.252	1.232	1.217	1.225	1.225	1.183	1.155	1.188	1.200	1.221	1.247
Si	2.748	2.768	2.783	2.775	2.775	2.817	2.845	2.812	2.800	2.779	2.753
Oxide Sum	96.56	95.66	95.96	96.52	95.44	95.92	95.75	95.54	95.66	95.62	95.95

South-central Maine

Sample*	TP-6b	TP-29b	TP-29c	T-57	T-66	T-78	TP-89b	TP-89c	F-A9	F-B7
K	0.885	0.888	0.906	0.870	0.860	0.891	0.887	0.892	0.898	0.904
Na	0.012	0.010	0.009	0.012	0.004	0.013	0.011	0.008	0.009	0.006
Fe	0.585	0.966	0.930	0.631	0.887	0.588	0.680	0.697	0.624	0.597
Mg	1.844	1.398	1.453	1.778	1.378	1.820	1.734	1.674	1.811	1.821
Mn	0.000	0.001	0.002	0.002	0.002	0.003	0.002	0.002	0.000	0.000
Ti	0.062	0.090	0.085	0.078	0.089	0.078	0.072	0.068	0.076	0.081
Al^{VI}	0.382	0.412	0.402	0.372	0.470	0.366	0.366	0.407	0.355	0.357
Al^{IV}	1.152	1.222	1.234	1.132	1.162	1.137	1.120	1.141	1.161	1.158
Si	2.848	2.779	2.766	2.868	2.838	2.863	2.880	2.859	2.839	3.842
Oxide Sum	95.34	95.78	96.08	95.95	95.38	95.90	95.59	95.25	95.39	95.31

TABLE 2

(continued)

C. Chlorite.

East-central Vermont

Sample*	16cm-a	16cm-c	16cm-g	16cm-i	5m-6	5m-8	5m-12	5m-14	35m-6	35m-7	35m-13a	35m-17
Fe	1.646	1.668	1.489	1.608	1.650	0.956	0.667	0.831	0.833	0.849	1.495	1.579
Mg	2.666	2.923	3.061	3.060	2.943	3.588	3.918	3.834	3.731	3.704	3.053	2.968
Mn	0.007	0.008	0.006	0.006	0.011	0.000	0.002	0.001	0.002	0.001	0.003	0.012
Ti	0.007	0.008	0.006	0.010	0.010	0.004	0.003	0.002	0.009	0.003	0.005	0.011
Al	2.618	2.701	2.698	2.600	2.614	2.670	2.540	2.521	2.642	2.696	2.710	2.695
Si	2.832	2.663	2.683	2.690	2.724	2.711	2.793	2.767	2.721	2.696	2.682	2.685
Oxide Sum	88.63	88.13	88.57	88.72	87.34	87.58	87.28	87.23	87.64	87.83	88.15	88.11

South-central Maine

Sample*	TP-6a	TP-6b	TP-29b	TP-29c	T-57	T-66	T-78	TP-89b	TP-89c	F-A9	F-B7
Fe	1.102	0.999	1.679	1.603	1.073	1.630	1.018	1.210	1.231	1.087	1.034
Mg	3.469	3.588	2.847	2.937	3.477	2.878	3.537	3.366	3.339	3.532	3.528
Mn	0.001	0.000	0.005	0.005	0.006	0.005	0.007	0.005	0.006	0.000	0.000
Ti	0.002	0.003	0.004	0.004	0.002	0.003	0.002	0.003	0.002	0.007	0.006
Al	2.650	2.611	2.734	2.721	2.614	2.697	2.606	2.613	2.618	2.609	2.649
Si	2.725	2.746	2.680	2.684	2.760	2.717	2.762	2.746	2.746	2.725	2.721
Oxide Sum	87.57	87.56	87.61	87.66	87.53	88.06	87.61	87.72	87.51	87.62	87.09

D. Ankerite.

East-central Vermont

Sample*	16cm-a	16cm-c	16cm-g	16cm-i	5m-6	5m-8	5m-12	5m-14	35m-6	35m-7	35m-13a	35m-17
Ca	1.046	1.018	1.016	1.003	1.014	1.008	1.012	1.013	1.013	1.010	1.032	0.989
Mg	0.768	0.736	0.758	0.768	0.721	0.905	0.904	0.897	0.898	0.897	0.783	0.724
Fe	0.173	0.226	0.198	0.203	0.229	0.083	0.078	0.085	0.083	0.089	0.177	0.215
Mn	0.013	0.020	0.027	0.026	0.036	0.003	0.005	0.005	0.005	0.005	0.008	0.072
Oxide Sum	53.88	54.81	54.48	54.76	53.92	52.11	52.99	52.29	52.21	52.61	54.05	55.46

South-central Maine

Sample*	TP-6a	TP-6b	TP-29b	TP-29c	T-52	T-57	T-66	T-78	TP-89b	TP-89c	F-A9	F-B7
Ca	1.016	1.015	1.033	1.029	1.018	1.022	1.017	1.022	1.009	1.012	1.008	1.014
Mg	0.834	0.851	0.713	0.726	0.841	0.816	0.769	0.819	0.838	0.817	0.858	0.859
Fe	0.142	0.126	0.233	0.221	0.135	0.141	0.189	0.132	0.133	0.151	0.131	0.124
Mn	0.007	0.008	0.021	0.023	0.007	0.022	0.025	0.027	0.020	0.021	0.003	0.003
Oxide Sum	53.39	53.38	54.53	54.35	52.63	52.74	53.26	53.86	53.47	53.79	52.93	52.96

E. Calcite.

East-central Vermont

Sample*	16cm-a	16cm-c	16cm-g	16cm-i	5m-6	5m-8	5m-12	5m-14	35m-6	35m-7	35m-13a	35m-17
Ca	0.937	0.931	0.914	0.924	0.924	0.940	0.948	0.942	0.945	0.957	0.934	0.911
Mg	0.040	0.038	0.050	0.048	0.038	0.046	0.041	0.046	0.042	0.033	0.043	0.040
Fe	0.018	0.023	0.026	0.023	0.026	0.012	0.009	0.010	0.011	0.009	0.020	0.026
Mn	0.004	0.007	0.010	0.005	0.012	0.002	0.002	0.002	0.002	0.002	0.003	0.023
Oxide Sum	55.35	55.70	56.16	55.86	55.42	55.39	55.60	55.59	55.94	55.85	55.79	56.35

South-central Maine

Sample*	TP-6a	TP-6b	TP-29b	TP-29c	T-52	T-57	T-66	T-78	TP-89b	TP-89c	F-A9	F-B7
Ca	0.951	0.952	0.938	0.939	0.949	0.945	0.931	0.944	0.942	0.944	0.959	0.953
Mg	0.034	0.033	0.034	0.032	0.037	0.035	0.040	0.035	0.036	0.035	0.028	0.034
Fe	0.012	0.011	0.021	0.021	0.011	0.012	0.021	0.012	0.015	0.014	0.012	0.012
Mn	0.003	0.003	0.008	0.008	0.003	0.008	0.009	0.010	0.008	0.008	0.001	0.001
Oxide Sum	56.06	55.87	55.98	55.79	55.88	56.23	56.19	56.15	56.29	56.34	55.66	55.87

TABLE 2

(continued)

F. Plagioclase.

East-central Vermont

Sample*	16cm-a	16cm-c	16cm-g	16cm-i	5m-6	5m-8	5m-12	5m-14	35m-6	35m-7	35m-13a	35m-17
Average X_{an}	0.320	0.312	0.324	0.320	0.317	0.104	0.238	0.283	0.175	0.112	0.312	0.283
Average X_{ab}	0.676	0.685	0.674	0.677	0.680	0.893	0.758	0.713	0.825	0.887	0.685	0.714
Average X_{or}	0.003	0.003	0.003	0.003	0.003	0.003	0.004	0.004	0.001	0.001	0.003	0.003
Oxide Sum	99.74	99.73	99.68	99.90	99.99	99.66	100.18	99.91	99.64	99.73	99.42	100.62
Max X_{an}	0.37	0.38	0.39	0.40	0.41	0.37	0.49	0.48	0.41	0.19	0.48	0.37

South-central Maine

Sample*	TP-6a	TP-6b	TP-29b	TP-29c	T-52	T-57	T-66	T-78	TP-89b	TP-89c	F-A9	F-B7
Average X_{an}	0.375	0.435	0.540	0.516	0.363	0.521	0.294	0.516	0.325	0.329	0.202	0.380
Average X_{ab}	0.622	0.561	0.557	0.479	0.635	0.477	0.703	0.480	0.671	0.668	0.795	0.615
Average X_{or}	0.003	0.004	0.003	0.005	0.002	0.002	0.003	0.004	0.004	0.003	0.003	0.005
Oxide Sum	99.81	99.85	99.93	100.01	99.67	100.06	99.94	100.07	100.34	100.27	99.70	100.06
Max X_{an}	0.45	0.68	0.72	0.67	0.52	0.84	0.32	0.75	0.39	0.41	0.30	0.58

Micas: cations per 11 oxygen atoms (less H_2O). Chlorite: cations per 14 oxygen atoms (less H_2O). Ankerite: cations per 2 oxygen atoms (less CO_2). Calcite: cations per oxygen atom (less CO_2). Plagioclase: mole fraction anorthite (an), albite (ab), and orthoclase (or) components. "Oxide Sum" refers to sum of metal oxides (less H_2O and CO_2). Both structural formulas and "Oxide Sum" consider all Fe as FeO.

*Sample notation as in footnote to table 1.

and others, 2002). Values of $\delta^{18}O_{carbonate}$ and $\delta^{13}C_{carbonate}$ can be less than those in table 4 near the contact between the Waits River and Gile Mountain Formations and where the Waits River Formation is intruded by Acadian granites. Other values of $\delta^{18}O_{carbonate}$ and $\delta^{13}C_{carbonate}$ are greater than those in table 4 in parts of Vermont outside the area in figure 1 where the Waits River Formation occurs at lower grades of metamorphism.

Measured $\delta^{18}O_{carbonate}$ and $\delta^{13}C_{carbonate}$ for samples from location 5 in Maine fall in the range 17.3 to 20.4 permil and −4.0 to 0.0 permil, respectively, and are slightly more variable than those from the three locations in Vermont. Values of $\delta^{18}O_{carbonate}$ and $\delta^{13}C_{carbonate}$ in table 4 fall within the range reported by Bickle and others (1997) for the limestone member of the Waterville Formation both at location 5 and at lower grades.

PROGRADE MINERAL REACTIONS, MEASUREMENT OF REACTION PROGRESS, AND INITIAL MINERALOGY AND MINERAL COMPOSITIONS

Micaceous carbonate rocks from locations 21-21 and 21-32 in Vermont and location 5 in Maine differ from equivalent rocks at lower grades primarily in the occurrence of Bt, Chl, and intermediate to calcic Pl. The equivalents at an immediately lower grade of metamorphism lack Bt, contain no or only trace Chl, and contain more sodic Pl (Ferry, 1987, 1992, 1994). The mineralogical differences are explained by prograde net-transfer reactions that were formulated following Thompson (1982). Carbonate rocks from both the Waits River and limestone member of the Waterville Formations are considered to have bulk chemistry described by 12 system components (SiO_2, TiO_2, Al_2O_3, MgO, FeO, CaO, Na_2O, K_2O, P_2O_5, CO_2, H_2O, S_2). Biotite, Ms, Chl, Ank, and Cal are considered Fe-Mg solid solutions with each represented by two phase components; Pl is represented by two phase components (ab, $NaAlSi_3O_8$, and an, $CaAl_2Si_2O_8$); Qtz, Rt, pyrrhotite, and apatite are considered pure substances; and fluid is taken as a CO_2-H_2O solution. Accessory minerals that occur in abundances <1 modal percent (allanite, titanite, garnet, ilmenite, zircon, tourmaline, paragonite, sphalerite) are not significant participants in the prograde reactions and are ignored. There are then 18 phase components and 18 − 12 = 6 linearly independent reaction relationships that can be written among the phase components. Four of the six are

TABLE 3

Average mineral formulas and Fe-Mg exchange coefficients

	East-central Vermont		South-central Maine	
Mineral	Average formula*	Fe/(Fe+Mg)†	Average formula§	Fe/(Fe+Mg)‡
Calcite	$Ca_{0.93}(Mg,Fe)_{0.07}CO_3$	0.10-0.42	$Ca_{0.94}(Mg,Fe)_{0.06}CO_3$	0.23-0.42
Ankerite	$Ca_{1.02}(Mg,Fe)_{0.98}(CO_3)_2$	0.04-0.26	$Ca_{1.02}(Mg,Fe)_{0.98}(CO_3)_2$	0.11-0.25
Muscovite	$K_{0.90}Na_{0.07}(Mg,Fe)_{0.22}Ti_{0.05}Al_{2.61}Si_{3.13}O_{10}(OH)_2$	0.11-0.39	$K_{0.91}Na_{0.05}(Mg,Fe)_{0.20}Ti_{0.03}Al_{2.65}Si_{3.14}O_{10}(OH)_2$	0.20-0.41
Biotite	$K_{0.89}(Mg,Fe)_{2.39}Ti_{0.12}Al_{1.59}Si_{2.77}O_{10}(OH)_2$	0.14-0.45	$K_{0.89}Na_{0.01}(Mg,Fe)_{2.38}Ti_{0.08}Al_{1.57}Si_{2.83}O_{10}(OH)_2$	0.23-0.43
Chlorite	$(Mg,Fe)_{4.60}Ti_{0.01}Al_{2.68}Si_{2.67}O_{10}(OH)_8$	0.12-0.39	$(Mg,Fe)_{4.56}Al_{2.65}Si_{2.73}O_{10}(OH)_8$	0.21-0.37

	East-central Vermont		South-central Maine	
K_D	Average Value*	1σ*	Average value§	1σ§
$K_{Bt/Ank} = [(Fe/Mg)_{Bt}/(Fe/Mg)_{Ank}]$	2.35	0.28	2.17	0.20
$K_{Cal/Ank} = [(Fe/Mg)_{Cal}/(Fe/Mg)_{Ank}]$	1.88	0.20	2.14	0.24
$K_{Ms/Ank} = [(Fe/Mg)_{Ms}/(Fe/Mg)_{Ank}]$	1.89	0.21	2.01	0.19
$K_{Chl/Ank} = [(Fe/Mg)_{Chl}/(Fe/Mg)_{Ank}]$	1.92	0.24	1.90	0.21

*Average formula, K_D, and standard deviation (σ) of K_D based on all analyzed samples along the 16-cm traverse, location 21-32.
†Range in Fe/(Fe+Mg) based on all analyzed samples from east-central Vermont.
§Average formula, K_D, and standard deviation (σ) of K_D based on all analyzed samples along the 100-m traverse, location 5.
‡Range in Fe/(Fe+Mg) based on all analyzed samples from south-central Maine.

TABLE 4

Oxygen and carbon isotope compositions of carbonate

A. East-central Vermont.

Sample*	$\delta^{18}O_{carb}$ (‰)	$\delta^{13}C_{carb}$ (‰)	$\delta^{18}O_{Cal}$ (‰)	$\delta^{13}C_{Cal}$ (‰)
9cm-a[†]	19.1	0.0	19.0	-0.2
9cm-c[†,§]	19.1, 19.1	-0.2, 0.0	19.1, 19.0	-0.3, -0.1
9cm-e	18.8	-0.3	18.7	-0.4
9cm-g[§]	18.7, 19.0	-0.8, -0.4	18.7, 19.0	-0.9, -0.5
16cm-a	19.0	-0.8	19.0	-0.8
16cm-c	19.3	-1.3	19.2	-1.3
16cm-e	19.0	-1.4	19.0	-1.4
16cm-g	19.3	-0.9	19.3	-0.9
16cm-i	19.3	-1.1	19.3	-1.1
5m-1	19.5	-1.0	19.5	-1.0
5m-5	19.1	-0.9	19.0	-1.0
5m-7	19.0	-0.6	19.0	-0.8
5m-8	19.2	+0.1	19.1	-0.2
5m-10	19.4	+0.1	19.3	-0.1
5m-11	19.4	-0.2	19.3	-0.4
5m-12	19.6	-0.2	19.5	-0.4
5m-13	19.6	-0.2	19.5	-0.3
5m-14	19.4	-0.3	19.4	-0.5
5m-15	19.7	-0.8	19.7	-0.9
35m-1a	18.6	+0.3	18.5	+0.1
35m-1	19.0	-0.2	18.9	-0.5
35m-2	19.3	-0.6	19.3	-0.7
35m-3	19.6	-0.2	19.6	-0.2
35m-4	19.1	-0.2	19.1	-0.3
35m-5	19.2	-0.3	19.1	-0.6
35m-6	19.1	+0.4	19.0	+0.2
35m-7	19.0	+0.5	18.9	+0.2
35m-7a	19.0	-0.4	19.0	-0.5
35m-7b	18.2	-0.6	18.2	-0.7
35m-8	18.8	-0.1	18.8	-0.2
35m-9	18.6	-0.7	18.6	-0.8
35m-10t	18.3	-0.7	18.3	-0.8
35m-10b	18.4	-0.7	18.4	-0.7
35m-10a	18.9	-0.5	18.9	-0.5
35m-11	18.8	-0.6	18.8	-0.6
35m-12	19.3	-0.5	19.2	-0.6
35m-13	19.1	-0.7	19.0	-0.9
35m-13a	19.1	-0.6	19.1	-0.7
35m-14	19.0	-0.6	19.0	-0.7
35m-15	19.1	-0.9	19.1	-1.0

TABLE 4

(continued)

A. East-central Vermont.

Sample*	distance (cm)‡	$\delta^{18}O_{carb}$ (‰)	$\delta^{13}C_{carb}$ (‰)	$\delta^{18}O_{Cal}$ (‰)	$\delta^{13}C_{Cal}$ (‰)
21-35-1	2.0	18.5	-1.2	18.4	-1.3
21-35-2	8.7	18.4	-1.1	18.4	-1.2
21-35-3	16.1	18.4	-1.2	18.4	-1.3
21-35-4	25.5	18.4	-1.2	18.4	-1.3
21-35-5	36.7	18.3	-1.2	18.3	-1.3
21-35-6	50.6	18.4	-1.2	18.3	-1.3
21-35-7	64.6	18.3	-1.4	18.3	-1.5
21-35-8	75.8	18.3	-1.7	18.3	-1.8
21-35-9	84.7	18.3	-1.6	18.3	-1.7
21-35-10	92.6	18.4	-1.6	18.3	-1.8
21-35-11	100.2	18.4	-1.7	18.4	-1.9
21-35-12	106.4	18.4	-1.8	18.3	-1.9
21-35-A	46.3	18.1	-1.8	18.0	-1.9
21-35-B	43.0	18.4	-1.5	18.4	-1.6
21-35-C	39.0	18.0	-1.7	18.0	-1.8
21-35-D	34.4	18.1	-1.4	18.1	-1.5
21-35-E	30.7	18.1	-1.6	18.0	-1.7
21-35-F	24.9	18.3	-1.6	18.2	-1.7
21-35-G	19.0	18.3	-1.6	18.2	-1.8
21-35-H	13.5	17.9	-1.8	17.9	-1.9
21-35-I	13.8	18.2	-1.9	18.2	-2.0
21-35-J	9.2	18.1	-3.2	18.0	-3.4
21-35-K	5.8	18.6	-3.4	18.5	-3.6
21-35-L	1.5	18.3	-3.5	18.2	-3.7

Values of $\delta^{18}O_{carb}$ and $\delta^{13}C_{carb}$ are measured for bulk Cal + Ank in each sample; values of $\delta^{18}C_{Cal}$ and $\delta^{13}C_{Cal}$ are estimated values for Cal computed from measured $\delta^{18}O_{carb}$ and $\delta^{13}C_{carb}$, measured modes, and the Dol-Cal O- and C-isotope fractionation factors at the T of metamorphism from Sheppard and Schwarcz (1970). Values of $\delta^{18}O$ relative to VSMOW; values of $\delta^{13}C$ relative to VPDB. 2σ uncertainty in $\delta^{13}C$ is ±0.2‰ for all analyses except for samples FT-A1 to FT-F; 2σ uncertainity in $\delta^{18}O$ is ±0.2‰ for all analyses except for samples 9cm-e, 35m-1, 21-35-A, 21-35-B, 21-35-D to 21-35-F, 21-35-I, and 21-35-L (±0.3‰), samples 21-35-1 to 21-35-10, and 21-35-K (±0.4‰) and samples FT-A1 to FT-F. The $\delta^{18}O$ and $\delta^{13}C$ reported for samples FT-A1 to FT-F are the weighted mean of 5-8 analyses of the same specimen that are statistically consistent with a single value (MSWD = 0.4-1.4); "i" refers to groups of analyses not statistically consistent with a single value (MSWD = 2.9-7.8). The 95% confidence interval of the weighted mean values of $\delta^{18}O$, based on the standard error, is ±0.10‰ (FT-E), ±0.11‰ (FT-F), or ±0.16‰ (FT-A1, FT-B, FT-C); the 95% confidence interval of the weighted mean value of $\delta^{13}C$ of sample FT-C is ±0.14‰.

*9-cm traverse is from sample location 21-21 (fig. 1). Samples with the "21-35" prefix are from traverses across thick carbonate layers within pelitic schist at location 21-35 (fig. 1). Samples with "FT" prefix are from a 12-cm-long traverse across folded layers A and B (figs. 4, 13). Samples T-82A and T-82B are located <1 m apart along the 100-m traverse but are not from the same hand specimen. Other sample notation as in footnote to table 1.

†Bulk measurement of layers a1 and a2 and of layers c1, c2, and c3.

§Pairs of values refer to analyses of 2 samples separated by ≈3 cm parallel to layering.

‡Measured from center of sample perpendicular to layer from its western contact with pelite.

TABLE 4

(continued)

B. South-central Maine.

Sample*	$\delta^{18}O_{carb}$ (‰)	$\delta^{13}C_{carb}$ (‰)	$\delta^{18}O_{Cal}$ (‰)	$\delta^{13}C_{Cal}$ (‰)
T-3	17.9	-2.4	17.9	-2.4
T-4	17.9	-0.7	17.8	-0.8
TP-6a	17.7	-1.2	17.7	-1.2
TP-6b	17.9	-2.0	17.9	-2.1
TP-8a	18.2	-4.0	18.2	-4.0
TP-8c	17.8	-3.5	17.8	-3.5
T-12A	19.0	-0.4	19.0	-0.4
TP-17a	19.5	0.0	19.4	-0.2
TP-17b	19.7	-0.2	19.6	-0.3
TP-23a	18.7	-0.3	18.7	-0.4
T-24	19.0	-0.2	19.0	-0.3
TP-29b	17.6	-2.8	17.6	-2.8
TP-29c	18.0	-3.1	17.9	-3.2
TP-47a	17.3	-2.6	17.2	-2.6
TP-47b	17.5	-3.1	17.5	-3.2
T-50	18.5	-0.7	18.4	-0.9
T-52	19.3	-0.2	19.3	-0.2
T-57	19.8	-0.5	19.8	-0.5
T-62	19.5	-0.5	19.5	-0.6
T-66	19.5	-0.6	19.5	-0.6
TP-72a	19.6	-0.6	19.6	-0.6
TP-72b	19.7	-0.7	19.7	-0.7
T-78	20.4	-0.4	20.4	-0.4
T-82A	19.9	-0.3	19.8	-0.5
T-82B	19.4	-0.2	19.3	-0.6
T-87	20.1	-0.5	20.1	-0.6
TP-89b	19.5	-0.4	19.2	-0.9
TP-89c	19.7	-0.5	19.6	-0.6
F-A3	19.4	-0.3	19.4	-0.4
F-A4	19.5	-0.3	19.4	-0.5
F-A5	19.3	-0.3	19.3	-0.5
F-A6	19.4	-0.2	19.3	-0.4
F-A7	19.6	-0.3	19.5	-0.4
F-A8	19.5	-0.3	19.4	-0.5
F-A9	19.5	-0.3	19.4	-0.5
F-B1	20.2	-0.4	20.1	-0.4
F-B2	19.9	-0.3	19.8	-0.4
F-B3	20.1	-0.2	20.1	-0.2
F-B4	19.9	-0.1	19.9	-0.3
F-B5	19.9	-0.2	19.9	-0.3
F-B6	19.9	-0.2	19.9	-0.3
F-B7	19.9	-0.3	19.8	-0.4
FT-A1	19.63	i	19.61	i
FT-B	19.42	i	19.34	i
FT-C	19.54	-0.15	19.45	-0.35
FT-E	19.90	i	19.88	i
FT-F	20.06	i	20.03	i

linearly-independent Fe-Mg exchange reactions among Bt, Ms, Ank, Chl, and Cal. The other two are net-transfer reactions that explain the development of Bt and Chl and the change in Pl composition. In schematic form, the two adopted are:

$$\text{Mg-ms} + \text{Mg-ank} + \text{qtz} + \text{rt} + H_2O = \text{Mg-bt} + \text{Mg-cal} + \text{an} + \text{ab} + CO_2 \qquad (2)$$

and

$$\text{Mg-ank} + \text{an} + \text{qtz} + \text{rt} + H_2O = \text{Mg-chl} + \text{Mg-cal} + CO_2, \qquad (3)$$

where Mg-ms, Mg-ank, Mg-bt, Mg-cal, and Mg-chl represent the Mg-components of the minerals, and qtz and rt represent the phase components SiO_2 and TiO_2. Formal consideration of MnO as a system component introduces four additional linearly-independent exchange reactions but no additional net-transfer reactions. Stoichiometric coefficients are omitted from reactions (2) and (3) because they depend in detail on the compositions of Ms, Ank, Bt, Cal, and Chl in each sample. Using average mineral compositions in sample 5m-12 from Vermont (table 2), examples of balanced reactions are:

$$\begin{aligned} 0.97\ &K_{0.90}Na_{0.06}Mg_{0.22}Ti_{0.03}Al_{2.63}Si_{3.15}O_{10}(OH)_2 + 2.36\ Ca_{1.01}Mg_{0.99}(CO_3)_2 \\ &+ 0.90\ SiO_2 + 0.03\ TiO_2 + 0.03\ H_2O \\ = 1.00\ &K_{0.88}Na_{0.01}Mg_{2.45}Ti_{0.06}Al_{1.53}Si_{2.85}O_{10}(OH)_2 + 2.00\ Ca_{0.95}Mg_{0.05}CO_3 \\ &+ 0.49\ CaAl_2Si_2O_8 + 0.04\ NaAlSi_3O_8 + 2.72\ CO_2 \end{aligned} \qquad (2a)$$

and

$$\begin{aligned} 4.96\ &Ca_{1.01}Mg_{0.99}(CO_3)_2 + 1.27\ CaAl_2Si_2O_8 + 0.25\ SiO_2 + 4\ H_2O \\ = &\ Mg_{4.59}Al_{2.54}Si_{2.79}O_{10}(OH)_8 + 6.60\ Ca_{0.95}Mg_{0.05}CO_3 + 3.32\ CO_2 \end{aligned} \qquad (3a)$$

Because the formulas of minerals are similar in analyzed samples from Vermont and Maine (tables 2 and 3), the stoichiometric coefficients of net-transfer reactions (2) and (3) are also similar.

Reactions (2) and (3), and the analysis upon which they are based, assume isochemical metamorphism in the petrologic sense. Isochemical metamorphism of the Waits River Formation and the Waterville limestone at the regional scale is indicated by the absence of any statistically significant difference in the average major-element composition of metacarbonate rocks in the different metamorphic zones, except in H_2O and CO_2 (Ferry, 1988b, 1992). Prograde changes in mineral assemblages, however, suggest that some K- and Na-metasomatism may have occurred at the outcrop or smaller scales. Possible effects of K-metasomatism were ignored in this study for two reasons. First, loss of K from metacarbonate rocks in both Vermont and Maine is associated petrographically with the prograde formation of calcic amphibole and diopside (Ferry, 1988b, 1992). None of the rocks considered in this study contain amphibole or diopside. Second, Evans and Bickle (2005) conclude that K-metasomatism of metacarbonate rocks at location 5 in Maine cannot explain the observed range in Bt modes. The conservative assumption of isochemical metamorphism is adopted because it leads to an adequate quantitative understanding of the variations in reaction progress observed in metacarbonate rocks from Vermont and Maine. Nevertheless, for completeness, the effect of possible Na-metasomatism at the cm- to dm-scale on the progress of reactions (2) and (3) is evaluated in a later section.

Progress of reactions (2) and (3), ξ_2 and ξ_3, were simply taken as the number of moles Bt and Chl per L rock, respectively (table 5); measured values then are with reference to 1 L rock after reaction. The determination of ξ_3 ignores the trace

Table 5

Measured reaction progress, $lnK_s(6)$, and calculated fluid composition

A. East-central Vermont.

Sample*	Dist†	ξ_2 (mol/L)§	ξ_3 (mol/L)§	$lnK_s(6)$‡	X_{CO_2}**
9cm-a1	0.1	0	0	<-0.641 (0.183)	>0.126 (+0.011/-0.010)
9cm-a2	0.4	0.32 (0.08)	0.01 (0.01)	-0.728 (0.134)	0.131 (+0.009/-0.008)
9cm-b	1.4	0.27 (0.03)	0.07 (0.01)	-0.755 (0.162)	0.133 (+0.011/-0.010)
9cm-c1	2.5	0.39 (0.08)	0.03 (0.02)	-0.699 (0.116)	0.130 (+0.007/-0.007)
9cm c2	2.7	0	0	<-0.524 (0.143)	>0.120 (+0.008/-0.007)
9cm-c3	3.0	0.38 (0.10)	0.04 (0.03)	-0.714 (0.121)	0.131 (+0.008/-0.007)
9cm-d	3.7	0.28 (0.04)	0.06 (0.02)	-0.665 (0.127)	0.128 (+0.008/-0.007)
9cm-e	5.2	0.24 (0.03)	0.03 (0.01)	-0.755 (0.110)	0.133 (+0.007/-0.007)
9cm-f	6.9	0.36 (0.06)	0.07 (0.02)	-0.785 (0.112)	0.135 (+0.008/-0.007)
9cm-g	8.1	0.36 (0.07)	0.02 (0.01)	-0.712 (0.153)	0.131 (+0.010/-0.009)
16cm-a	0.4	0.24 (0.05)	0.01 (0.01)	-1.406 (0.401)	0.185 (+0.046/-0.035)
16cm-b	3.0	0.43 (0.07)	0.05 (0.02)	-1.333 (0.185)	0.178 (+0.019/-0.016)
16cm-c	5.9	0.97 (0.10)	0.10 (0.03)	-1.340 (0.287)	0.179 (+0.030/-0.025)
16cm-d	7.0	0.72 (0.09)	0.03 (0.02)	-1.381 (0.205)	0.183 (+0.021/-0.018)
16cm-e	7.7	0.83 (0.10)	0.10 (0.03)	-1.316 (0.147)	0.176 (+0.014/-0.013)
16cm-f	8.4	0.55 (0.08)	0.03 (0.02)	-1.547 (0.333)	0.199 (+0.041/-0.032)
16cm-g	9.9	0.33 (0.06)	0.01 (0.01)	-1.344 (0.181)	0.179 (+0.018/-0.016)
16cm-h	13.3	0.83 (0.10)	0.03 (0.02)	-1.276 (0.305)	0.173 (+0.031/-0.025)
16cm-i	14.7	0.54 (0.07)	0.02 (0.01)	-1.294 (0.335)	0.174 (+0.034/-0.027)
5m-1	0.1	0.89 (0.10)	0.06 (0.02)	-1.389 (0.204)	0.183 (+0.021/-0.019)
5m-2	0.4	0.39 (0.07)	0.05 (0.02)	-1.407 (0.529)	0.185 (+0.063/-0.044)
5m-3	0.7	0.33 (0.06)	0.06 (0.02)	-1.658 (0.266)	0.212 (+0.034/-0.029)
5m-4	1.0	0.32 (0.06)	0.05 (0.02)	-1.665 (0.303)	0.213 (+0.040/-0.032)
5m-5	1.7	0.27 (0.05)	0	-1.210 (0.178)	0.167 (+0.016/-0.014)
5m-6	2.4	0.55 (0.08)	0.03 (0.02)	-1.231 (0.183)	0.169 (+0.017/-0.015)
5m-7	2.5	0.09 (0.03)	0.03 (0.02)	-1.419 (0.331)	0.186 (+0.037/-0.029)
5m-8	3.0	0.02 (0.02)	<0.01 (0.01)	-1.111 (0.142)	0.159 (+0.012/-0.011)
5m-9	3.4	0	0.04 (0.02)	<-0.873 (0.221)	>0.141 (+0.016/-0.014)
5m-10	3.5	0.02 (0.02)	0.01 (0.01)	-0.924 (0.119)	0.145 (+0.009/-0.008)
5m-11	3.7	0.27 (0.06)	0.06 (0.02)	-0.727 (0.154)	0.131 (+0.010/-0.009)
5m-12	3.8	0.39 (0.07)	0.07 (0.02)	-0.742 (0.152)	0.132 (+0.010/-0.009)
5m-13	3.9	0.22 (0.05)	0.06 (0.02)	-0.790 (0.166)	0.135 (+0.011/-0.010)
5m-14	4.0	0.16 (0.04)	0.04 (0.02)	-0.776 (0.164)	0.135 (+0.011/-0.010)
5m-15	4.7	0.26 (0.05)	<0.01 (<0.01)	-1.157 (0.285)	0.162 (+0.026/-0.022)
35m-1a	1.1	0.03 (0.03)	0.04 (0.02)	-1.029 (0.138)	0.152 (+0.011/-0.010)
35m-1	2.3	0.34 (0.04)	0.09 (0.03)	-0.741 (0.123)	0.132 (+0.008/-0.007)
35m-2	4.3	0.47 (0.08)	0.08 (0.03)	-0.795 (0.091)	0.136 (+0.006/-0.006)
35m-3	6.5	0.42 (0.07)	0.06 (0.02)	-0.835 (0.114)	0.138 (+0.008/-0.007)
35m-4	8.2	0.14 (0.04)	0.05 (0.02)	-0.833 (0.111)	0.138 (+0.008/-0.007)
35m-5	9.3	0.07 (0.03)	0.04 (0.02)	-0.892 (0.128)	0.142 (+0.009/-0.009)
35m-6	12.4	<0.01 (<0.01)	0.01 (0.01)	-0.802 (0.093)	0.136 (+0.006/-0.006)
35m-7	12.8	0	0.05 (0.02)	<-1.454 (0.221)	>0.190 (+0.024/-0.021)
35m-7a	13.8	0.03 (0.02)	0.01 (0.01)	-1.084 (0.154)	0.156 (+0.013/-0.012)
35m-7b	15.8	0.10 (0.04)	<0.01 (0.01)	-0.760 (0.201)	0.134 (+0.014/-0.012)
35m-8	18.1	0.01 (0.01)	<0.01 (<0.01)	-0.723 (0.177)	0.131 (+0.012/-0.010)
35m-9	19.1	0.01 (0.01)	0.01 (0.01)	-0.825 (0.161)	0.138 (+0.011/-0.010)
35m-10t	19.7	<0.01 (0.01)	0.02 (0.01)	-0.963 (0.254)	0.147 (+0.020/-0.017)
35m-10b	19.7	0	0.01 (0.01)	<-0.992 (0.120)	>0.149 (+0.009/-0.009)
35m-10a	21.4	<0.01 (<0.01)	0.03 (0.02)	-0.948 (0.082)	0.146 (+0.006/-0.006)
35m-11	21.9	<0.01 (0.01)	0.04 (0.02)	-0.719 (0.238)	0.131 (+0.016/-0.014)
35m-12	23.9	<0.01 (<0.01)	0.01 (0.01)	-0.952 (0.197)	0.147 (+0.015/-0.013)
35m-13	24.9	0	0.06 (0.02)	<-0.842 (0.259)	>0.139 (+0.019/-0.016)
35m-13a	26.0	0.06 (0.03)	<0.01 (0.01)	-1.368 (0.221)	0.181 (+0.023/-0.020)
35m-14	27.1	<0.01 (0.01)	0.01 (0.01)	-1.441 (0.487)	0.188 (+0.059/-0.042)
35m-15	28.1	0.26 (0.05)	0.06 (0.02)	-1.247 (0.162)	0.170 (+0.015/-0.014)
35m-17	31.2	0.51 (0.08)	0.02 (0.01)	-1.434 (0.288)	0.188 (+0.032/-0.026)
35m-18	32.1	0.36 (0.06)	0.06 (0.02)	-1.281 (0.190)	0.173 (+0.018/-0.016)
35m-22	34.8	0.70 (0.09)	0.02 (0.01)	-1.329 (0.156)	0.178 (+0.015/-0.014)

TABLE 5

(continued)

B. South-central Maine.

Sample*	Dist†	ξ_2 (mol/L)§	ξ_3 (mol/L)§	$ln K_s(6)$‡	X_{CO_2}**
T-3	3	1.52 (0.13)	0.03 (0.02)	>-0.737 (0.116)	<0.117 (+0.007/-0.007)
T-4	4	0.07 (0.03)	0.01 (0.01)	-1.169 (0.206)	0.148 (+0.019/-0.016)
TP-6a	6	0	0.01 (0.01)	<-0.937 (0.122)	>0.130 (+0.009/-0.008)
TP-6b	6	0.92 (0.10)	0.09 (0.03)	-0.896 (0.086)	0.127 (+0.006/-0.006)
TP-8a	8	2.40 (0.14)	<0.01 (<0.01)	>-1.243 (0.116)	<0.154 (+0.011/-0.010)
TP-8c	8	0.76 (0.09)	0.01 (0.01)	>-1.289 (0.132)	<0.159 (+0.013/-0.012)
T-12A	12	0.44 (0.07)	0.16 (0.04)	-1.139 (0.094)	0.145 (+0.008/-0.007)
T-12B	12	2.75 (0.14)	0.11 (0.03)	>-1.111 (0.138)	<0.143 (+0.012/-0.011)
TP-17a	17	<0.01 (<0.01)	0.01 (0.01)	-1.164 (0.142)	0.148 (+0.012/-0.012)
TP-17b	17	0.60 (0.08)	0.04 (0.02)	-1.089 (0.118)	0.141 (+0.010/-0.009)
TP-23a	23	0	0	<-1.191 (0.168)	>0.150 (+0.015/-0.014)
TP-23b	23	n.m.	n.m.	-1.091 (0.164)	0.141 (+0.014/-0.012)
T-24	24	0	0	<-1.297 (0.172)	>0.159 (+0.018/-0.015)
TP-29b	29	0.32 (0.06)	0.01 (0.01)	-1.281 (0.154)	0.158 (+0.015/-0.014)
TP-29c	29	1.46 (0.12)	0.03 (0.02)	-1.203 (0.134)	0.151 (+0.012/-0.011)
T-33	33	2.21 (0.l4)	<0.01 (<0.01)	>-1.513 (0.140)	<0.182 (+0.016/-0.015)
TP-47a	47	0.12 (0.04)	0.07 (0.02)	-1.057 (0.128)	0.139 (+0.010/-0.010)
TP-47b	47	1.84 (0.13)	0.18 (0.04)	-1.015 (0.116)	0.136 (+0.009/-0.009)
T-50	50	0.30 (0.06)	0.02 (0.01)	-1.023 (0.160)	0.136 (+0.013/-0.011)
T-52	52	0	0	<-0.983 (0.118)	>0.133 (+0.009/-0.008)
T-57	57	0.29 (0.06)	0.01 (0.01)	-0.893 (0.126)	0.127 (+0.009/-0.008)
T-62	62	0	0	<-1.857 (0.180)	>0.226 (+0.030/-0.025)
T-66	66	0.04 (0.02)	0.01 (0.01)	-1.772 (0.156)	0.214 (+0.023/-0.020)
TP-72a	72	0.04 (0.02)	0.01 (0.01)	-0.906 (0.108)	0.128 (+0.007/-0.007)
TP-72b	72	0.25 (0.06)	0.04 (0.02)	-0.933 (0.136)	0.130 (+0.010/-0.010)
T-78	78	1.79 (0.13)	0.08 (0.03)	-0.804 (0.122)	0.121 (+0.008/-0.008)
T-82A	82	0.68 (0.09)	0.05 (0.02)	-0.938 (0.102)	0.130 (+0.008/-0.007)
T-82B	82	0	0.01 (0.01)	<-1.132 (0.180)	>0.145 (+0.016/-0.014)
T-87	87	1.47 (0.12)	0.13 (0.03)	-0.948 (0.102)	0.131 (+0.007/-0.007)
TP-89b	89	0.65 (0.09)	0.05 (0.02)	-1.113 (0.114)	0.143 (+0.010/-0.009)
TP-89c	89	0.06 (0.03)	0.02 (0.01)	-1.072 (0.134)	0.140 (+0.011/-0.010)
BB1b	--	0	0	<-1.158 (0.128)	>0.147 (+0.011/-0.010)
BB1c	--	2.39 (0.14)	0.13 (0.03)	>-1.108 (0.134)	<0.143 (+0.011/-0.010)
F-A3		n.m.	n.m.	-1.282 (0.194)	0.158 (+0.020/-0.017)
F-A4		0	<0.01 (0.01)	<-1.217 (0.172)	>0.152 (+0.016/-0.014)
F-A5		n.m.	n.m.	-1.142 (0.144)	0.146 (+0.012/-0.012)
F-A6		0.02 (0.02)	0.02 (0.01)	-1.481 (0.154)	0.178 (+0.018/-0.016)
F-A7		n.m.	n.m.	-1.222 (0.146)	0.153 (+0.013/-0.013)
F-A8		0.10 (0.04)	0.02 (0.01)	-1.382 (0.166)	0.168 (+0.018/-0.016)
F-A9		0.02 (0.01)	0.01 (0.01)	-1.284 (0.146)	0.158 (+0.015/-0.013)

amount of Chl (<0.01 mol/L) that occurs in a few samples of carbonate rock at lower grades of metamorphism. Measured ξ_2 varies widely in the range 0 to 0.97 and 0 to 2.75 mol/L in Vermont and Maine, respectively; corresponding ranges in ξ_3 are 0 to 0.10 and 0 to 0.18. Decarbonation of micaceous carbonate rocks during metamorphism in both areas therefore was largely controlled by the formation of Bt by reaction (2).

The initial molar abundance of each mineral i prior to reactions (2) and (3), n_i^o, was calculated for all analyzed samples from the present molar abundance of mineral i, n_i (computed from modes and molar volumes of minerals) and measured values of ξ_2 and ξ_3:

$$n_i^o = n_i - \nu_{i,2}\xi_2 - \nu_{i,3}\xi_3, \quad (4)$$

where $\nu_{i,2}$ and $\nu_{i,3}$ are the coefficients of mineral i in reactions (2) and (3). The compositions of minerals prior to reaction were also calculated. Initial plagioclase composition (X_{an}^o) is $n_{an}^o/(n_{an}^o + n_{ab}^o)$, with n_{an}^o and n_{ab}^o calculated from equation (4).

TABLE 5

(continued)

B. South-central Maine.

Sample*	Dist†	ξ_2 (mol/L)§	ξ_3 (mol/L)§	$ln K_s(6)$‡	X_{CO_2}**
F-B1		n.m.	n.m.	-0.817 (0.096)	0.122 (+0.006/-0.006)
F-B2		0.66 (0.09)	0.14 (0.03)	-0.894 (0.084)	0.127 (+0.006/-0.006)
F-B3		n.m.	n.m.	-0.926 (0.142)	0.129 (+0.011/-0.009)
F-B4		1.06 (0.11)	0.06 (0.02)	-1.031 (0.090)	0.137 (+0.007/-0.007)
F-B5		0.69 (0.09)	0.08 (0.03)	-1.000 (0.200)	0.134 (+0.017/-0.013)
F-B6		n.m.	n.m.	-0.888 (0.118)	0.126 (+0.009/-0.007)
F-B7		0.89 (0.10)	0.16 (0.04)	-0.943 (0.116)	0.130 (+0.009/-0.008)
FT-A3	0.3			-0.887 (0.120)	0.126 (+0.009/-0.007)
FT-A1	0.9	0.15 (0.04)#	0.03 (0.01) #	-1.072 (0.112)	0.140 (+0.009/-0.009)
FT-B	2.7	0.05 (0.03)	0.05 (0.02)	-1.067 (0.150)	0.140 (+0.012/-0.012)
FT-C	5.4	0.01 (0.01)	0.01 (0.01)	-1.370 (0.180)	0.166 (+0.020/-0.016)
FT-D	-1.0	2.29 (0.14)	0.18 (0.04)	-0.802 (0.094)	0.121 (+0.006/-0.006)
FT-E	-3.5	1.03 (0.11)	0.06 (0.02)	-0.830 (0.118)	0.123 (+0.008/-0.008)
FT-F	-6.1	0.71 (0.09)	0.09 (0.03)	-0.859 (0.090)	0.124 (+0.007/-0.005)

*Samples T-12A and T-12B and samples T-82A and T-82B are located <1 m apart along the 100-m traverse but are not from the same hand specimen. Samples BB1b and BB1c are adjacent layers in the same thin section of a sample collected at location 5 (fig. 2) away from the 100-m traverse. Other sample notation as in footnotes to tables 1 and 3.

†Distance along traverse perpendicular to lithologic layering measured at center of layer or sample. East-central Vermont: origin placed arbitrarily close to first sample. South-central Maine: 100-m traverse measured to the southeast from the origin at limestone-pelite contact; traverse across fold in fig. 4 measured in direction of layer A from origin at contact between layers A and B. Units are cm for samples 9cm-a1 to 9cm-g, 16cm-a to 16cm-i, and FT-A3 to FT-F, and m for sample 5m-1 to 5m-15, 35m-1a to 35m-22, and T-3 to T-89c.

§Progress of reactions (2) and (3) with reference to 1 L rock after reaction. Uncertainties in parentheses represent 2σ based on the statistics of point counting (Chayes, 1956). n.m. = not measured.

‡$ln K_s$ based on equilibrium (6) evaluated using measured mineral compositions and mixing models for minerals as described in text. Uncertainties in parentheses represent 2σ based exclusively on variations in mineral composition in each sample.

**X_{CO_2} calculated from equilibrium (6) using measured values of $ln K_s(6)$ and thermodynamic data and mixing models for fluid components as described in text. Uncertainties in parentheses represent ±2σ based exclusively on variations in mineral composition in each sample.

#FT-A1 and FT-A3 are two areas in the same thin section. Value of reaction progress refers to both areas combined.

The Mn-content of minerals is small (table 2); initial compositions of Ms, Ank, and Cal therefore were calculated from mass balance of Fe assuming that the minerals were Fe-Mg solutions:

$$Fe_T = X^o_{FeMs}\epsilon_{M,Ms}n^o_{Ms} + X^o_{FeAnk}\epsilon_{M,Ank}n^o_{Ank} + X^o_{FeCal}\epsilon_{M,Cal}n^o_{Cal}, \quad (5)$$

where Fe_T is the moles Fe per L contained in Bt, Chl, Ms, Ank, and Cal (estimated from modes and mineral compositions), X^o_{Fei} is the Fe/(Fe+Mg) of mineral i prior to reaction, and $\epsilon_{M,i}$ is the moles Fe+Mg+Mn per mole mineral i. The three X^o_{Fei} terms are computed from equation (5) and the values of $K_{Cal/Ank}$ and $K_{Ms/Ank}$ in table 3.

A small number of irregularities emerged in the set of 104 samples for which initial amounts and compositions of minerals were computed. Calculated values of n^o_{an} (and hence X^o_{an}) are negative for four samples from Vermont and four from Maine. In all but one sample, however, the negative values are statistically indistinguishable from 0, considering errors in point counting. In an additional seven samples from Vermont and three from Maine, calculated values of n^o_{Cal} are negative. The negative values cannot be explained simply by statistical errors in point counting and probably indicate that the volume of rock involved in reactions (2) and (3) in a few cases was larger than the thin section or portion of thin section in which Bt and Chl modes were measured for determination of ξ_2 and ξ_3.

MEASUREMENT OF PROXIES OF FLUID COMPOSITION

Activity of CO_2

The proxy for a_{CO_2} considered is $K_s(6)$ for the equilibrium,

$$\underset{\text{muscovite}}{KAl_3Si_3O_{10}(OH)_2} + 3\ \underset{\text{ankerite}}{CaMg(CO_3)_2} + 2\ \underset{\text{quartz}}{SiO_2} = \underset{\text{biotite}}{KMg_3AlSi_3O_{10}(OH)_2}$$

$$+ 2\ \underset{\text{calcite}}{CaCO_3} + \underset{\text{plagioclase}}{CaAl_2Si_2O_8} + 4\ \underset{\text{fluid}}{CO_2}, \quad (6)$$

defined as $[(a_{phl})(a_{an})(a_{cal})^2]/[(a_{ms})(a_{dol})^3(a_{qtz})^2]$, where subscripts refer to the relevant mineral component. The proxy $K_s(6)$ was considered, rather than a_{CO_2} or X_{CO_2}, to avoid uncertainties introduced by thermodynamic data for mineral and fluid species, by estimates of P and T, and by making any assumption about the approach to mineral-fluid equilibrium during metamorphism. Activities of components in minerals were calculated assuming an ideal ionic model for carbonates, equations in Holland and Powell (1990) for micas, and the equations in figure 5 for Pl (see Appendix for details). Average mineral compositions for all but Pl were used as input to the estimates of activity. Because $\xi_2 >> \xi_3$,

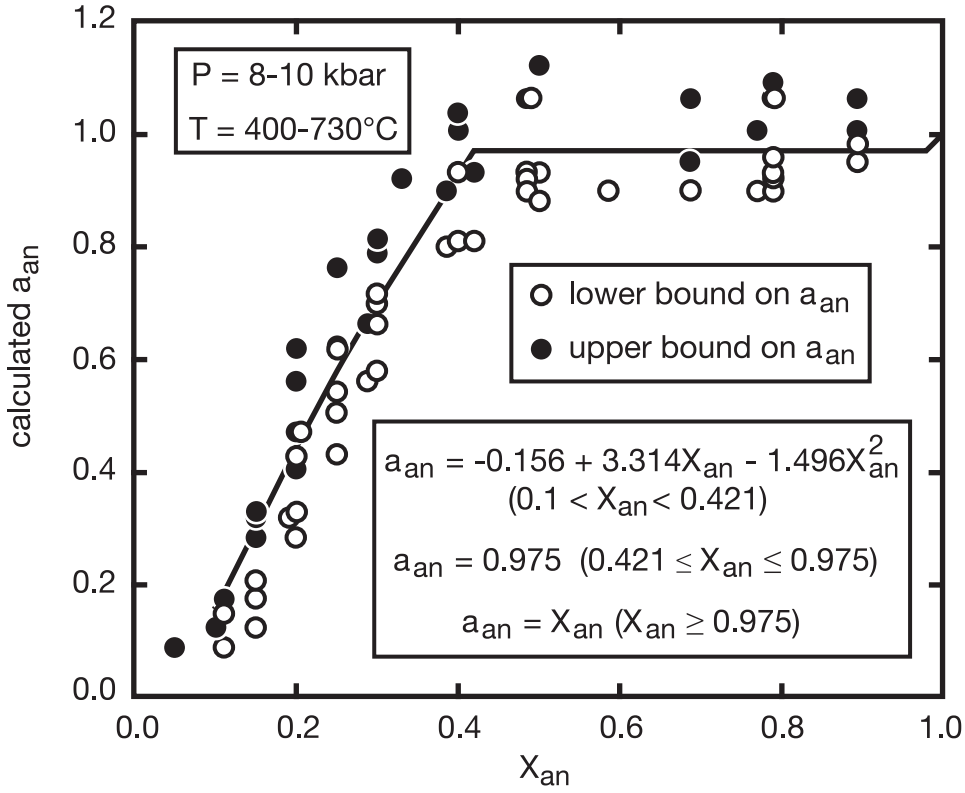

Fig. 5. Activity of $CaAl_2Si_2O_8$ in Pl (a_{an}) calculated from experimental data of Goldsmith (1982) at 8 to 10 kbar and 400° to 730°C following the general method of Carpenter and Ferry (1984) but consistent with the Berman (1988, updated June, 1992) thermodynamic database. Each experimental datum defines either an upper or lower bound on a_{an}. Solid curve and equations are empirical representations of X_{an}-a_{an} relations that are consistent with experimental results within error of measurement. See Appendix for details.

X_{an} increased in almost all samples during progress of reactions (2) and (3). The most calcic rather than average measured Pl in each sample therefore was used to compute a_{an}. For rocks that lack Bt because reaction (2) did not initiate, a fictive Bt formula was estimated either from the average of Bt compositions in samples from the same layer (sample F-A4, Maine), from the composition of Bt in the adjacent layer (adjacent layer pairs, Maine), or from the average of Bt compositions along the same traverse (all other Bt-free samples). The Fe/(Fe+Mg) of the fictive Bt was then calculated from the composition of Ank in the sample and the average $K_{Bt/Ank}$ of the same group of samples used to estimate the Bt formula. A model a_{phl} was estimated from the fictive Bt composition. The value of $K_s(6)$, computed using the model activity for Bt-free samples, represents an upper limit. For rocks that lack Ank and/or Ms because reactions (2) and (3) went to completion (Maine only), fictive Ank and/or Ms formulas were estimated similarly as for Bt. Model a_{dol} or a_{ms} was estimated from the fictive Ank or Ms composition. The value of $K_s(6)$, computed using the model activities for Ank- or Ms-free samples, represents a lower limit.

Because the goal of the study is to compare differences in $K_s(6)$ among samples from the same location and because P and T were probably uniform during metamorphism at the scale of each location, uncertainties in $K_s(6)$ were computed by only considering uncertainties introduced by variations in mineral composition within individual samples. The approach further assumes that any errors in calculated $K_s(6)$ introduced by the activity-composition relations are the same for all samples compared. Values of a_{ms}, a_{dol}, a_{phl} and a_{cal} were calculated from each individual mineral analysis for each sample; from these, σ was then computed for each average activity in the sample. The 2σ uncertainty in a_{an} was taken as 0.025 which approximately corresponds both to a 2σ measurement uncertainty of $0.02X_{an}$ propagated through the equation in figure 5 for Pl with $0.1<X_{an}<0.421$ and to a reasonable uncertainty in $a_{an} = 0.975$ for Pl with $X_{an}>0.421$ (see Appendix). Uncertainties in $K_s(6)$ and $ln K_s(6)$, in turn, were calculated by propagating the uncertainties in mineral activities through the computation of $K_s(6)$ and $ln K_s(6)$.

Results for all analyzed samples are listed in table 5. Samples that contain Ms, Ank, Qtz, Bt, Cal, and Pl record $ln K_s(6) = -0.79$ to -0.67 and -1.67 to -0.72 at locations 21-21 and 21-32 in Vermont, respectively, and -1.77 to -0.80 at location 5 in Maine. Samples that record only upper or lower bounds on $K_s(6)$ give results consistent with these ranges. Except for location 21-21, the ranges are larger than the uncertainty of measurement, and significant differences in $K_s(6)$ existed among samples from the same outcrop during regional metamorphism.

Activities of mineral components and $K_s(6)$ were independently calculated for selected samples from Vermont using the program AX associated with Holland and Powell's (1998) thermodynamic database. Although absolute values of $K_s(6)$ differ slightly from those reported in table 5, differences in $K_s(6)$ among samples are indistinguishable from those in table 5 within estimated uncertainties.

$\delta^{18}O$ *and* $\delta^{13}C$ *of Fluid*

Values of $\delta^{18}O_{Cal}$ and $\delta^{13}C_{Cal}$ were used as proxies for $\delta^{18}O_{fluid}$ and $\delta^{13}C_{fluid}$ to avoid uncertainties introduced by estimates both of Cal-fluid O- and C-isotope fractionation factors and of X_{CO_2} and by any assumption about the degree to which mineral-fluid equilibrium was attained. Measured values of $\delta^{18}O_{carbonate}$ and $\delta^{13}C_{carbonate}$ were converted to estimates of $\delta^{18}O_{Cal}$ and $\delta^{13}C_{Cal}$ using measured modes of Ank and Cal and the Dol-Cal O- and C-isotope fractionation factors of Sheppard and Schwarcz (1970), as compiled in Friedman and O'Neil (1977). Because most samples contain much more Cal than Ank, the corrections in most cases are small, typically ≤ 0.1 permil. The difference between measured $\delta^{18}O_{carbonate}$ and estimated $\delta^{18}O_{Cal}$, however, may be as large as 0.3 permil for one sample from Maine. The difference between measured $\delta^{13}C_{carbonate}$ and estimated $\delta^{13}C_{Cal}$ may be as large as 0.3 permil for some samples from Vermont and as large as 0.5 permil for

one sample from Maine. Uncertainties in estimated $\delta^{18}O_{Cal}$ and $\delta^{13}C_{Cal}$ were taken as the same as the analytical precision in the measurement of $\delta^{18}O_{carbonate}$ and $\delta^{13}C_{carbonate}$.

Results are listed in table 4. Estimated $\delta^{18}O_{Cal}$ and $\delta^{13}C_{Cal}$ are 18.7 to 19.1 permil and −0.9 to −0.1 permil, respectively at location 21-21 in Vermont; 18.2 to 19.7 permil and −1.4 to +0.2 permil at location 21-32 in Vermont; 17.9 to 18.5 permil and −3.7 to −1.2 permil at location 21-35 in Vermont; and 17.2 to 20.4 permil and −4.0 to −0.2 permil at location 5 in Maine. Except for locations 21-21 and 21-35, the ranges in $\delta^{18}O_{Cal}$ are larger than the uncertainty of measurement, and significant differences in $\delta^{18}O_{fluid}$ existed among samples from the same outcrop during regional metamorphism. Significant differences in $\delta^{13}C_{Cal}$ occur among samples at each of the locations.

SPATIAL DISTRIBUTION OF REACTION PROGRESS AND PROXIES FOR FLUID COMPOSITION

East-central Vermont

Centimeter scale.—Significant differences in ξ_2 exist across layering between samples even at the smallest spatial scales investigated along the 9-cm traverse at location 21-21 (0-0.39 mol/L) and along the 16-cm traverse at location 21-32 (0.24-0.97 mol/L) (figs. 6 and 7). Some differences in ξ_2 between adjacent layers <1 cm thick are outside the error of measurement (fig. 6). A calculated mean square weighted deviation (MSWD) of 0.39 (Mahon, 1996), however, demonstrates that all measured $ln K_s(6)$ along the 9-cm traverse at location 21-21 are statistically consistent with a single value whose best estimate is the weighted mean, −0.728 ± 0.055 (uncertainties here and elsewhere are 95 percent confidence intervals based on the standard error unless stated otherwise). Likewise, values of $\delta^{18}O_{Cal}$ along the 9-cm traverse are statistically consistent with a single value whose best estimate is 18.94 ± 0.12 permil (fig. 6). Values of $\delta^{13}C_{Cal}$, on the other hand, are not consistent with a single value (MSWD = 8.00). Similarly, along the 16-cm traverse, $ln K_s(6)$ and $\delta^{18}O_{Cal}$ are statistically consistent with single values whose best estimates are −1.345 ± 0.089 and 19.16 ± 0.14 permil (fig. 7), respectively, but values of $\delta^{13}C_{Cal}$ are not (MSWD = 6.50). There does not appear to be any systematic correlation between either $ln K_s(6)$, $\delta^{18}O_{Cal}$, or $\delta^{13}C_{Cal}$ and proximity to Qtz veins at the scale of the 16-cm traverse (fig. 7). Over distances of at least 8 to 15 cm across layering, significant differences in the progress of reaction (2) developed during regional metamorphism while at the same time values of the proxies, $K_s(6)$ and $\delta^{18}O_{Cal}$, were uniform within error of measurement. An explanation for the apparently discrepant behavior of ^{13}C is presented later.

Meter scale.—As is observed along the 9- and 16-cm traverses, measured ξ_2 varies significantly along the 5-m traverse at location 21-32, 0-0.89 mol/L (fig. 8). Values between samples as close as 0.1 m apart differ outside the error of measurement. Unlike along the 9- and 16-cm traverses, $K_s(6)$ and $\delta^{18}O_{Cal}$ are not statistically consistent with single values over the entire 5-m traverse (fig. 8). Nevertheless, there are three regions in which measured $ln K_s(6)$ is statistically uniform: −1.520 ± 0.297 at 0.1 to 1.0 m along the traverse, −1.191 ± 0.197 at 1.7 to 3.0 m, and −0.826 ± 0.089 at 3.5 to 4.7 m. Measured $\delta^{18}O_{Cal}$ within two of the regions is also statistically consistent with single values (diagonally ruled areas in fig. 8). There are insufficient O-isotope data to assess whether $\delta^{18}O_{Cal}$ is statistically uniform as well in the third region 0.1 to 1.0 m along the traverse. As along the 9-cm and 16-cm traverses, $\delta^{13}C_{Cal}$ is not consistent with a single value within error of measurement along the entire 5-m traverse or even in regions where $\delta^{18}O_{Cal}$ is uniform.

Two traverses at location 21-35 further constrain the distance over which $\delta^{18}O_{Cal}$ is uniform at the m scale. Measurements of $\delta^{18}O_{Cal}$ along the 0.5- and 1.1-m traverses are statistically consistent with single values whose best estimates are 18.11 ± 0.09 permil and 18.34 ± 0.10 permil, respectively (figs. 9 and 10). As along the other traverses,

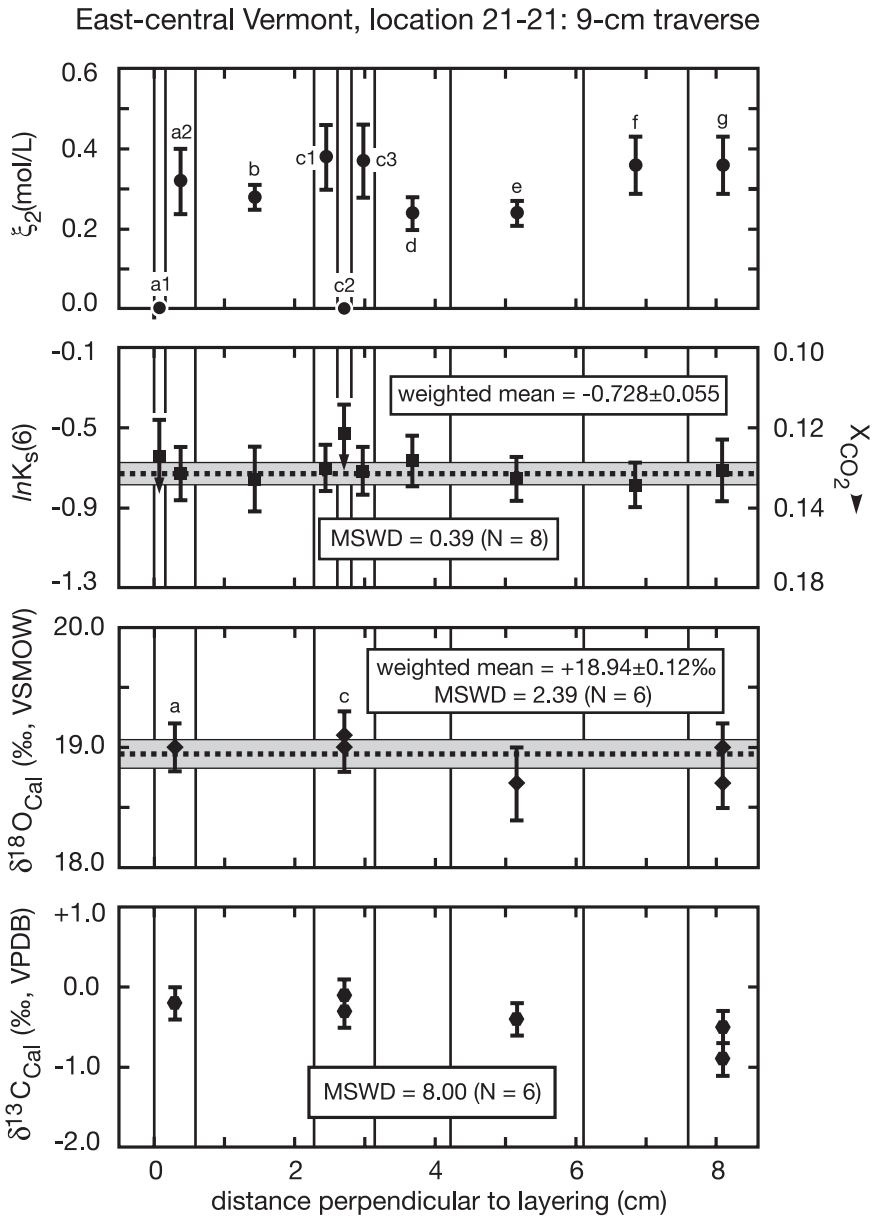

Fig. 6. Values of progress of reaction (2), $ln K_s(6)$, $\delta^{18}O_{Cal}$, and $\delta^{13}C_{Cal}$ for 10 samples along the 9-cm-long traverse perpendicular to lithologic layering at location 21-21, Vermont. Sample numbers have "9cm" prefix omitted. Thin vertical lines represent boundaries between visually distinct adjacent layers. For the purposes of O- and C-isotope analyses, layers a1 and a2 and layers c1, c2, and c3 were treated as single layers, a and c, respectively. Error bars are $\pm 2\sigma$; error bars omitted when smaller than size of symbol. Scale for X_{CO_2}, computed from mineral-fluid equilibrium, is not linear. Downward pointing arrows indicate an upper bound on $ln K_s(6)$ in samples that lack Bt because reaction (2) did not occur. The $ln K_s(6)$ and $\delta^{18}O_{Cal}$ are statistically consistent with single values along the traverse, -0.728 ± 0.055 and 18.94 ± 0.12‰, respectively (dashed horizontal lines are weighted means; horizontal gray bands are 95% confidence intervals based on the standard error). The $\delta^{13}C_{Cal}$, however, are not statistically consistent with a single value.

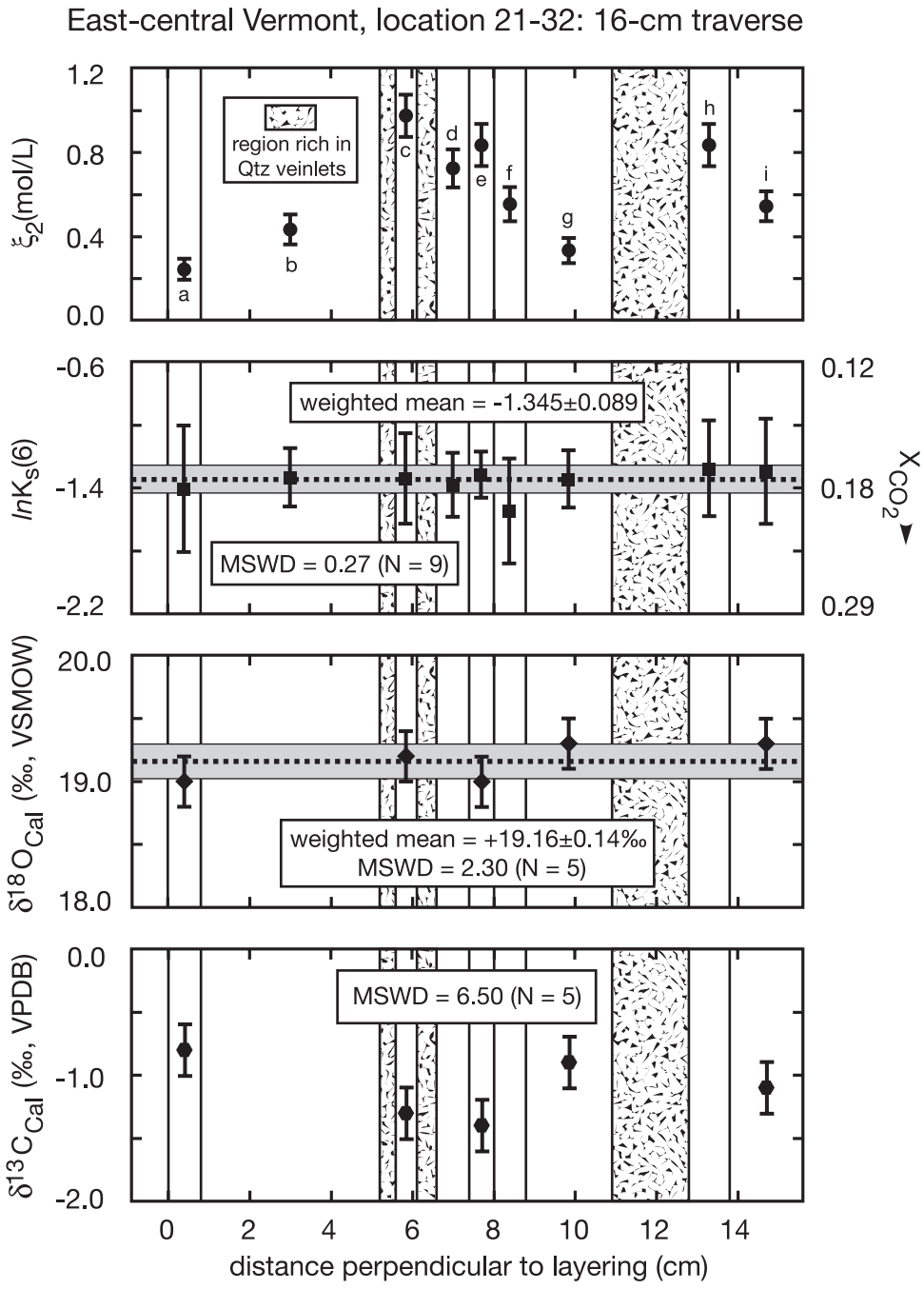

Fig. 7. Values of progress of reaction (2), $ln K_s(6)$, $\delta^{18}O_{Cal}$, and $\delta^{13}C_{Cal}$ for nine samples along the 16-cm-long traverse perpendicular to lithologic layering at location 21-32, Vermont. Sample numbers have "16cm" prefix omitted. Format the same as in figure 6. The $ln K_s(6)$ and $\delta^{18}O_{Cal}$ are statistically consistent with single values along the traverse, -1.345 ± 0.089 and 19.16 ± 0.14‰, respectively. The $\delta^{13}C_{Cal}$, however, are not statistically consistent with a single value.

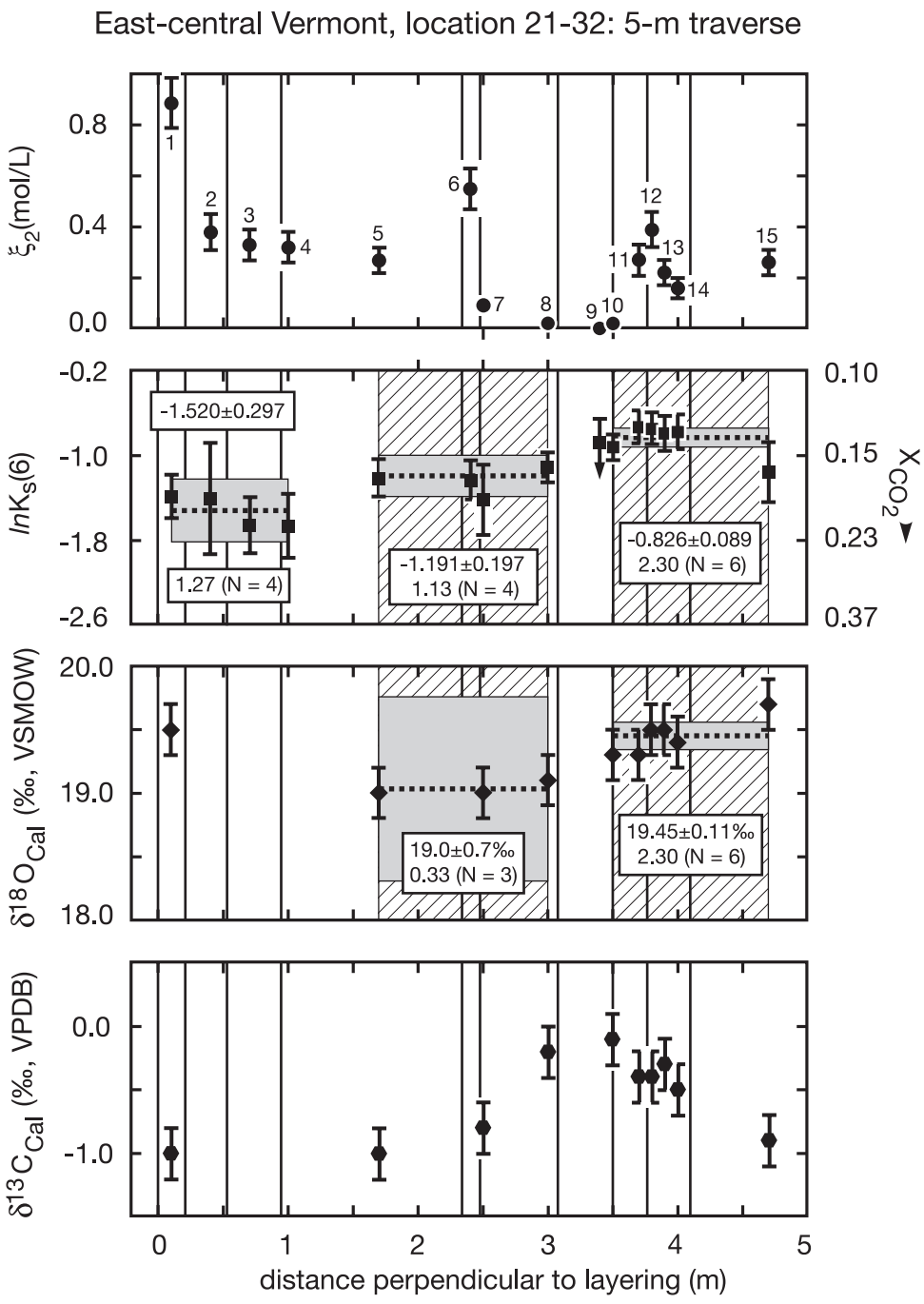

Fig. 8. Values of progress of reaction (2), $ln K_s(6)$, $\delta^{18}O_{Cal}$, and $\delta^{13}C_{Cal}$ for 15 samples along the 5-m-long traverse perpendicular to lithologic layering at location 21-32, Vermont. Sample numbers have "5m" prefix omitted. Format the same as in figure 6. Boxes contain weighted means, 95% confidence intervals based on the standard error, and values of MSWD. The $ln K_s(6)$, $\delta^{18}O_{Cal}$, and $\delta^{13}C_{Cal}$ are not statistically consistent with single values across the entire traverse. Along three segments of the traverse, however, the $ln K_s(6)$ are statistically consistent with single values, and along two of the segments both $ln K_s(6)$ and $\delta^{18}O_{Cal}$ are consistent with single values (diagonally-ruled regions).

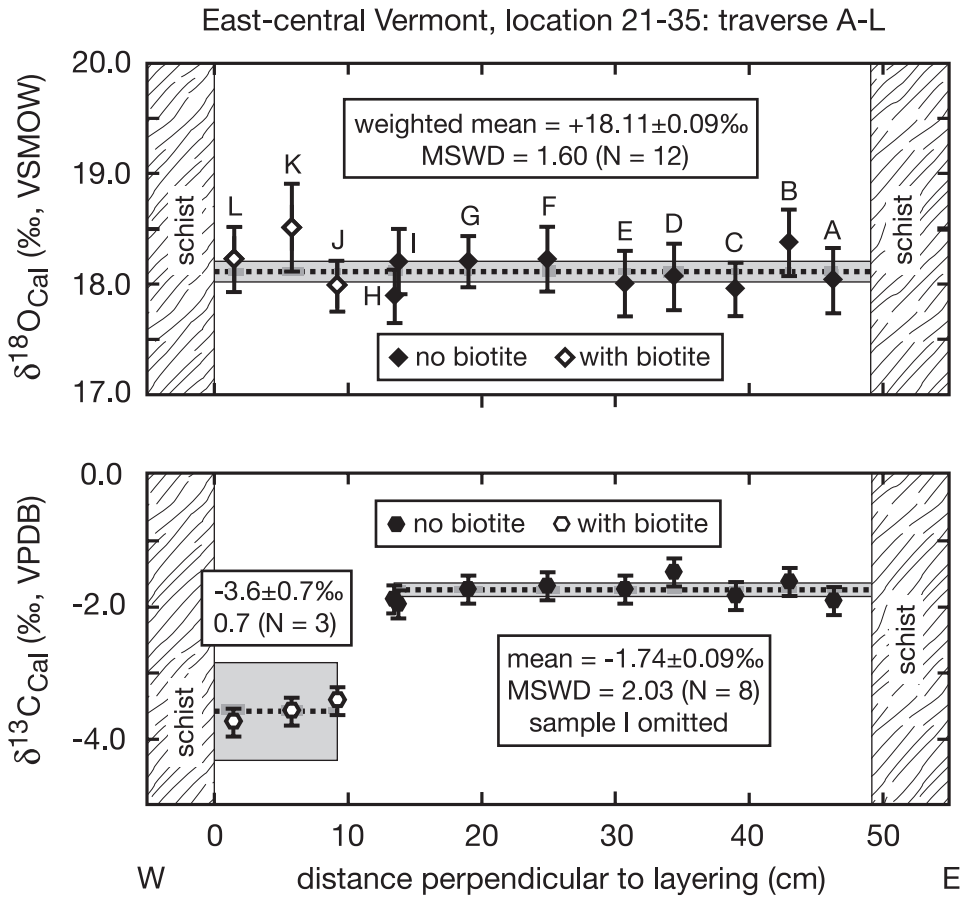

Fig. 9. Values of $\delta^{18}O_{Cal}$ and $\delta^{13}C_{Cal}$ for 12 samples along a 0.5-m-long traverse perpendicular to a carbonate layer surrounded by pelitic schist at location 21-35, Vermont. Sample numbers have "21-35" prefix omitted. Format the same as in figures 6 and 8. The $\delta^{18}O_{Cal}$ are statistically consistent with a single value along the traverse, 18.11 ± 0.09‰. The $\delta^{13}C_{Cal}$, however, are not statistically consistent with a single value.

however, $\delta^{13}C_{Cal}$ is not consistent with a single value. Nevertheless, both traverses can be divided into two segments along which $\delta^{13}C_{Cal}$ is uniform within error of measurement. No measurements of reaction progress or estimates of $K_s(6)$ were made for samples from location 21-35.

Values of $K_s(6)$ and $\delta^{18}O_{Cal}$ are uniform over distances up to 1.3 m along the 5-m traverse at location 21-32 and along the two traverses at location 21-35. Evans and others (2002) observed a similar scale of uniformity in $\delta^{18}O_{carbonate}$ across five marl layers from other regions of the Waits River Formation outside the area of figure 1. Data from the 5-m traverse further reveal at what spatial scale uniformity in $K_s(6)$ and $\delta^{18}O_{Cal}$ was not attained. Specifically, some groups of samples separated by as little as 0.5 to 0.7 m record values of $K_s(6)$ that fail to overlap at the 95 percent confidence level (between 1.0 and 1.7 m and between 3.0 and 3.5 m along the 5-m traverse, fig. 8). The MSWD test additionally indicates that while samples 1.7-3.0 and 3.5-4.7 m along the traverse record statistically uniform $\delta^{18}O_{Cal}$, measured $\delta^{18}O_{Cal}$ is not consistent with a single value over the entire distance 1.7 to 4.7 m at a >95 percent level of confidence. The proxies for a_{CO_2} and $\delta^{18}O_{fluid}$ appear to have been uniform across layering within error of measurement during metamorphism in Vermont certainly over a distance

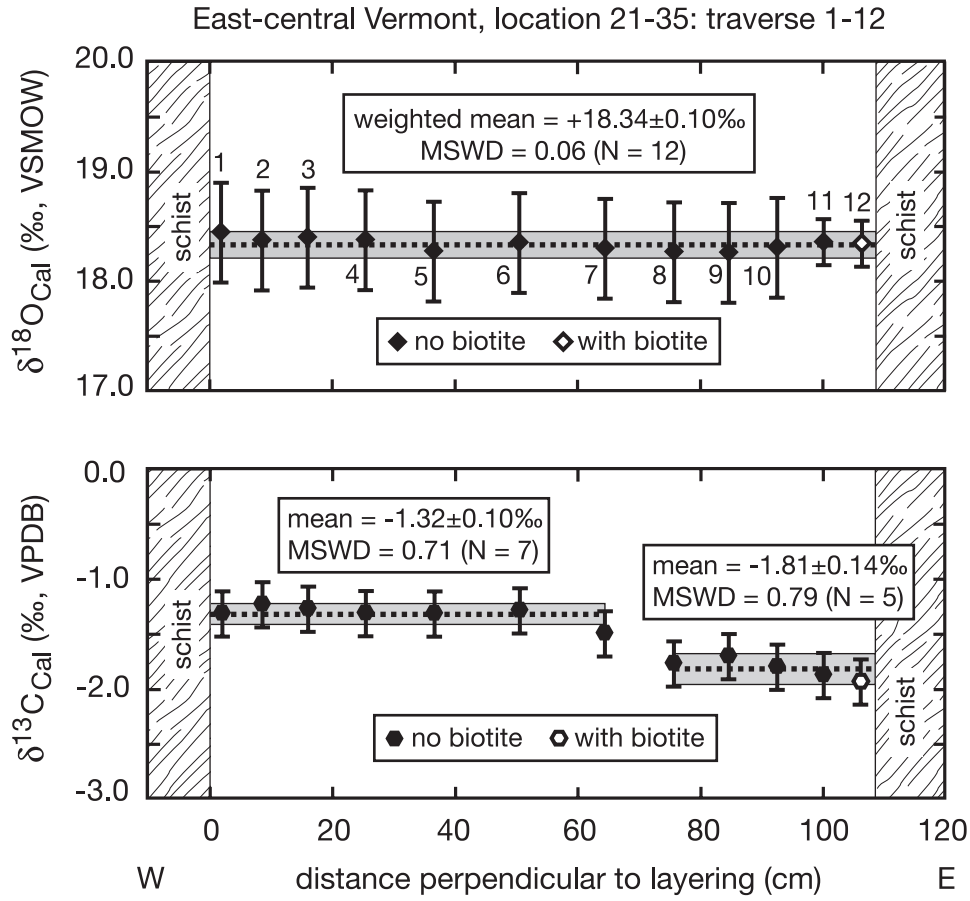

Fig. 10. Values of $\delta^{18}O_{Cal}$ and $\delta^{13}C_{Cal}$ for 12 samples along a 1.1-m-long traverse perpendicular to a carbonate layer surrounded by pelitic schist at location 21-35, Vermont. Sample designations have "21-35" prefix omitted. Format the same as in figures 6 and 8. The $\delta^{18}O_{Cal}$ are statistically consistent with a single value along the traverse, 18.34 ± 0.10‰. The $\delta^{13}C_{Cal}$, however, are not statistically consistent with a single value.

≥15 cm (figs. 6 and 7), and in some cases up to ≈1 m (figs. 8 and 10), but not always at significantly larger scales (fig. 8).

Decameter scale.—The spatial distributions of ξ_2, $K_s(6)$, $\delta^{18}O_{Cal}$, and $\delta^{13}C_{Cal}$ along the 35-m traverse at location 21-32 (fig. 11) are similar to those along the 5-m traverse (fig. 8). Significant differences in ξ_2 are observed across layering at the dkm scale, some between samples separated by as little as ≈1 m. Values of $K_s(6)$, $\delta^{18}O_{Cal}$, and $\delta^{13}C_{Cal}$ are not uniform along the entire traverse. Nevertheless, measured $ln K_s(6)$ is statistically consistent with a single value in three regions: −0.833 ± 0.054 at 1.1 to 12.4 m along the traverse, −0.881 ± 0.074 at 15.8 to 23.9 m, and −1.316 ± 0.116 at 26.0 to 34.8 m (fig. 11). Because of the larger spacing of samples along the 35-m traverse compared to the 5-m traverse, however, it probably would be unsafe to conclude that $K_s(6)$ was necessarily uniform within error of measurement over distances as large as 8 to 11 m across layering during metamorphism without additional data. In portions of two of the regions, 8.2-12.4 and 26.0-28.1 m along the traverse, measured $\delta^{18}O_{Cal}$ is also statistically consistent with a single value (diagonally ruled areas in fig. 11). Within the third region, 15.8 to 23.9 m along the traverse, no triplet of adjacent $\delta^{18}O_{Cal}$

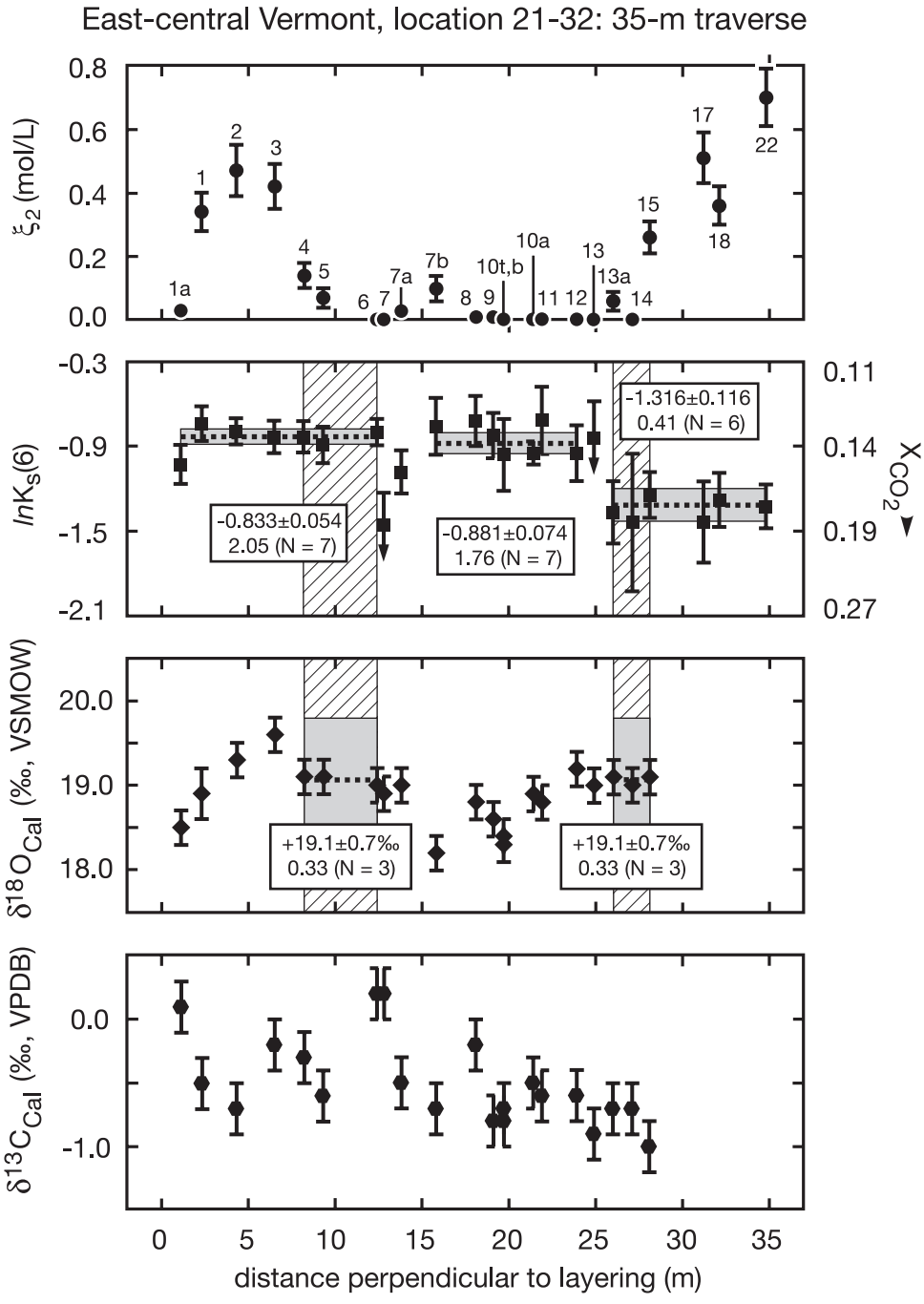

Fig. 11. Values of progress of reaction (2), $ln K_s(6)$, $\delta^{18}O_{Cal}$, and $\delta^{13}C_{Cal}$ for 23 samples along the 35-m-long traverse perpendicular to lithologic layering at location 21-32, Vermont. Sample numbers have "35m" prefix omitted. Format the same as in figures 6 and 8. The $ln K_s(6)$, $\delta^{18}O_{Cal}$, and $\delta^{13}C_{Cal}$ are not statistically consistent with single values across the entire traverse. Along three segments of the traverse, however, the $ln K_s(6)$ are statistically consistent with single values and along portions of two of the segments both $ln K_s(6)$ and $\delta^{18}O_{Cal}$ are consistent with single values (diagonally-ruled regions).

measurements are consistent with a single value. The scale over which both $K_s(6)$ and $\delta^{18}O_{Cal}$ are uniform, 2.1 to 4.2 m, is the same order of magnitude as that along the 5-m traverse.

The 2.1 to 3.4 m separation of the three regions with statistically uniform $ln K_s(6)$, between 12.4 and 15.8 m and between 23.9 and 26.0 m along the traverse, however, documents that uniformity in the proxy for a_{CO_2} in some cases did not occur over distances more than ≈2-3 m across layering. In assessing the significance of data for individual samples from the 35-m and other traverses, overlap at the $\pm 2\sigma$ level is considered agreement; difference at more than the $\pm 3\sigma$ level is considered significant; and difference at the 2 to 3σ level is considered inconclusive. On this basis, sample 35m-6 records $ln K_s(6)$ (-0.802, $3\sigma = 0.140$) that is significantly greater than the value recorded by sample 35m-7 (<-1.454, $3\sigma = 0.332$); the separation between the two samples is 0.4 m (fig. 11). The two pairs of samples with the smallest separation that record significantly different values of $\delta^{18}O_{Cal}$ (difference >0.6‰) are 35m-1a (18.5‰) and 35m-2 (19.3‰), separated by 3.2 m, and sample 35m-7a (19.0‰) and 35m-7b (18.2‰), separated by 2.0 m (fig. 11). Data from the 35-m traverse, along with those for the 5-m traverse, demonstrate that the upper limit of the distance over which proxies for a_{CO_2} and $\delta^{18}O_{fluid}$ were uniform within error of measurement is on the order of ≈1 m across layering. As along the shorter traverses, $\delta^{13}C_{Cal}$ along the 35-m traverse is not necessarily uniform even in regions where both $K_s(6)$ and $\delta^{18}O_{Cal}$ are (for example, 8.2-12.4 m along the traverse).

Data from the 35-m traverse additionally provide estimates of the scale at which reversals in gradients in the proxies for a_{CO_2} and $\delta^{18}O_{fluid}$ occurred across layering during regional metamorphism. The information constrains the geometry of metamorphic fluid flow and the processes that drove decarbonation reaction. Samples 35m-6 and 35m-7b both record $ln K_s(6)$ (-0.802, $3\sigma = 0.140$; -0.760, $3\sigma = 0.302$, respectively) that is significantly greater than the value recorded by sample 35m-7 in between (<-1.454, $3\sigma = 0.332$). A reversal in the gradient of $K_s(6)$ therefore occurs over the distance between samples 35m-6 and 35m-7b, 3.4 m (fig. 11). Samples 35m-7a and 35m-10a both record $\delta^{18}O_{Cal}$ (19.0‰ and 18.9‰, respectively) that is significantly greater than the value recorded by sample 35m-7b in between (18.2‰). A reversal in the gradient of $\delta^{18}O_{Cal}$ therefore occurs over the distance between samples 35m-7a and 35m-10a, 7.6 m (fig. 11). Statistically resolvable reversals in the gradient in proxies for fluid composition appear to occur across lithologic layering over distances of ≈4 to 8 m or less.

South-central Maine

Centimeter scale.—Significant differences in ξ_2 exist between each of the eight, cm-thick, adjacent layer pairs from the same thin section of samples collected at location 5 in Maine (samples with "TP" and "BB1" prefixes). The smallest difference is 0.21 mol/L between layers TP-72a and TP-72b, and the largest difference is 2.39 mol/L between samples BB1b and BB1c (table 5, fig. 12A). Measured $ln K_s(6)$ for each adjacent pair, on the other hand, overlap at the $\pm 1\sigma$ level, and values of $\delta^{18}O_{Cal}$ overlap at the $\pm 2\sigma$ level (figs. 12B and 12C). Values of $\delta^{13}C_{Cal}$ for three adjacent pairs, however, do not overlap at the $\pm 2\sigma$ level, and values for one pair do not overlap at a $>\pm 3\sigma$ level; the different behavior of $\delta^{13}C_{Cal}$ is explained later. Similar to the area in Vermont, large differences in progress of reaction (2) developed during metamorphism at the same cm scale over which proxies for fluid composition, $K_s(6)$ and $\delta^{18}O_{Cal}$, were uniform within error of measurement.

Meter scale.—Seven samples were investigated from each of two adjacent layers exposed over an ≈1 m^2 area in the hinge of the isoclinal fold at location 5 (fig. 4). In one layer (A) ξ_2 is relatively low (0-0.10 mol/L); in the other (B) ξ_2 is relatively high (0.66 – 1.06 mol/L). Measured $ln K_s(6)$, $\delta^{18}O_{Cal}$, and $\delta^{13}C_{Cal}$ are statistically consistent (MSWD = 0.18 – 2.50) with single values in each layer (fig. 4). All three proxies

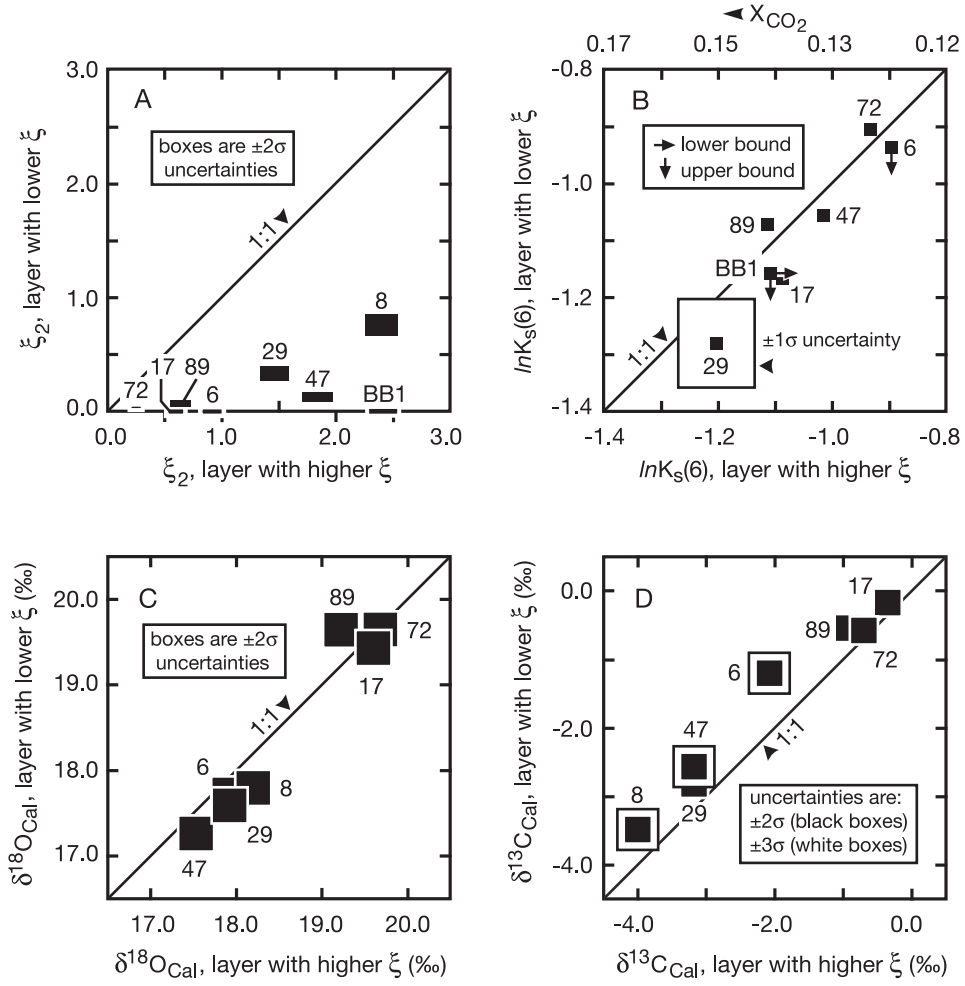

Fig. 12. Comparison of values of progress of reaction (2), $ln K_s(6)$, $\delta^{18}O_{Cal}$, and $\delta^{13}C_{Cal}$ between pairs of adjacent cm-thick lithologic layers along the 100-m-long traverse perpendicular to lithologic layering at location 5, Maine. Sample numbers have "TP" prefix omitted. Error boxes are $\pm 2\sigma$ for ξ_2 and $\delta^{18}O_{Cal}$, $\pm 1\sigma$ for $ln K_s(6)$, and either $\pm 2\sigma$ (black) or $\pm 3\sigma$ (white) for $\delta^{13}C_{Cal}$. Scale for X_{CO_2}, computed from mineral-fluid equilibrium, is not linear. Upper bounds on $ln K_s(6)$ refer to samples that lack Bt because reaction (2) did not occur; lower bound on $ln K_s(6)$ refers to sample that lacks Ank because reaction (2) went to completion. Values of $ln K_s(6)$ for sample pair TP-8 omitted because both members record lower bounds only. No O- and C-isotope data measured for samples BB1b and BB1c.

evidently were uniform within each layer during metamorphism, but the 99 percent confidence intervals of both $ln K_s(6)$ and $\delta^{18}O_{Cal}$ for the two layers fail to overlap. Data for six additional samples collected along a 12-cm traverse across the contact between layers A and B (FT traverse, fig. 4) more precisely constrain the distance over which the changes in $K_s(6)$ and $\delta^{18}O_{Cal}$ occur between the layers to <10 cm (fig. 13). The two proxies for fluid composition were uniform within error of measurement across layering certainly over a distance no more than ≈ 1 m (fig. 4) and probably over a distance no more than ≈ 10 cm (fig. 13). Additionally, the spatial distribution of $K_s(6)$ and $\delta^{18}O_{Cal}$ in figure 4 documents a reversal in gradients of their values over a distance $\approx$ 1m across layering.

Decameter scale.—The spatial distributions of ξ_2, $K_s(6)$, $\delta^{18}O_{Cal}$, and $\delta^{13}C_{Cal}$ along the 100-m traverse (fig. 14) confirm earlier conclusions. Over a distance of ≈ 90 m

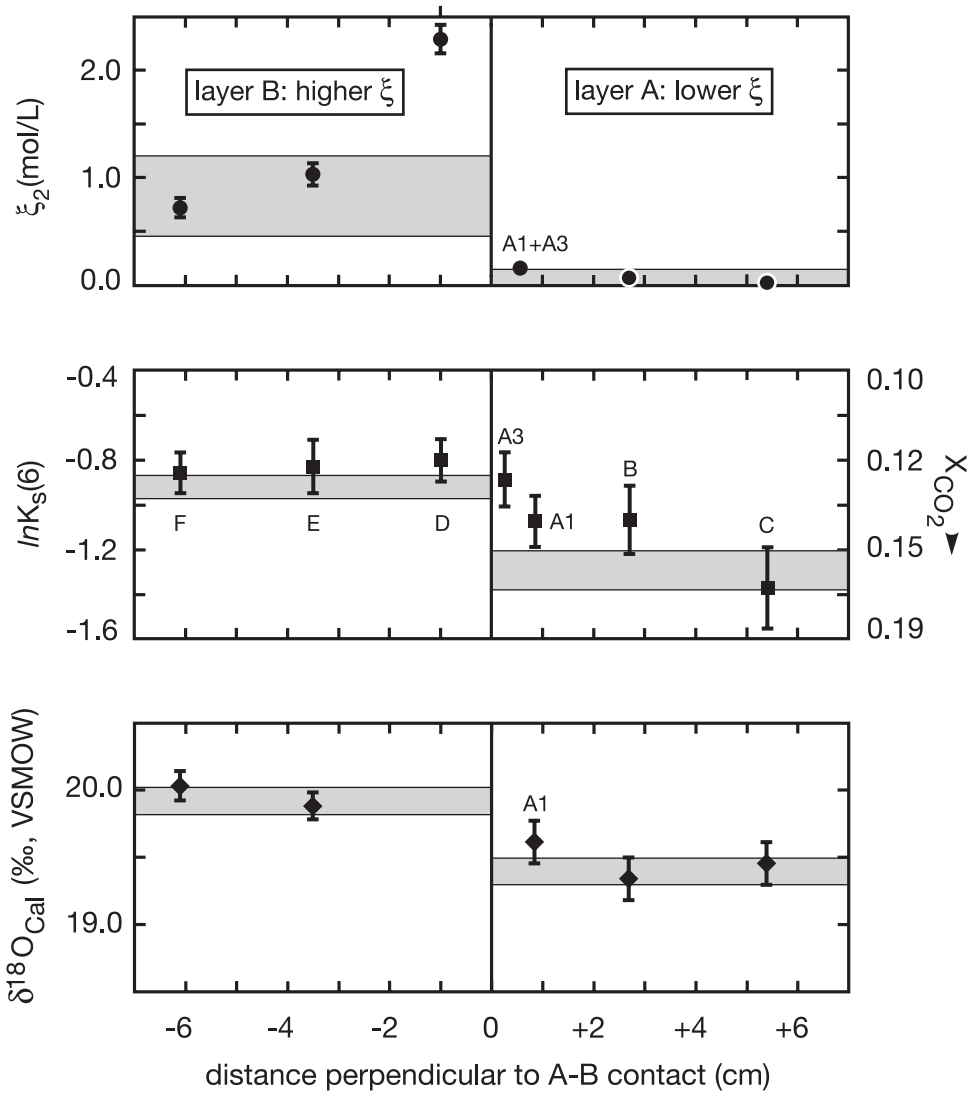

Fig. 13. Values of progress of reaction (2), $ln K_s(6)$, and $\delta^{18}O_{Cal}$ for six samples along the 12-cm-long traverse perpendicular to the contact between layers A and B in the hinge of the isoclinal fold at location 5, Maine (see fig. 4). Sample numbers have "FT" prefix omitted. Format the same as in figure 6. Values of $ln K_s(6)$ were calculated for two portions of the same thin section of sample A (A1 and A3); $\delta^{18}O_{Cal}$ refers to the portion A1; ξ_2 refers to both portions combined. Error bars for ξ_2 and $ln K_s(6)$ are $\pm 2\sigma$. Values of $\delta^{18}O_{Cal}$ represent the weighted mean of 5 to 8 analyses of each specimen; error bar is the 95% confidence interval based on the standard error. Shaded gray bands represent either $\pm 2\sigma$ (ξ_2) or 95% confidence intervals based on the standard error [$ln K_s(6)$, $\delta^{18}O_{Cal}$] in layers A and B away from their mutual contact (from fig. 4).

across layering, the total range in measured ξ_2 (0 – 2.75 mol/L) is only slightly larger than that measured in adjacent layer pairs (0 – 2.40 mol/L). The pairs of layers therefore are representative of the outcrop as a whole. Over the length of the 100-m traverse, the ranges in $ln K_s(6)$, $\delta^{18}O_{Cal}$, and $\delta^{13}C_{Cal}$ are -1.77 to -0.80, 17.2-20.4 permil, and -4.0 to -0.2 permil, respectively. Results for some samples that record just a lower or just an upper bound on $ln K_s(6)$ are consistent with the range in $ln K_s(6)$ recorded by the other samples. As shown by the $\pm 3\sigma$ error bars in figure 14, significant

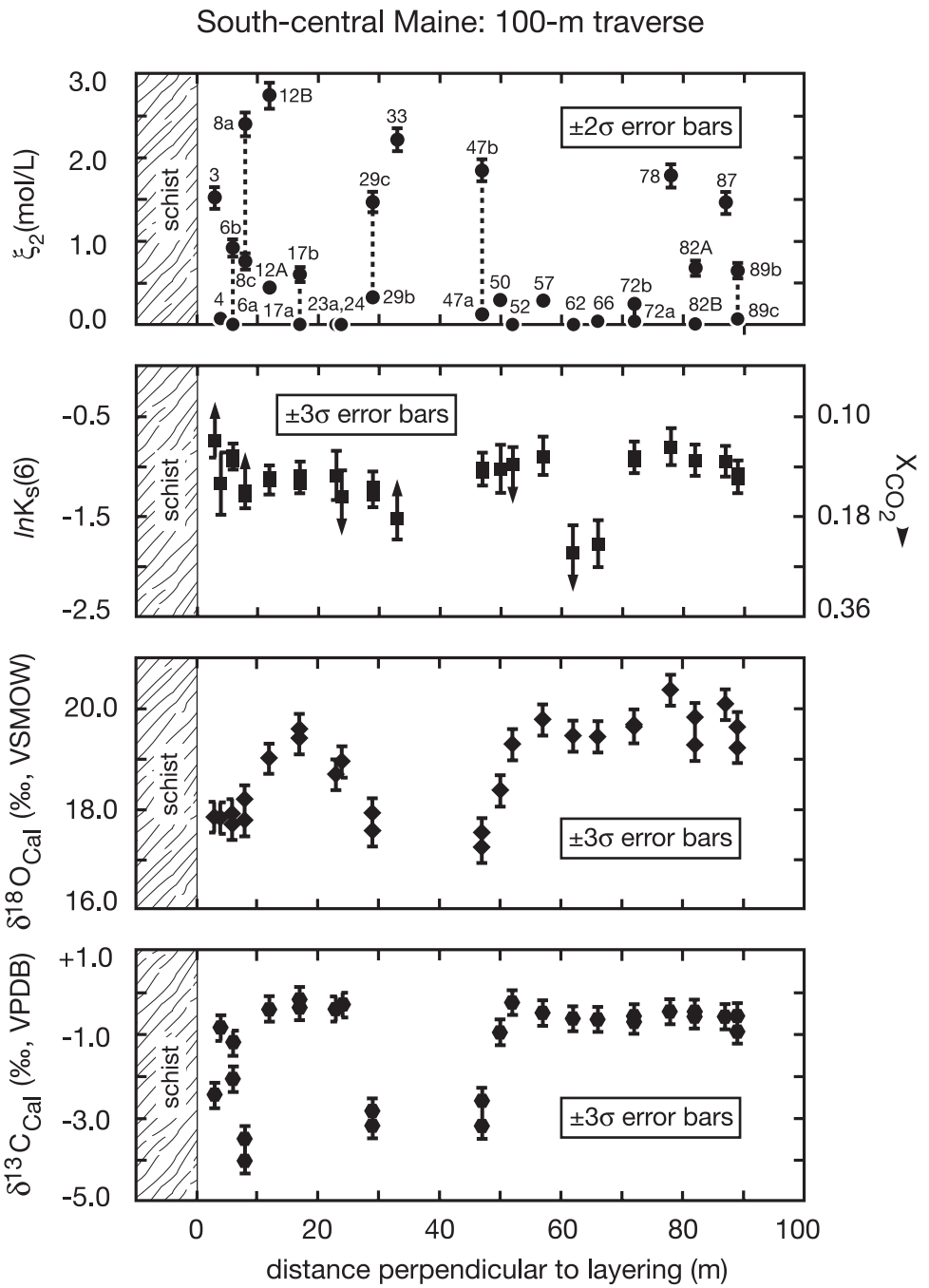

Fig. 14. Values of progress of reaction (2), $ln K_s(6)$, $\delta^{18}O_{Cal}$, and $\delta^{13}C_{Cal}$ for samples along the 100-m-long traverse perpendicular to lithologic layering at location 5, Maine, starting at the NW contact between the normal and limestone members of the Waterville Formation. Sample numbers have "T" and "TP" prefixes omitted and correspond to the samples' positions along the traverse, measured in m. Format the same as in figure 6. Values of ξ_2 for adjacent layer pairs connected with vertical dashed line. Samples 12A and 12B and samples 82A and 82B were collected <1 m apart but are not adjacent layers. Upper and lower bounds on $ln K_s(6)$ the same as in figure 12. Error bars for $ln K_s(6)$, $\delta^{18}O_{Cal}$, and $\delta^{13}C_{Cal}$ are $\pm 3\sigma$ to highlight significant differences between individual samples; for adjacent layer pairs the error bar is the overlap in the $\pm 3\sigma$ errors of the two samples. No triplet of adjacent samples is consistent with both a single value of $ln K_s(6)$ and with a single value of $\delta^{18}O_{Cal}$ (adjacent layer pairs treated as a single sample in this analysis).

differences in $ln K_s(6)$ and $\delta^{18}O_{Cal}$ occur between samples as close as several m apart: $ln K_s(6)$ differs at a $>\pm 3\sigma$ level over 5 m between samples T-57 and T-62, and $\delta^{18}O_{Cal}$ differs at a $>\pm 3\sigma$ level over 2 m between samples T-50 and T-52. Calculation of MSWDs further demonstrates that there are no triplets of adjacent samples along the 100-m traverse in which both $ln K_s(6)$ and $\delta^{18}O_{Cal}$ are statistically consistent with single values (taking adjacent layer pairs as a single sample). Uniformity in proxies for a_{CO_2} and $\delta^{18}O_{fluid}$ did not occur within error of measurement over a distance more than several m during regional metamorphism along the 100-m traverse, consistent with conclusions drawn from samples from the hinge of the fold illustrated in figure 4. Reversals in gradients in both $ln K_s(6)$ and $\delta^{18}O_{Cal}$ occur along the 100-m traverse. For example, the gradient in $ln K_s(6)$ reverses over a distance of $\leq$15 m between samples T-57 and TP-72a,b (fig. 14). The gradient in $\delta^{18}O_{Cal}$ reverses over a distance of $\leq$15 m between samples TP-8a,c and sample T-23a and over $\leq$10 m between samples TP-72a,b and T-82B (fig. 14). The reversals in gradients in proxies for fluid composition across layering over distances no greater than $\approx$10-20 m are consistent with data for samples summarized in figure 4. Values of $\delta^{18}O_{Cal}$ along the 100-m traverse in figure 14 are also broadly consistent with the results of Bickle and others (1997) who concluded that $\delta^{18}O_{carbonate}$ homogenized over a distance on the order of several m at location 5, figure 2.

EXPLANATION OF SPATIAL VARIATIONS IN REACTION PROGRESS

Conventional Explanation

Because of the relationship between time-integrated fluid flux and reaction progress specified by equation (1), cm- to m-scale layer-by-layer variations in progress of the decarbonation reactions in east-central Vermont and south-central Maine have been explained by spatial variations in time-integrated fluid flux with elevated flow in layers with higher ξ and reduced or no flow in layers with low ξ (Ferry, 1987, 1988b, 1994). The conventional explanation, however, is valid only if rocks were chemically isolated from each other during metamorphism at the same cm scale over which variations in ξ are observed. Otherwise ξ in any one sample will depend on infiltration and reaction in adjacent samples. Because reactants and products of reactions (2) and (3) are solid solutions, $K_s(6)$ increases monotonically with reaction progress in a given sample (fig. 15). The predicted change in $K_s(6)$ during reaction ($\approx$0.6 *ln* units) is significantly larger than the error of measurement (table 5). If individual layers of micaceous carbonate were chemically isolated from each other during regional metamorphism, a measurable positive correlation between $K_s(6)$ and ξ_2 would be expected. No such correlation is observed (figs. 6-8, 11-12). Moreover, in regions between $\approx$1-dm- and $\approx$1-m-wide in which there are significant differences in ξ_2, measured $K_s(6)$ is statistically consistent with a uniform value. Not only does the conventional explanation for cm- to m-scale layer-by-layer variations in progress of decarbonation reactions appear to be incorrect, but any successful explanation also must consider the cross-layer uniformity in $K_s(6)$ at that same scale.

New Explanation

Qualitative description.—Layer-by-layer variations in progress of an infiltration-driven reaction will inevitably develop in rocks that experience the same reaction if (a) one or more mineral participants is a solid solution, (b) different layers initially contained different amounts and/or compositions of reactant minerals, and (c) K_s of the relevant mineral-fluid equilibrium is the same, or nearly so, in the layers during subsequent reaction (Ferry and others, 2005). The process can be explained qualitatively with reference to reaction (2) in micaceous carbonate rocks in Vermont and Maine. Consider two rocks that contain Ms, Ank, Cal, Pl, Qtz, Rt, and other accessory minerals but no Bt or Chl prior to reaction; for the sake of simplicity Ms, Ank, and Cal

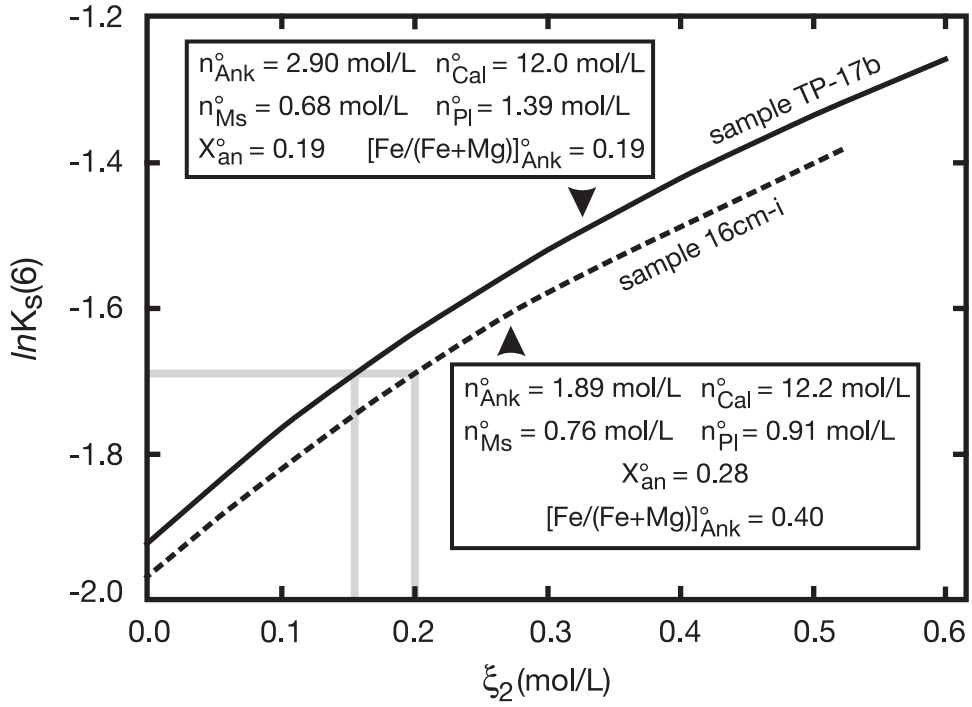

Fig. 15. Calculated evolution of $ln K_s(6)$ with ξ_2 for two representative samples, 16cm-i from Vermont and TP-17b from Maine. Initial amounts and compositions of minerals prior to reaction specified in the insets. For each value of ξ_2, $\xi_3 = (n_{Chl}/n_{Bt})\xi_2$ where n_{Chl} and n_{Bt} are present measured mole concentrations Chl and Bt in the samples. Moles of Ms, Ank, Bt, Chl, Cal, $CaAl_2Si_2O_8$, and $NaAlSi_3O_8$ were calculated from equation (4), and compositions of the Fe-Mg minerals were calculated from an equation analogous to equation (5) (with terms added for Bt and Chl), using measured mineral formulas and the Fe-Mg exchange constants in table 3. The composition of Pl is considered homogeneous. Values of the activity of components in the solid solutions and $ln K_s(6)$ were then computed as described in the text. Curves for both samples terminate at the measured value of ξ_2.

are pure Mg compounds without Fe or Mn. The first rock contains 1 mole Pl/L with $X^0_{an} = 0$, and the second rock contains 2 moles Pl/L with same composition. Both rocks are infiltrated by chemically reactive fluid and reaction (2) proceeds at constant T and P; for simplicity, reaction (3) is considered not to occur. When reaction (2) initiates and at all times afterwards, $K_s(6)$ in both rocks is the same; X_{an} must be the same as well. As reaction proceeds and X_{an} increases in both rocks, ξ_2 in the second rock must be twice ξ_2 in the first rock to maintain the equality in Pl composition. The difference in ξ_2 between the two rocks develops because, from a mass balance constraint, the rate of reaction (2) on a volume basis in the second Pl-rich rock is twice that in the first Pl-poor rock. All else being equal, rocks that start with a greater abundance of Pl prior to reaction will experience a higher rate of reaction (on a volume basis) and record a higher value of ξ_2 than rocks with less Pl.

Alternatively, consider two rocks that both contain the same amount of Pl (for example, 1 mol/L) but the Pl differs in composition prior to reaction. Plagioclase in the first rock, as before, has $X^o_{an} = 0$, but the second rock contains a more calcic Pl, $X^o_{an} = 0.2$. Both rocks are infiltrated by chemically reactive fluid, reaction (2) proceeds at constant T and P, and reaction (3) does not occur. Consideration of $K_s(6)$ leads to the conclusion that as long as X_{an} in the first rock remains <0.20, reaction (2) initially proceeds in the first rock but not in the second. With continued infiltration and reaction, however, X_{an} in the first rock eventually reaches 0.2; with further infiltration,

reaction (2) then proceeds in both. If reaction (2) progresses until $X_{an} = 0.4$ in both rocks, for example, ξ_2 in the first rock will be approximately twice ξ_2 in the second. In this case, the difference in ξ_2 develops not so much because of a difference in rate of reaction between the two rocks but because of the longer duration of reaction (2) in the first rock compared to the second. All else being equal, rocks that start out with more sodic Pl prior to reaction will experience a longer duration of reaction and record a higher value of ξ_2 than rocks with initially more calcic Pl.

As qualitatively explained for another reaction by Ferry and others (2005), differences in the amounts and compositions of reactant Fe-Mg minerals among rocks prior to reaction likewise will result in significant differences in reaction progress by the same mechanism. Specifically, carbonate rocks from Vermont and Maine with a relatively greater abundance of Ank, Ms, and/or Cal and rocks that contain minerals with relatively higher Fe/(Fe+Mg) prior to reaction will develop greater progress of reactions (2) and (3) than rocks with initially smaller amounts of Ank, Ms, and/or Cal or that contain minerals with lower initial Fe/(Fe+Mg).

Quantitative analysis.—The effect of different initial amounts and compositions of Pl work together with different initial amounts and compositions of Ank, Ms, and Cal to control the layer-by-layer variations in ξ_2 and ξ_3 at the dm to m scale over which $K_s(6)$ was uniform during regional metamorphism. A systematic quantitative analysis of the process appears in figure 16, specifically for the progress of reactions (2) and (3). The analysis is with specific reference to samples along the 16-cm traverse at location 21-32, Vermont, but applies to other samples from both Vermont and Maine. Calculations follow those described in the caption to figure 15 using the average mineral formulas and Fe-Mg exchange coefficients for the 16-cm traverse in table 3. In one set of calculations (fig. 16A), the initial amounts and compositions of Ms, Ank, and Cal were held constant at representative values for samples along the 16-cm traverse (see inset to fig. 16A), and initial amounts and compositions of Pl were varied within limits relevant to the samples. Reactions (2) and (3) were allowed to proceed until a value of $ln\mathrm{Ks}(6) = -1.35$ was attained (fig. 7), and reaction progress recorded. As predicted from the qualitative analysis of the process, ξ_2 is larger in rocks with an initially greater abundance of Pl and/or more sodic Pl. The effect of Pl alone can produce differences in ξ_2 of up to 0.3 to 0.4 mol/L. In a second set of calculations (fig. 16B) the initial amounts and compositions of Ms, Cal, and Pl were held constant at representative values for samples along the 16-cm traverse (see inset to fig. 16B), and initial amounts and compositions of Ank were varied within limits relevant to the samples. Reactions (2) and (3) were allowed to proceed until a value of $ln\mathrm{K_s}(6) = -1.35$ was attained, and reaction progress recorded. As predicted from the qualitative analysis of the process by Ferry and others (2005), ξ_2 is larger in rocks with an initially greater abundance of Ank and/or Ank with higher Fe/(Fe+Mg). The effect of Ank alone can produce differences in ξ_2 of up to $\approx$1.0 mol/L. Figure 16 illustrates the results of two additional sets of calculations in which the initial amounts and compositions of Cal (fig. 16C) and Ms (fig. 16D) are allowed to vary with everything else held constant (as specified by the insets). Variations in the initial amounts of Ms and Cal have little effect on ξ_2 because the minerals contain much less Mg+Fe per mole than do Ank, Bt, and Chl. The effect of variation in initial Fe/(Fe+Mg) of Ank, Cal, and Ms on ξ_2 are almost the same because they cannot vary independently; Fe/(Fe+Mg) of the minerals are always interrelated by the Fe-Mg exchange coefficients in table 3. Taken together, inferred variations in the amounts and compositions of Pl, Ank, Cal, and Ms prior to reaction can adequately explain the variations in ξ_2 between 0.24 and 0.97 mol/L along the 16-cm traverse provided that $K_s(6)$ was spatially uniform at the end of reaction (as is indicated by data in fig. 7). Furthermore, the mechanism effectively produces significant layer-by-layer differences in reaction progress even if homogenization of K_s only proceeds until small but non-zero differences occur between layers.

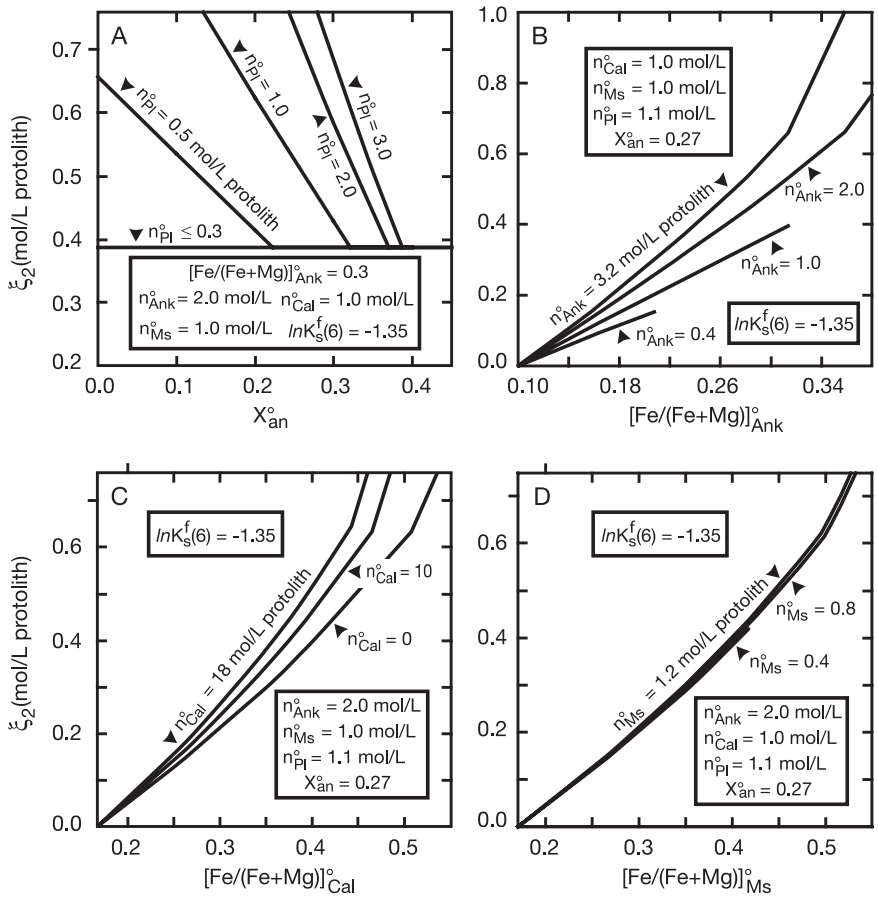

Fig. 16. Systematic evaluation of the effect of variations in initial amounts and compositions of minerals on reaction progress calculated following the method described in caption to figure 15. Calculations are with reference to samples from the 16-cm traverse, location 21-32, Vermont. Mineral formulas and Fe-Mg exchange constants from table 3. All calculations take initial amounts and compositions of minerals as specified by the inset, abscissa, and contours of each panel. Model $\xi_3 = 0.0477\xi_2$ (Penniston-Dorland, ms, 2004). Calculation of ξ_2 proceeds until a final $ln K_s(6) = -1.35$; some curves terminate in the interior of the diagram where a reactant mineral is exhausted before $ln K_s(6) = -1.35$ is attained. (A) Effect of variations in initial amount (n°_{Pl}) and composition (X°_{an}) of Pl with initial amounts and compositions of other minerals held constant as specified by the inset. Effect of variations in initial amount and composition of Ank (B), Cal (C), and Ms (D). Termination of curves in (A) at the horizontal line and kinks in curves in panels (B)-(D) result from the stoichiometry of the reactions and the X_{an}-a_{an} relations for Pl in figure 5.

Validity tests.—The validity of the new explanation for cm- to m-scale variations in progress of reactions (2) and (3) in Vermont and Maine was tested by two additional sets of calculations. The first involved seven pairs of the adjacent cm-thick layers from location 5 in Maine (fig. 12). (A comparison of pair TP-8 is meaningless because reactions (2) and (3) have gone to completion in both layers.) The effect of variations in the initial amounts and compositions of Pl, Ank, Ms, and Cal on ξ_2 effectively can be reduced to a consideration of Pl and Ank alone (fig. 16). If the new explanation is correct, therefore, the member of each pair with higher ξ_2 should have initially contained a greater abundance of Pl, more sodic Pl, a greater abundance Ank, and/or more Fe-rich Ank than its companion with lower ξ_2. Initial amounts and compositions of Pl and Ank were computed for all 14 samples from measured modes and mineral compositions using equations (4) and (5); results are presented in figure 17. Consis-

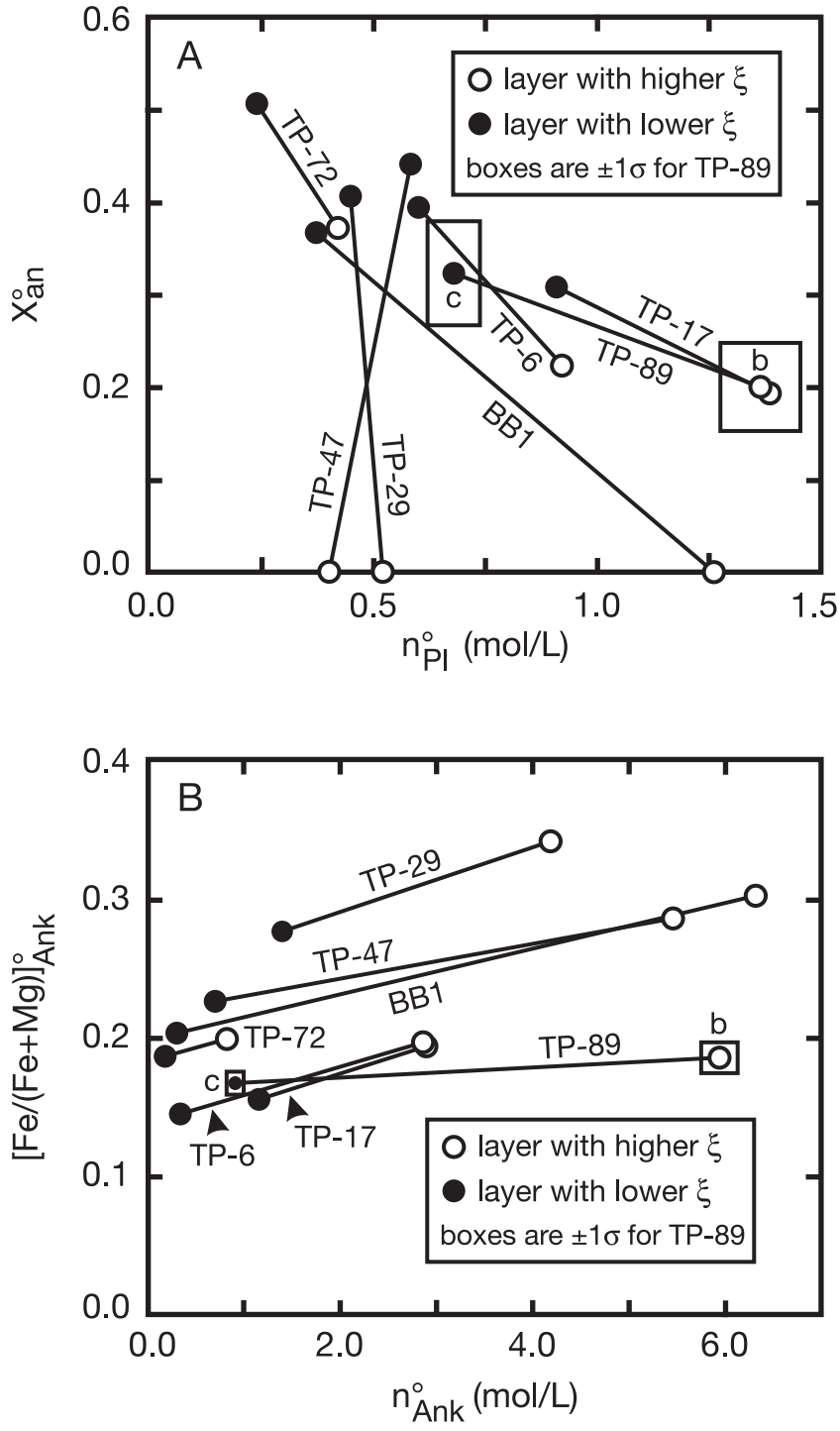

Fig. 17. Initial amounts and compositions of Pl and Ank in the seven pairs of adjacent layers from the 100-m traverse, location 5, Maine, calculated from equations (4) and (5). Calculated $X^{\circ}_{an}<0$ in three samples represented as $X_{an} = 0$. In every pair, the layer that records higher ξ_2 contained a greater abundance of Ank, more sodic Pl, and Ank with higher Fe/(Fe+Mg) than its companion prior to reaction, and, in all but one case, the layer with higher ξ contained a greater abundance of Pl than its companion. Representative $\pm 1\sigma$ uncertainties in calculated results are shown as boxes for layer pair TP89.

tent with the new explanation, the sample of every pair with higher ξ_2 contained a more sodic Pl prior to reaction, and in all but one pair (TP-47), the sample with higher ξ_2 initially contained a greater abundance of Pl as well (fig. 17A). Further consistent with the new explanation, the sample of every pair with higher ξ_2 contained both a greater abundance of Ank and Ank with a higher Fe/(Fe+Mg) prior to reaction (fig. 17B).

Results in figure 17 additionally argue against the conventional explanation of cm-scale spatial variations in reaction progress. If reaction was just controlled by variations in time-integrated flux in chemically isolated channels that correspond to lithologic layers and was independent of amounts and compositions of minerals prior to reaction, it would be a surprising coincidence that in the case of every adjacent pair of layers investigated, fluid was preferentially focused into the layer that initially contained more Ank, Ank with higher Fe/(Fe+Mg), and more sodic Pl, and, in all but one pair, the layer that initially contained more Pl. On the other hand, the new explanation provides a straightforward explanation for the systematic correlations between reaction progress and the amount and composition of Pl and Ank in adjacent pairs of layers prior to reaction (fig. 17).

A second test was applied both to the adjacent layer pairs from Maine and to representative samples from the 16-cm traverse from location 21-32 in Vermont. In the case of samples from the 16-cm traverse, ξ_2 in samples 16cm-a, -d, -e, and -g was simulated as a function of ξ_2 in sample 16cm-c (that records the highest value of ξ_2 along the traverse) following calculations described in the caption to figure 15. For a given value of ξ_2 in sample 16cm-c, ξ_2 in the other samples has a unique value determined by the constraint that $K_s(6)$ in all samples is the same at all times during reaction. (As a hypothetical example, if $K_s(6)$ were the same during reaction in samples 16cm-i and TP-17b, fig. 15, ξ_2 in sample TP-17b is $\approx$0.15 when ξ_2 in sample 16cm-i is 0.20.) Results are illustrated in figure 18. All simulations start at the origin of the diagram ("S," fig. 18). In two samples (16cm-e, -g) reaction begins after reaction has already started in reference sample 16cm-c (their initial trajectories in the simulation follow the abscissa of fig. 18). Reaction starts in the other two samples (16cm-a, -d) prior to reaction in the reference sample (their initial trajectories in the simulation follow the ordinate of fig. 18). The trajectory of a sample enters the interior of the diagram when reaction occurs simultaneously in it and the reference sample. The simulation ends for each sample ("E," fig. 18) when the measured value of ξ_2 for the sample is attained. Final values of ξ_2 predicted for sample 16cm-c in the four simulations, 0.89 to 1.13 mol/L, agree with the measured value (0.97 mol/L) within the uncertainty of the modal analyses of Bt and Chl. Perfect agreement between measured and predicted values of ξ_2, in any case, is not expected because the simulations do not account for the chemical zonation observed in natural Pl. Results in figure 18 indicate that not all layers started reaction at the same time. Specifically, layer 16cm-a began first, followed in order by layers -d, -c, -e, and -g. Thus, part of the reason ξ_2 is larger in sample 16cm-c than in samples -e and -g is that reaction occurred for a longer duration in sample 16cm-c. Duration of reaction, however, cannot explain larger ξ_2 in sample 16cm-c than in samples -a and -d. The slope of the trajectory of all samples in the interior of the diagram is <1. Measured ξ_2 is highest in sample 16cm-c additionally because the rate of reaction was higher in sample 16cm-c than in any of the others. This is explained by higher initial amounts of both Pl and Ank in sample 16cm-c than in the others.

Simulations were similarly conducted for reaction in the six adjacent layer pairs from Maine in which reaction (2) proceeded in both layers (fig. 19). For five pairs (all but TP-8), reaction progress in the layer with lower ξ_2 was computed as a function of reaction progress in the layer with higher ξ_2, subject to the constraint of equal $K_s(6)$ in each pair during reaction, and the simulation was ended when the measured value of

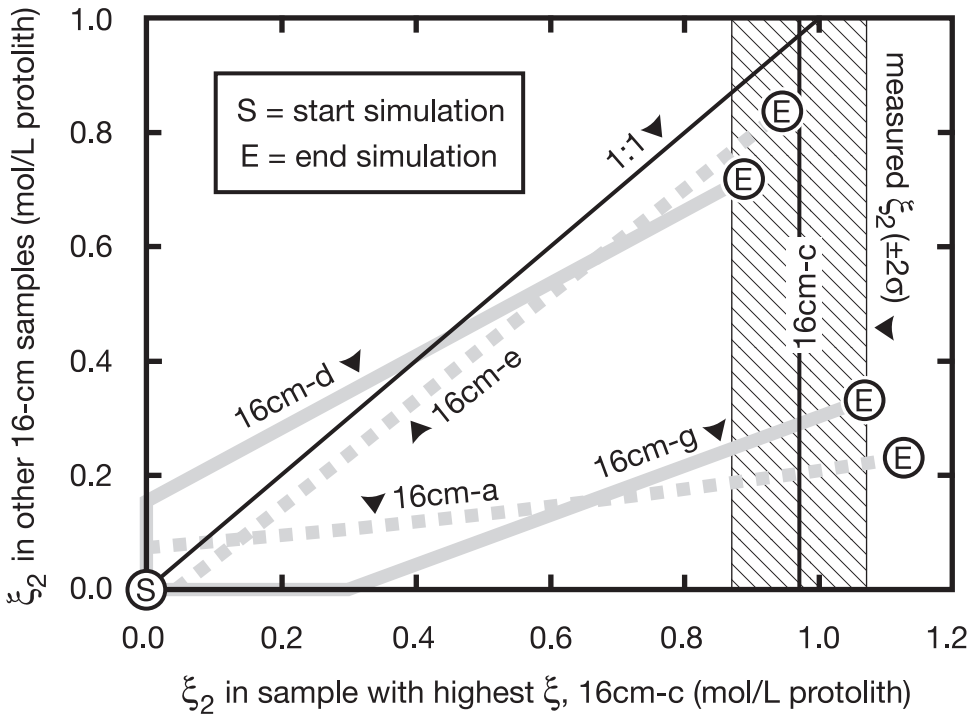

Fig. 18. Quantitative simulation of reaction progress in samples 16cm-a, -d, -e, and -g as a function of ξ_2 in sample 16cm-c, location 21-32, Vermont (thick solid and dashed gray curves). Calculations followed the method described in caption to figure 15 with the constraint that $K_s(6)$ at any stage of reaction is the same in all samples. Initial amounts and compositions of minerals prior to reaction computed from equations (4) and (5). All simulations start at "S" and terminate at "E." For measured values of ξ_2 in samples 16cm-d, -e, and -g, the simulated value of ξ_2 for sample 16cm-c agrees with the measured value within $\pm 2\sigma$ (vertical black line and diagonally-ruled band); there is also agreement between predicted and measured values for the simulation of sample 16cm-a if $\pm 2\sigma$ uncertainties in both ξ_2 and ξ_3 are considered.

ξ_2 in the layer with lower ξ_2 was attained. The final value of ξ_2 predicted by the simulations for the layer with higher ξ_2 agrees with the measured value within the uncertainty of the modal analyses. Perfect agreement between measured and predicted values of ξ_2 is not expected because the simulations do not account for the chemical zonation observed in natural Pl. For pair TP-8, the simulation ended when measured ξ_2 in the layer with higher ξ_2 was attained because reaction (2) went to completion in the layer with lower ξ_2 before the measured value of ξ_2 in its companion was attained. In all pairs but TP-8, reaction started in the layer with higher ξ_2 before it started in its companion (fig. 19A). In addition, reaction (2) never occurred at all in the member of two other pairs with lower ξ_2 (TP-6, BB1; not illustrated in fig. 19A because their simulations simply follow the abscissa). When both layers of pairs TP-29, -47, -72, and -89 were reacting at the same time, the rate of reaction was nearly the same (trajectories of simulations in the interior of fig. 19A have slope ≈ 1). Thus for seven adjacent layer pairs, the layer with higher ξ_2 records a larger value of reaction progress because it experienced reaction for a longer duration than its companion with lower ξ_2. This, in turn, occurred because the member of each pair with higher ξ_2 contained both more sodic Pl and Ank with higher Fe/(Fe+Mg) than its companion with lower ξ_2 prior to reaction (fig. 17). Layer pair TP-8 is the exception (fig. 19B). The layer with lower ξ_2 began reaction before the layer with higher ξ_2. The layer with higher ξ_2 has higher measured ξ_2 because once reaction started in the layer with higher ξ_2, the rate

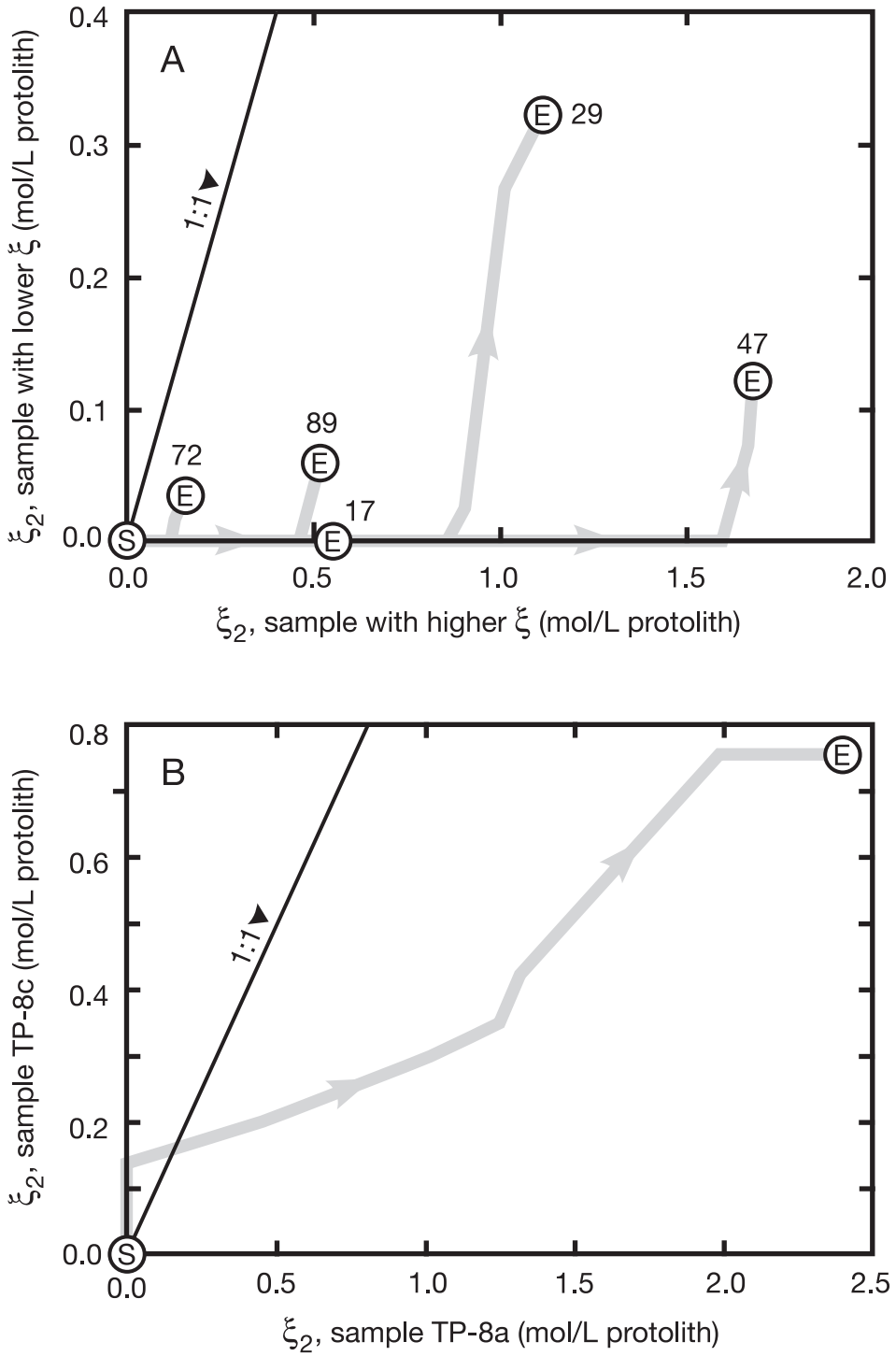

Fig. 19. Quantitative simulation of reaction progress in each of the six adjacent layer pairs from the 100-m traverse, location 5, Maine, in which reaction (2) has occurred in both members. Progress of reaction (2) in the member of each pair with lower ξ was calculated as a function of ξ_2 in the member with higher ξ using the same method to compute curves in figure 18. Kinks in calculated curves result from X_{an}-a_{an} relations assumed for Pl (fig. 5). For measured ξ_2 in the member of each pair with lower ξ in panel (A), the calculated value of ξ_2 for its companion reproduces the measured value within the uncertainty of the modal analyses.

of reaction greatly exceeded that in its companion (slope of trajectory of the simulation in the interior of fig. 19B <1). This, in turn, occurred because the layer with higher ξ_2 contained both more Pl and more Ank than its companion prior to reaction.

The good agreement between predicted and measured values of ξ_2 in both sets of simulations (figs. 18 and 19) is quantitative confirmation of the new explanation for spatial variations in reaction progress. Additionally, the good agreement emphasizes that it is the effects of variations in the initial amounts and compositions of Pl, Ank, Cal, and Ms acting in concert that account for the layer-by-layer variations in ξ_2 observed along the traverse.

DISCUSSION

Uniformity in Proxies for Fluid Composition and Attainment of Equilibrium

Mechanism for development of uniformity in proxies for fluid composition.—The explanation presented in the last section for layer-by-layer variations in reaction progress is strictly based on the empirical observation that $K_s(6)$ is uniform at a spatial scale larger than layering, and the explanation does not require an understanding of what caused the uniformity in $K_s(6)$. Nevertheless, the likeliest mechanism for producing uniformity in $K_s(6)$ and $\delta^{18}O_{Cal}$, the proxies for a_{CO_2} and $\delta^{18}O_{fluid}$, is homogenization of metamorphic fluid composition across layering at the 1 to 10 m scale, probably by diffusion/dispersion, as has been argued by others on the basis of field, theoretical, and laboratory experiment (Bickle and others, 1997; Ague and Rye, 1999; Ague, 2000, 2002, 2003; Evans and others, 2002; Wark and Watson, 2004).

Attainment of mineral-fluid equilibrium.—The numerical values of proxies for a_{CO_2} and $\delta^{18}O_{fluid}$ in those regions where they are uniform are open to several interpretations. One is that mineral-fluid equilibrium was attained, or nearly so, during metamorphism. In this case, fluid composition can be calculated from values of the proxies using thermodynamic data for minerals and fluid, an equation of state for the fluid, and estimates of the P-T conditions of equilibration. If the fluid was a CO_2-H_2O solution, measured values of $K_s(6)$ correspond to $X_{CO_2} = 0.13$-0.21 for samples from east-central Vermont and to $X_{CO_2} = 0.12$-0.21 for samples from south-central Maine. In more detail, values of equilibrium X_{CO_2} can be read from the righthand or top scales of the panels for $ln K_s(6)$ in figures 6-8 and 11-14 and are listed for every analyzed sample in table 5.

Numerous studies, however, have argued that mineral-fluid equilibrium is not necessarily closely approached during infiltration-driven metamorphism (for example, Lasaga and Rye, 1993; Lasaga and others, 2000, 2001; Lüttge and others, 2004). In this case, estimation of X_{CO_2} from measured values of $K_s(6)$ would require a kinetic model for coupled fluid flow and mineral-fluid reaction that is beyond the scope of this study. If a kinetically controlled steady state were attained during infiltration-driven metamorphism, the difference between the true X_{CO_2} and the fictive equilibrium X_{CO_2} would be some constant value (or nearly so) for a given set of P, T, and fluid flow conditions (Lasaga and others, 2000). In the circumstance of a decarbonation reaction driven by infiltration of rock by chemically reactive H_2O-rich CO_2-H_2O fluid, the kinetically controlled value of X_{CO_2} is less than the equilibrium value (Lasaga and others, 2000, 2001).

Alternatively, if the metamorphic fluid-rock system were far from equilibrium, there might not be any simple relationship between the values of proxies for fluid composition and fluid composition itself. Even in this case, however, simply the empirical observation that $K_s(6)$ is spatially uniform at a scale larger than that of lithologic layering is a sufficient basis for the explanation of layer-by-layer variations in reaction progress presented in the last section.

Reaction Rate During Infiltration-driven Regional Metamorphism

The standard treatment of the kinetics of metamorphic mineral-fluid reactions considers that the rate at which a mineral product is produced is controlled by the intrinsic rate constant and order of the reaction, the change in Gibbs free energy of reaction at the conditions of reaction (ΔG), and the surface area (A_i) of the rate-limiting mineral i (for example, Ague and Rye, 1999). This study demonstrates that there is an additional control on reaction rate in individual layers that fundamentally is based on mass balance. Specifically, if K_s associated with the reaction is uniform over some region across layering, the rate of reaction on a volume basis in all but one layer in that region depends on the abundance of mineral solid solutions involved in the reaction. The phenomenon is illustrated in figure 16 specifically for layers undergoing reactions (2) and (3). With reference to figure 16A, for example, if X^o_{an} is the same in two samples, reaction will initiate and end at the same time in both. The final value of ξ_2, however, will be larger in the sample that initially contained a greater abundance of Pl; the rate of reaction (2) therefore also must be larger in the sample that initially contained a greater abundance of Pl.

The two different considerations of reaction rate are not incompatible. In a sequence of rock layers of variable bulk composition composed of the same mineral reactants and products, some or all of which are solid solutions, the mineral-fluid reaction and its order and intrinsic rate constant will be the same (or nearly so) in all layers. If uniformity in K_s associated with the reaction develops by efficient homogenization of fluid composition across layering by diffusion/dispersion, ΔG will be the same (or nearly so) in all layers undergoing reaction. There will be one layer, however, in which the rate-limiting mineral i has a surface area, A_i, that sets a rate of reaction slower than in all the other layers. Provided K_s is uniform, the rate of reaction (on a volume basis) in the other layers undergoing reaction then is set relative to the slowest reacting layer by the amounts of solid solutions in them that participate in the reaction (fig. 16).

In a sequence of rocks all with the same mineral reactants, some or all of which are solid solutions, reaction may occur in some layers but not in others depending on the composition of the reactants. Figure 16, for example, illustrates the phenomenon specifically for the initial Fe/(Fe+Mg) of mineral reactants of reactions (2) and (3). In terms of the standard theory of reaction kinetics, the absence of reaction is appropriately considered as controlled by a value of ΔG that is either zero or of the wrong algebraic sign in non-reacted layers.

Advection, Diffusion/Dispersion, and Mineral-fluid Reaction during Regional Metamorphism

The mechanism of infiltration-driven reaction.—Reaction progress and its spatial variation in micaceous carbonate rocks from east-central Vermont and south-central Maine are best understood in terms of the coupled effects of transport of CO_2 and H_2O by both fluid flow and diffusion/dispersion. The evidence for reactive fluid flow is the significant progress of decarbonation reactions (2) and (3) in rocks that coexisted during reaction with H_2O-rich CO_2-H_2O fluid ($X_{CO_2} \leq$ 0.12-0.21 with exact values depending on the degree to which mineral-fluid equilibrium was attained). Because there are no significant local sources of H_2O-rich fluid exposed within outcrops 21-21 and 21-32 in Vermont and outcrop 5 in Maine (for example, other rock types that underwent dehydration or synmetamorphic granitic rocks) and because the length scale of mass transport of CO_2 and H_2O by diffusion/dispersion across layering during metamorphism was certainly no more than $\approx$1 to 10 m (documented by this study), H_2O must have been transported at the outcrop and larger scales by flow that then drove the decarbonation reactions. After reactions (2) and (3) initiated in favorable layers, diffusion/dispersion caused CO_2 transport from layers undergoing reaction to

adjacent layers that were not and H_2O transport in the opposite direction. Assuming homogenization of fluid composition by diffusion/dispersion is what caused the observed m-scale uniformity in K_s(6), variations in the amounts and compositions of minerals prior to reaction, in turn, controlled ξ within individual layers over distances up to $\approx$1 to 10 m (figs. 16, 18, and 19). Specifically, decarbonation reactions proceeded for a longer duration in layers with relatively more sodic Pl and/or Ank with relatively higher Fe/(Fe+Mg) prior to reaction and proceeded at a faster rate in layers with relatively greater initial amounts of Pl and/or Ank. Cross-layer transport of CO_2 and H_2O by diffusion/dispersion effectively inhibited reaction in some layers and promoted reaction in others depending on the amount and composition of minerals present prior to reaction (in turn controlled by sedimentation and diagenesis). Results for the areas in Vermont and Maine demonstrate that the combination of fluid flow and cross-layer mass transport by diffusion/dispersion controls decarbonation of micaceous carbonate rocks during regional metamorphism in both intermediate-P Barrovian terrains and low-P Buchan terrains over a depth interval of at least 15 km in the crust. Further, results firmly substantiate the conclusion of Ague and Rye (1999) and Ague (2000, 2002) that cross-layer diffusion/dispersion of CO_2 and H_2O is a vital driving force for decarbonation reactions during metamorphism and the important conclusion of Evans and Bickle (2005) that cm-scale variations in ξ at location 5 in Maine are controlled by variations in bulk rock composition.

Resolution of an apparent contradiction.—This study resolves the apparent contradiction between cm-scale layer-by-layer variations in progress of infiltration-driven decarbonation reactions and field and theoretical evidence for transport of CO_2 and H_2O by diffusion/dispersion across layering at a scale of a meter or more (Bickle and others, 1997; Ague 2000, 2002, 2003; Evans and others, 2002). If the cm-scale variations in reaction progress resulted from channeled fluid flow at the scale of lithologic layering (Ferry, 1987, 1988a, 1994), the scale of CO_2 and H_2O transport by diffusion/dispersion could not have been greater than the width of individual layers. Our results resolve the apparent contradiction by verifying that the scale of transport of CO_2 and H_2O by diffusion/dispersion across layering during regional metamorphism is on the order of 1 m or more and by demonstrating that cm-scale spatial variations in progress of decarbonation reactions are better explained in terms of layer-by-layer variations in modes and compositions of minerals prior to reaction than in terms of layer-by-layer variations in fluid flow.

Spatial variations in reaction progress as an image of fluid flow channels.—When mineral reactants and products of an infiltration-driven reaction are solid solutions and the relevant K_s is completely homogenized (or nearly so) over some distance, spatial variations in reaction progress at that scale simply image spatial variations in the amounts and compositions of reactant minerals prior to reaction (that is, bulk composition). The distribution of reaction progress cannot image fluid flow pathways over the length scale of homogenization of K_s. On the other hand, when mineral reactants and products of an infiltration-driven reaction either are pure substances (such as calcite, quartz, and wollastonite) or have compositions fixed by mineral equilibria (such as calcite and dolomite during the dolomite-periclase-calcite reaction), reaction progress is independent of the amounts and compositions of minerals prior to reaction. Unless there is a control by differences in grain size, reaction progress in those circumstances does faithfully image pathways of fluid flow, with elevated flow in areas where reaction has occurred and reduced flow where it has not. Thus, many studies of contact metamorphism that have used progress of the calcite-quartz-wollastonite and dolomite-periclase-calcite reactions to directly image channelways of reactive fluid flow remain valid (Ferry and Rumble, 1997; Roselle, ms, 1997; Ferry and others, 1998, 2001, 2002; Lackey and Valley, 2004).

A limit on the scale of investigation of the geometry of fluid flow.—Progress of reaction (2) in metamorphosed carbonate rocks from Vermont and Maine cannot image pathways of reactive fluid flow at scales smaller than the one over which $K_s(6)$ is uniform. As a generalization, regardless of the geochemical tracer considered (isotopes, molecular fluid species, trace elements) and regardless of whether mineral-fluid reactions involve solid solutions or not, the geometry of reactive fluid flow in any fossil hydrothermal system can never be determined at a spatial scale smaller than the one at which the proxy for that geochemical tracer is homogenized, presumably by diffusion/dispersion. Diffusion/dispersion simply obliterates any geochemical record of flow geometry. Over the scale of homogenization of the proxy, it is impossible to distinguish whether the physical mechanism of flow was along a single thin fracture, pervasive and uniform, or something in-between and/or more complicated.

Reactive Fluid Flow during Regional Metamorphism in Northern New England

Layer-parallel reactive fluid flow.—To what extent, if any, do earlier arguments for layer-parallel flow of reactive fluid during metamorphism of carbonate rocks in east-central Vermont and south-central Maine remain correct? In cases of decarbonation reactions driven by infiltration of rock by reactive H_2O-rich fluid, X_{CO_2} increases monotonically along the flow path regardless of the approach to mineral-fluid equilibrium at the reaction site, regardless of whether reactants and products are solid solutions or not, and regardless of whether mineral-fluid reaction is driven by the gradient flow mechanism or the disequilibrium flow mechanism (Ferry and Gerdes, 1998). Reversals in gradients in the proxy for a_{CO_2}, $K_s(6)$, at locations 21-32 in Vermont (fig. 11) and at location 5 in Maine (figs. 4 and 14) therefore rule out a significant cross-layer component of fluid flow at a scale larger than the reversals ($\approx$1 – 15 m). By default, large-scale flow of reactive fluids in both areas must have been largely parallel to lithologic layering. The study confirms, as have many others (for example, Kohn and Valley, 1994; Vyhnal and Chamberlain, 1996; Bickle and others, 1997; Wing and Ferry, 2002; Ague, 2003), the occurrence of layer-parallel flow during Acadian regional metamorphism in New England. Results of this study, however, do not disprove earlier conclusions of cm- to m-scale layer-by-layer channeled fluid flow during regional metamorphism in Vermont and Maine (Ferry, 1987, 1988b, 1994); rather they demonstrate that the spatial distribution of reaction progress is *inconclusive* about whether channeled fluid flow occurred or not at the layer-by-layer scale.

Time-integrated fluid flux.—There are now two reasons to reconsider published values of time-integrated fluid flux (q) during regional metamorphism of the Waterville and Waits River Formations (Ferry, 1992, 1994). First, this study establishes that q should be computed from the value of reaction progress averaged over the distance that K_s was uniform during metamorphism rather than from individual samples as was done in the earlier studies. Second, the earlier studies computed q assuming that the widespread spatial distribution of reactants and products of reaction (2) in east-central Vermont and south-central Maine indicates the gradient flow mechanism for the decarbonation reaction. Solid solution in reactants and products or sluggish reaction kinetics, however, can stabilize a widespread spatial distribution of mineral reactants and products even if decarbonation results from the disequilibrium flow mechanism (Ague and Rye, 1999; Lasaga and others, 2001). A way to circumvent the question of reaction mechanism in calculating q is to compute a fluid-rock ratio for the entire flow system; q then is the product of the fluid-rock ratio and the distance of reaction along the flow path (Ferry, 1991). A minimum whole-system fluid-rock ratio was estimated for the two terrains from equation (1) of Ferry (1991) taking the average of all measured values of ξ_2 and X_{CO_2} for each area in table 5 and assuming infiltration of the system by pure H_2O fluid; values are 3.8 and 11.8 mol/L for Vermont and Maine, respectively. For flow and reaction over a distance on the order of 10 km, either horizontal, vertical, or inclined (figs. 1 and 2), q = 3800 and 12,000 mol fluid/cm^2

rock for Vermont and Maine, respectively. These are minimum values because calculations assume infiltration of pure H_2O, mineral-fluid equilibrium at the site of reaction, and reaction at the inferred maximum metamorphic T. Previously reported average q $\approx$5000 mol/cm^2 for locations 21-21 and 21-32 in east-central Vermont and $\approx$20,000 mol/cm^2 for location 5 in Maine (Ferry, 1994), therefore, are consistent with the new values. The new estimates of q confirm that enormous quantities of reactive fluid were involved in driving mineral reactions during Acadian regional metamorphism in northern New England.

Source of reactive fluid.—Several sources of the reactive H_2O-rich fluid that drove decarbonation reactions in micaceous carbonate rocks during regional metamorphism in New England have been suggested. One is that H_2O is derived by dehydration in nearby pelitic rocks and transported by diffusion/dispersion across layering into the carbonate rocks (Ague and Rye, 1999; Ague, 2000, 2002). In the case of location 21-32 in Vermont and location 5 in Maine, however, reversals in the gradients in the proxy for a_{CO_2}, $K_s(6)$, over distances of 1 to 15 m indicate that diffusion/dispersion could not have transported H_2O over the >50 m distance that separates carbonate rocks that have experienced progress of reactions (2) and (3) from the nearest exposures of pelitic schist. In other areas of New England, reactive H_2O-rich fluids appear to have been introduced along fractures (now Qtz veins), probably from a plutonic source (for example, Ague, 1994, 2003; van Haren and others, 1996). This possibility is appealing in the case of east-central Vermont because locations 21-21 and 21-32 are $\approx$20 percent Qtz veins by volume (Ferry, 1994). Unfortunately, no spatial correlation between locations of Qtz veins and either reaction progress, $K_s(6)$, or $\delta^{18}O_{Cal}$ were detected because the spacing of veins is smaller than the distance over which $K_s(6)$ and $\delta^{18}O_{Cal}$ are uniform. Consequently, this study is inconclusive whether Qtz veins represent fossil channels for the reactive fluid flow or whether the veins were precipitated from fluid derived from or equilibrated with igneous rock. The source of reactive fluid during regional metamorphism in New England where many 1000s km^3 of rock experienced infiltration-driven reactions remains an unsolved problem.

Mass Transport of Na, Ca, and C Isotopes

Two puzzling results of the study lead to additional considerations of mass transport of Na and Ca and of C isotopes during regional metamorphism.

Intergranular Na-Ca interdiffusion.—Two irregularities in the estimated modes and mineral compositions prior to reactions (2) and (3) point to possible Na-Ca-metasomatism during metamorphism of the adjacent layer pairs of carbonate rock from Maine. First, for three of the pairs (TP-29, TP-47, BB1), calculated Pl composition prior to reaction in the layer with higher ξ_2 is impossible ($X^o_{an}<0$), although X^o_{an} in only one sample is statistically different from 0 given the uncertainties in measured Pl modes. Second, estimated X^o_{an} in every member with lower ξ_2 of the analyzed adjacent pairs of layers is surprisingly large (fig. 17A; up to 0.51). The large value of X^o_{an} cannot be easily explained by isochemical metamorphism because equivalent rocks at lower grades contain albite ($X_{an}<0.1$), and no prograde reactions are observed at lower grades that produced the $CaAl_2Si_2O_8$ component of Pl without Bt or Chl. Both irregularities can be explained by Ca-Na exchange at the cm- to dm-scale between adjacent layers and subsequent Pl-fluid reaction:

$$CaAl_2Si_2O_8 + 4\ SiO_2 + 2\ Na^+ = 2\ NaAlSi_3O_8 + Ca^{++} \qquad (7)$$

(speciation of Na and Ca in the fluid is irrelevant to the discussion and is chosen arbitrarily). When the member with higher ξ_2 of an adjacent pair of layers started reaction (2) first, as was typically the case (fig. 19), the increase in X_{an} locally drove reaction (7) forward, which, in turn drove Ca-Na exchange between the adjacent layers. As Ca and Na transport proceeded, reaction (7) was driven forward in the layer

with higher ξ_2 (producing Pl with lower X_{an} than it otherwise would have) while reaction (7) was driven in reverse in the layer with lower ξ_2 (producing Pl with higher X_{an} than it otherwise would have). Exchange of Ca and Na between adjacent layers, coupled with reaction (7), thus can explain the anomalously high calculated X^o_{an} in the layers with lower ξ_2, the negative calculated X^o_{an} in some layers with higher ξ_2, and the complicated chemical zoning in Pl. Significantly, the effect of reaction (7) on the layers with higher ξ_2 is the same as increasing the amount of Pl prior to reaction and lowering X^o_{an}, causing reaction (2) to proceed further than it would otherwise (fig. 16A). The complementary effect of reaction (7) on the layers with lower ξ_2 is the same as decreasing the initial amount of Pl and raising X^o_{an}, inhibiting progress of reaction (2). The Ca-Na exchange between adjacent layers is an additional process that in part can explain the difference in ξ_2 between adjacent pairs of layers. Reaction (7) may have also occurred in the Waits River Formation, but the evidence is not as conclusive. A quantitative analysis of the effect of reaction (7) on progress of reactions (2) and (3) could not be made in an uncontrived fashion without additional data to constrain the amount and scale of Na and Ca transport.

Intracrystalline ^{13}C-^{12}C interdiffusion.—Values of $\delta^{18}O_{Cal}$ are uniform within error of measurement over ≈50-100 cm across entire layers of marl in pelitic schist at location 21-35 of the Waits River Formation, Vermont, while values of $\delta^{13}C_{Cal}$ can differ over a distance <5 cm (figs. 9 and 10). Similarly, measured $\delta^{18}O_{Cal}$ is uniform over distances on the order of ≈100 cm across layering in marls from locations 21-21 and 21-32 of the Waits River Formation (figs. 8 and 11), while measured $\delta^{13}C_{Cal}$ is not uniform even over distances across layering as small as 9 cm (fig. 6). Considering the carbonate contents of rocks (table 1) and X_{CO_2} of fluid (table 5) involved, a comparison of the characteristic diffusion distances for $\delta^{18}O$ and $\delta^{13}C$ using equation (1) of Bickle and others (1997) predicts that the distance over which $\delta^{13}C_{Cal}$ is homogenized by intergranular diffusion should be 0.5 to 1.1 times the corresponding distance for $\delta^{18}O_{Cal}$ (≈50-100 cm). Direct measurement, however, indicates that the distance for $\delta^{13}C_{Cal}$ homogenization is much smaller (figs. 6, 7, 9, and 10). Equation (1) of Bickle and others (1997) assumes mass transport controlled by intergranular diffusion with intracrystalline diffusion of isotopic tracers fast in comparison to the time scale of intergranular diffusion. A simple explanation of diffusion distances for $\delta^{13}C$ that are smaller than expected therefore is that $\delta^{13}C_{Cal}$ failed to fully homogenize by intracrystalline diffusion at the time scale of metamorphism.

Prediction of intracrystalline homogenization of $\delta^{18}O_{Cal}$ but not of $\delta^{13}C_{Cal}$ during regional metamorphism is confirmed by measurements of the intracrystalline diffusion coefficients for C and O isotopes in calcite (Farver, 1994; Labotka and others, 2000). Using data for "wet" diffusion of O (C isotope diffusion appears independent of X_{CO_2} of coexisting fluid), the Dodson (1973) closure temperature (T_c) for a spherical calcite crystal with a representative 200 μm radius cooling at a rate of 20°C/My (appropriate for regional metamorphism), is 350°C for O isotopes and 540°C for C isotopes. The T_c for C isotopes is comparable to T recorded by mineral equilibria at locations 21-21, 21-32, and 21-35 in the Waits River Formation (500 – 550°C) while T_c for O isotopes is significantly below it. Slow intracrystalline C-isotope diffusion thus likely explains why the behavior of $\delta^{13}C_{Cal}$ in this study as a proxy for $\delta^{13}C_{fluid}$ seems to be aberrant in comparison to the behavior of $\delta^{18}O_{Cal}$ as a proxy for $\delta^{18}O_{fluid}$ (figs. 6 – 12).

ACKNOWLEDGMENTS

We thank A. J. Kaufman for providing access to his laboratory at the University of Maryland. Patient, thoughtful, and insightful reviews by Mike Bickle, William Peck, Joe Pyle, and the Associate Editor were much appreciated. Research supported by grant EAR-0229267 from the Division of Earth Sciences, National Science Foundation, and

by endowed funds for fieldwork from the Department of Earth and Planetary Sciences at Johns Hopkins University.

Appendix

Activity-composition relations for plagioclase solid solutions were derived from experiments by Goldsmith (1982) on the equilibrium among zoisite, kyanite, quartz, plagioclase solid solution, and H_2O fluid. Experiments determined the stability of zoisite + kyanite + quartz versus plagioclase + fluid as a function of P, T, and plagioclase composition. Although most experiments were synthesis experiments, Goldsmith verified that results obtained by several true reversals were the same. Given the reported values of P, T and X_{an}, each of Goldsmith's successful experiments can be used with Berman's (1988, updated June, 1992) thermodynamic database to calculate either an upper or lower bound on a_{an} (Carpenter and Ferry, 1984). Only experiments at 8, 9, and 10 kbar were considered. Additional experiments at 10.7 kbar in some cases are complicated by partial melting, and they do not span the entire plagioclase composition coordinate. Calculated results for all experiments at 8 to 10 kbar and 400 to 730°C (fig. 5) are consistent with a simple empirical representation within experimental error of the measurement of plagioclase composition ($\pm 0.02X_{an}$). A three-part subdivision of the a_{an}-X_{an} relations follows Orville (1972). For $0.1<X_{an}<0.421$, upper and lower bounds on a_{an} are separated by a quadratic curve based on a visual fit to the data. For $0.421<X_{an}<0.975$, $a_{an} = 0.975$ correctly separates upper and lower bounds within $\pm 0.025a_{an}$ (considering that values of $a_{an}>1$ are impossible). For $X_{an}>0.975$, Raoult's Law is assumed. Activity-composition relations for $X_{an}<0.1$ are not specified, but they must follow Henry's Law at some sufficiently low value of X_{an}. The implied limited dependence of the a_{an}-X_{an} relations on P and T is firmly based on Goldsmith's experimental data. For example, the change from a_{an} as a function of X_{an} to constant $a_{an} = 0.975$ occurs in the experimental data over a range of P and T (615°C at 8 kbar; 665°C at 9 kbar; 715°C at10 kbar) but at the same $X_{an} \approx 0.42$.

References

Ague, J. J., 1994, Mass transfer during Barrovian metamorphism of pelites, south-central Connecticut. II: channelized fluid flow and the growth of staurolite and kyanite: American Journal of Science, v. 294, p. 1061–1134.

——— 2000, Release of CO_2 from carbonate rocks during regional metamorphism of lithologically heterogeneous crust: Geology, v. 28, p. 1123–1126.

——— 2002, Gradients in fluid composition across metacarbonate layers of the Wepawaug Schist, Connecticut, USA: Contributions to Mineralogy and Petrology, v. 143, p. 38–55.

——— 2003, Fluid infiltration and transport of major, minor, and trace elements during regional metamorphism of carbonate rocks, Wepawaug Schist, Connecticut, USA: American Journal of Science, v. 303, p. 753–816.

Ague, J. J., and Rye, D. M., 1999, Simple models of CO_2 release from metacarbonates with implications for interpretation of directions and magnitudes of fluid flow in the deep crust: Journal of Petrology, v. 40, p. 1443–1462.

Armstrong, J. T., 1988, Quantitative analysis of silicate and oxide minerals: comparison of Monte Carlo, ZAF and phi-rho-z procedures, *in* Newbury, D. E., editor, Microbeam Analysis – 1988: San Francisco, San Francisco Press, p. 239–246.

Barnett, D. E., and Chamberlain, C. P., 1991, Relative scales of thermal- and fluid infiltration-driven metamorphism in fold nappes, New England, U.S.A.: American Mineralogist, v. 76, p. 713–727.

Baumgartner, L. P., and Ferry, J. M., 1991, A model for coupled fluid-flow and mixed-volatile mineral reactions with applications to regional metamorphism: Contributions to Mineralogy and Petrology, v. 106, p. 273–285.

Berman, R. G., 1988, Internally-consistent thermodynamic data for minerals in the system Na_2O-K_2O-CaO-MgO-FeO-Fe_2O_3-Al_2O_3-SiO_2-TiO_2-H_2O-CO_2: Journal of Petrology, v. 29, p. 445–522.

Bickle, M. J., Chapman, H. J., Ferry, J. M., Rumble, D., III, and Fallick, A. E., 1997, Fluid flow and diffusion in the Waterville limestone, south-central Maine: constraints from strontium, oxygen and carbon isotope profiles: Journal of Petrology, v. 38, p. 1489–1512.

Carpenter, M. A., and Ferry, J. M., 1984, Constraints on the thermodynamic mixing properties of plagioclase feldspars: Contributions to Mineralogy and Petrology, v. 87, p. 138–148.

Chayes, F., 1956, Petrographic modal analysis: an elementary statistical appraisal: New York, John Wiley and Sons, 113 p.

Dodson, M. H., 1973, Closure temperature in cooling geochronological and petrological systems: Contributions to Mineralogy and Petrology, v. 40, p. 259–274.

Doll, C. G., Cady, W. M., Thompson, J. B., Jr., and Billings, M. P., compilers and editors, 1961, Centennial geologic map of Vermont: Montpelier, Vermont Geologic Survey, scale 1:250,000.

Evans, K. A., and Bickle, M. J., 2005, An investigation of the relationship between bulk composition, inferred reaction progress and fluid-flow parameters for layered micaceous carbonates from Maine, USA: Journal of Metamorphic Petrology, v. 23, p. 181–197.

Evans, K. A., Bickle, M. J., Skelton, A. D. L., Hall, M., and Chapman, H., 2002, Reductive deposition of graphite at lithological margins in east central Vermont: a Sr, C and O isotope study: Journal of Metamorphic Geology, v. 20, p. 781–798.

Farver, J. R., 1994, Oxygen self-diffusion in calcite: dependence on temperature and water fugacity: Earth and Planetary Science Letters, v. 121, p. 575–587.
Ferry, J. M., 1976, Metamorphism of calcareous sediments in the Waterville-Vassalboro area, south-central Maine: mineral reactions and graphical analysis: American Journal of Science, v. 276, p. 841–882.
——— 1979, A map of chemical potential differences within an outcrop: American Mineralogist, v. 64, p. 966–985.
——— 1980a, A case study of the amount and distribution of heat and fluid during metamorphism: Contributions to Mineralogy and Petrology, v. 71, p. 373–385.
——— 1980b, A comparative study of geothermometers and geobarometers in pelitic schists from south-central Maine: American Mineralogist, v. 65, p. 720–732.
——— 1984, A biotite isograd in south-central Maine, U.S.A.: mineral reactions, fluid transfer and heat transfer: Journal of Petrology, v. 25, p. 871–893.
——— 1987, Metamorphic hydrology at 13-km depth and 400–550°C: American Mineralogist, v. 72, p. 39–58.
——— 1988a, Infiltration-driven metamorphism in northern New England, USA: Journal of Petrology, v. 29, p. 1121–1159.
——— 1988b, Contrasting mechanisms of fluid flow through adjacent stratigraphic units during regional metamorphism, south-central Maine, USA: Contributions to Mineralogy and Petrology, v. 98, p. 1–12.
——— 1991, Dehydration and decarbonation reactions as a record of fluid infiltration: Reviews in Mineralogy, v. 26, p. 351–393.
——— 1992, Regional metamorphism of the Waits River Formation, eastern Vermont: delineation of a new type of giant metamorphic hydrothermal system: Journal of Petrology, v. 33, p. 45–94.
——— 1994, Overview of the petrologic record of fluid flow during regional metamorphism in northern New England: American Journal of Science, v. 294, p. 905–988.
Ferry, J. M., and Gerdes, M. L., 1998, Chemically reactive fluid flow during metamorphism: Annual Review of Earth and Planetary Sciences, v. 26, p. 255–287.
Ferry, J. M., and Rumble, D., III, 1997, Formation and destruction of periclase by fluid flow in two contact aureoles: Contributions to Mineralogy and Petrology, v. 128, p. 313–334.
Ferry, J. M., Sorensen, S. S., and Rumble, D., III, 1998, Structurally controlled fluid flow during contact metamorphism in the Ritter Range pendant, California, USA: Contributions to Mineralogy and Petrology, v. 130, p. 358–378.
Ferry, J. M., Wing, B. A., and Rumble, D., III, 2001, Formation of wollastonite by chemically reactive fluid flow during contact metamorphism, Mt. Morrison pendant, Sierra Nevada, California, USA: Journal of Petrology, v. 42, p. 1705–1728.
Ferry, J. M., Wing, B. A., Penniston-Dorland, S. C., and Rumble D., III, 2002, The direction of fluid flow during contact metamorphism of siliceous carbonate rocks: new data for the Monzoni and Predazzo aureoles, northern Italy, and a global review: Contributions to Mineralogy and Petrology, v. 142, p. 679–699.
Ferry, J. M., Rumble, D., III, Wing, B. A., and Penniston-Dorland, S. C., 2005, A new interpretation of centimetre-scale variations in the progress of infiltration-driven metamorphic reactions: case study of carbonated metaperidotite, Val d'Efra, Central Alps, Switzerland: Journal of Petrology, v. 46, p. 1725–1746.
Fisher, G. W., and Karabinos, P., 1980, Stratigraphic sequence of the Gile Mountain and Waits River Formations near Royalton, Vermont: Geological Society of America Bulletin, v. 91, p. 282–286.
Friedman, I., and O'Neil, J. R., 1977, Compilation of stable isotope fractionation factors of geochemical interest: United States Geological Survey Professional Paper 440-KK, 109 p.
Goldsmith, J. R., 1982, Plagioclase stability at elevated temperatures and water pressures: American Mineralogist, v. 67, p. 653–675.
Hatch, N. L., Jr., 1988a, New evidence for faulting along the "Monroe Line," eastern Vermont and westernmost New Hampshire: American Journal of Science, v. 288, p. 1–18.
——— 1988b, Some revisions to the stratigraphy and structure of the Connecticut Valley trough, eastern Vermont: American Journal of Science, v. 288, p. 1041–1059.
Holland, T. J. B., and Powell, R., 1990, An enlarged and updated internally consistent thermodynamic dataset with uncertainties and correlations: the system K_2O-Na_2O-CaO-MgO-MnO-FeO-Fe_2O_3-Al_2O_3-TiO_2-SiO_2-C-H_2-O_2: Journal of Metamorphic Geology, v. 8, p.89–124.
——— 1998, An internally consistent thermodynamic data set for phases of petrological interest: Journal of Metamorphic Geology, v. 16, p. 309–343.
Hueber, F. M., Bothner, W. A., Hatch, N. L., Jr., Finney, S. C., and Aleinikoff, J. N., 1990, Devonian plants from southern Quebec and northern New Hampshire and the age of the Connecticut Valley trough: American Journal of Science, v. 290, p. 360–395.
Kerrick, D. M., and Jacobs, G. K., 1981, A modified Redlich-Kwong equation for H_2O, CO_2, and H_2O-CO_2 mixtures at elevated pressures and temperatures: American Journal of Science, v. 281, p. 735–767.
Kohn, M. J., and Valley, J. W., 1994, Oxygen isotope constraints on metamorphic fluid flow, Townshend Dam, Vermont, USA: Geochimica et Cosmochimica Acta, v. 58, p. 5551–5566.
Kretz, R., 1983, Symbols for rock-forming minerals: American Mineralogist, v. 68, p. 277–279.
Labotka, T. C., Cole, D. R., and Riciputi, L. R., 2000, Diffusion of C and O in calcite at 100 MPa: American Mineralogist, v. 85, p. 488–494.
Lackey, J. S., and Valley, J. W., 2004, Complicated patterns of fluid flow during wollastonite formation in calcareous sandstones at Laurel Mountain, Mt. Morrison Pendant, California: Geological Society of America Bulletin, v. 116, p. 76–93.
Lasaga, A. C., and Rye, D. M., 1993, Fluid flow and chemical reaction kinetics in metamorphic systems: American Journal of Science, v. 293, p. 361–404.

Lasaga, A. C., Lüttge, A., Rye, D. M., and Bolton, E. W., 2000, Dynamic treatment of invariant and univariant reactions in metamorphic systems: American Journal of Science, v. 300, p. 173–221.
Lasaga, A. C., Rye, D. M., Lüttge, A., and Bolton, E. W., 2001, Calculation of fluid fluxes in Earth's crust: Geochimica et Cosmochimica Acta, v. 65, p. 1161–1185.
Lüttge, A., Bolton, E. W., and Rye, D. M., 2004, A kinetic model of metamorphism: an application to siliceous dolomites: Contributions to Mineralogy and Petrology, v. 146, p. 546–565.
Lyons, J. B., 1955, Geology of the Hanover quadrangle, New Hampshire-Vermont: Geological Society of America Bulletin, v. 66, p. 105–146.
Mahon, K. I., 1996, The new "York" regression: application of an improved statistical method to geochemistry: International Geology Review, v. 38, p. 293–303.
Menard, T., and Spear, F. S., 1993, Metamorphism of calcic pelitic schists, Strafford Dome, Vermont: compositional zoning and reaction history: Journal of Petrology, v. 34, p. 977–1005.
——— 1994, Metamorphic P-T paths from calcic pelitic schists from the Strafford Dome, Vermont, USA: Journal of Metamorphic Geology, v. 12, p. 811–826.
Orville, P. M., 1972, Plagioclase cation exchange equilibria with aqueous chloride solutions: results at 700°C and 2000 bars in the presence of quartz: American Journal of Science, v. 272, p. 234–272.
Osberg, P. H., 1968, Stratigraphy, structural geology, and metamorphism of the Waterville-Vassalboro area, Maine: Maine Geological Survey Bulletin 20, 64 p.
——— 1979, Geologic relations in south-central Maine, *in* Skehan, J. W., and Osberg, P. H., editors, The Caledonides in the U. S. A. Geological excursions in the northeast Appalachians: Weston, Massachusetts, Boston College, p. 37–62.
——— 1988, Geologic relations in the shale-wacke sequence in south-central Maine: Maine Geological Survey Studies in Maine Geology, v. 1, p. 51–73.
Osberg, P. H., Tull, J. F., Robinson, P., Hon, R., and Butler, J. R., 1989, The Acadian orogen, *in* Hatcher, R. D., Jr., Thomas, W. A., and Viele, G. W., editors, The Appalachian-Ouachita Orogen in the United States. The Geology of North America, v. F-2, Boulder: Geological Society of America, p. 179–232.
Penniston-Dorland, S. C., ms, 2004, Sources, mechanisms, and pathways of chemically reactive fluid transport during metamorphism from analysis of geochemical tracers: Maryland, Johns Hopkins University, Ph.D. thesis, 155 p.
Roselle, G. T., ms, 1997, Integrated petrologic, stable isotopic, and statistical study of fluid-flow in carbonates of the Ubehebe Peak contact aureole, Death Valley National Park, California: Madison, Wisconsin, University of Wisconsin, Ph.D. thesis, 258 p.
Rosenbaum, J., and Sheppard, S. M. F., 1986, An isotopic study of siderites, dolomites and ankerites at high temperatures: Geochimica et Cosmochimica Acta, v. 50, p. 1147–1150.
Sheppard, S. M. F., and Schwarcz, H. P., 1970, Fractionation of carbon and oxygen isotopes and magnesium between coexisting metamorphic calcite and dolomite: Contributions to Mineralogy and Petrology, v. 26, p. 161–198.
Stern, L. A., Chamberlain, C. P., Barnett, D. E., and Ferry, J. M., 1992, Stable isotope evidence for regional-scale fluid migration in a Barrovian metamorphic terrane, Vermont, USA: Contributions to Mineralogy and Petrology, v. 112, p. 475–489.
Swart, P. K., Burns, S. J., and Leder, J. J., 1991, Fractionation of the stable isotopes of oxygen and carbon in carbon dioxide during the reaction of calcite and phosphoric acid as a function of temperature and technique: Chemical Geology, v. 86, p. 89–96.
Thompson, J. B., Jr., 1982, Reaction space: an algebraic and geometric approach: Reviews in Mineralogy, v. 10, p. 33–52.
Thompson, J. B., Jr., and Norton, S. A., 1968, Paleozoic regional metamorphism in New England and adjacent areas, *in* Zen, E-an, White, W. S., Hadley, J. B., and Thompson, J. B., Jr., editors, Studies of Appalachian Geology: Northern and Maritime: New York, John Wiley and Sons, p. 319–327.
Thompson, J. B., Jr., Robinson, P., Clifford, T. N., and Trask, N. J., Jr., 1968, Nappes and gneiss domes in west-central New England, *in* Zen, E-an, White, W. S., Hadley, J. B., and Thompson, J. B., Jr., editors, Studies of Appalachian Geology: Northern and Maritime: New York, John Wiley and Sons, p. 203–218.
Tucker, R. D., Osberg, P. H., and Berry, H. N., IV, 2001, The geology of a part of Acadia and the nature of the Acadian orogeny across central and eastern Maine: American Journal of Science, v. 301, p. 205–260.
van Haren, J. L. M., Ague, J. J., and Rye, D. M., 1996, Oxygen isotope record of fluid infiltration and mass transfer during regional metamorphism of pelitic schist, south-central Connecticut, USA: Geochimica et Cosmochimica Acta, v. 60, p. 3487–3504.
Vyhnal, C. R., and Chamberlain, C. P., 1996, Preservation of early isotopic signatures during prograde metamorphism, eastern Vermont: American Journal of Science, v. 296, p. 394–419.
Wark, D. A., and Watson, E. B., 2004, Interdiffusion of H_2O and CO_2 in metamorphic fluids at ≈490 to 660°C and 1 GPa: Geochimica et Cosmochimica Acta, v. 68, p. 2693–2698.
White, W. S., and Jahns, R. H., 1950, Structure of central and east-central Vermont: Journal of Geology, v. 58, p. 179–220.
Wing, B. A., and Ferry, J. M., 2002, Three-dimensional geometry of metamorphic fluid flow during Barrovian regional metamorphism from an inversion of combined petrologic and stable isotopic data: Geology, v. 30, p. 639–642.
Wing, B. A., Ferry, J. M., and Harrison, T. M., 2003, Prograde destruction and formation of monazite and allanite during contact and regional metamorphism of pelites: petrology and geochronology: Contributions to Mineralogy and Petrology, v. 145, p. 228–250.
Woodland, B. G., 1977, Structural analysis of the Silurian-Devonian rocks of the Royalton area, Vermont: Geological Society of America Bulletin, v. 88, p. 1111–1123.